Portland State University

PDXScholar

10-2011

Bridge Damage Models for Seismic Risk Assessment of Oregon Highway Network

Peter Dusicka
Portland State University

Jeffery Roberts
Portland State University

Follow this and additional works at: https://pdxscholar.library.pdx.edu/trec_reports

Part of the Civil and Environmental Engineering Commons, and the Transportation Commons

Let us know how access to this document benefits you.

Recommended Citation

Dusicka, Peter and Jeffery Roberts. Bridge Damage Models for Seismic Risk Assessment of Oregon Highway Network. OTREC-RR-11-08. Portland, OR: Transportation Research and Education Center (TREC), 2011. https://doi.org/10.15760/trec.19

This Report is brought to you for free and open access. It has been accepted for inclusion in TREC Final Reports by an authorized administrator of PDXScholar. Please contact us if we can make this document more accessible: pdxscholar@pdx.edu.

OTREC

OREGON
TRANSPORTATION
RESEARCH AND
EDUCATION CONSORTIUM

FINAL REPORT

Bridge Damage Models for Seismic Risk Assessment of Oregon Highway Network

OTREC-RR-11-08
October 2011

A National University Transportation Center sponsored by the U.S. Department of Transportation's Research and Innovative Technology Administration

BRIDGE DAMAGE MODELS FOR SEISMIC RISK ASSESSMENT OF OREGON HIGHWAY NETWORK

Final Report

OTREC-RR-11-08

by

Jeff Roberts
Peter Dusicka
Portland State University

for

Oregon Transportation Research
and Education Consortium (OTREC)
P.O. Box 751
Portland, OR 97207

October 2011

Technical Report Documentation Page

1. Report No. OTREC RR-11-08	2. Government Accession No.	3. Recipient's Catalog No.
4. Title and Subtitle Bridge Damage Models For Seismic Risk Assessment of Oregon Highway Network		5. Report Date October 2011
		6. Performing Organization Code
7. Author(s) Peter Dusicka and Jeffery Roberts		8. Performing Organization Report No.
9. Performing Organization Name and Address Portland State University Department of Civil and Environmental Engineering PO Box 751 Portland, Oregon, 97207		10. Work Unit No. (TRAIS)
		11. Contract or Grant No.
12. Sponsoring Agency Name and Address Oregon Transportation Research and Education Consortium (OTREC) P.O. Box 751 Portland, Oregon 97207		13. Type of Report and Period Covered Final Report
		14. Sponsoring Agency Code
15. Supplementary Notes		

16. Abstract

The highway transportation network of the United States relies on the health and integrity of major infrastructure elements such as bridges. Frequently traveled parts of Oregon are within the seismically active Pacific Northwest and many of the bridges were designed and built to lateral demands that were assumed to be less than the current expectation, a deficiency caused by our growing awareness of seismic hazard and our enhanced understanding of the non-linear response of bridges. This vulnerability to damage from earthquakes can result in not only immediate damage, but also in potentially lingering economic impact caused by the disruption to traffic and freight mobility.

Using analytical methods, fragility curves were constructed assuming lognormal capacity and demand distributions. Probability of failure was determined for the four damage state conditions of slight, moderate, extensive, and complete levels of damage. These statistical values were compared to the median and dispersion values proposed by other researchers, in addition to those calculated using guidelines from the HAZUS Technical Manual. Older multiple-span Oregon bridges were found to be significantly more fragile than the HAZUS models.

As a result of this modeling and analysis effort, the relative fragility of the modeled typical 3-span and 5-span bridges was determined and quantified. Possible causes of the relatively high fragilities were also considered.

17. Key Words Seismic, fragility, bridge, structural performance, column, ductility		18. Distribution Statement No restrictions. Copies available from OTREC: www.otrec.us	
19. Security Classification (of this report) Unclassified	20. Security Classification (of this page) Unclassified	21. No. of Pages 106	22. Price

ACKNOWLEDGEMENTS

This project was funded by the Oregon Transportation Research and Education Consortium (OTREC). All dissemination should include the OTREC logo and reference as a sponsoring agency.

DISCLAIMER

The contents of this report reflect the views of the authors, who are solely responsible for the facts and the accuracy of the material and information presented herein. This document is disseminated under the sponsorship of the U.S. Department of Transportation University Transportation Centers Program and the Oregon Department of Transportation in the interest of information exchange. The U.S. Government and the Oregon Department of Transportation assume no liability for the contents or use thereof. The contents do not necessarily reflect the official views of the U.S. Government or the Oregon Department of Transportation. This report does not constitute a standard, specification, or regulation.

TABLE OF CONTENTS

EXECUTIVE SUMMARY ... 1

1.0 OVERVIEW OF BRIDGE FRAGILITY WORK ... 3

- 1.1 INTRODUCTION ... 3
- 1.2 OVERVIEW OF FRAGILITY FUNCTIONS ... 3
- 1.2.1 EMPERICAL FRAGILITY CURVES ... 4
- 1.2.2 EXPERT-BASED FRAGILITY FUNCTIONS ... 4
- 1.2.3 ANALYTICAL FRAGILITY FUNCTIONS ... 5

2.0 GROUND-MOTION SUMMARY ... 7

- 2.1 HISTORICAL EARTHQUAKES ... 7
- 2.2 PROPOSED GROUND MOTIONS IN THE PACIFIC NORTHWEST ... 8

3.0 BRIDGE INVENTORY ... 15

- 3.1 NATIONAL BRIDGE INVENTORY ... 15
- 3.2 DETERMINATION OF TYPICAL THREE-SPAN BRIDGE ... 15
- 3.3 DETERMINATION OF TYPICAL FIVE-SPAN BRIDGE ... 17

4.0 THREE-DIMENSIONAL MODELS OF TYPICAL BRIDGES ... 19

- 4.1 TYPICAL THREE-SPAN BRIDGE ... 21
- 4.1.1 BRIDGE LAYOUT ... 21
- 4.1.2 OPENSEES MODEL ... 22
- 4.1.2.1 MODEL VERIFICATION ... 25
- 4.1.3 MODEL RESPONSE ... 27
- 4.2 TYPICAL FIVE-SPAN BRIDGE ... 30
- 4.2.1 BRIDGE LAYOUT ... 30
- 4.2.2 OPENSEES MODEL ... 30
- 4.2.2.1 MODEL VERIFICATION ... 33
- 4.2.3 MODEL RESPONSE ... 34

5.0 PROBABALISTIC SEISMIC DEMAND ANALYSIS ... 39

- 5.1 PROBABALISTIC SEISMIC DEMAND ... 39
- 5.2 PSDM FOR TYPICAL THREE-SPAN BRIDGE ... 42
- 5.3 PSDM FOR TYPICAL FIVE-SPAN BRIDGE ... 44

6.0 SEISMIC FRAGILITY ANALYSIS OF BRIDGES ... 47

- 6.1 LIMIT STATES ... 47
- 6.2 FRAGILITY CURVE GENERATION ... 48
- 6.3 THREE-SPAN BRIDGE FRAGILITY CURVES ... 49
- 6.3.1 EFFECT OF ABUTMENTS ... 51
- 6.3.2 EFFECT OF GROUND-MOTION SUITE CHANGE ... 52
- 6.3.3 EFFECT OF DECREASING THE NUMBER OF RUNS ... 53
- 6.3.4 EFFECT OF GROUND-MOTION ORIENTATION ... 54
- 6.3.5 EFFECT OF CONCRETE CONFINEMENT RETROFIT ... 55
- 6.4 FIVE-SPAN BRIDGE FRAGILITY CURVES ... 58

7.0 DISCUSSION AND CONCLUSIONS ... 61

8.0 FUTURE WORK ... 65

9.0 REFERENCES 67
10.0 APPENDICES 71
10.1 OPENSEES SCRIPT FOR THREE-SPAN GEOMETRY 71
10.2 OPENSEES SCRIPT FOR THREE-SPAN GRAVITY LOADS 84
10.3 OPENSEES SCRIPT FOR THREE-SPAN EXTERNAL LOADS 88

LIST OF TABLES

Table 2.1: Selected U.S. Earthquakes of General Historic Interest (USGS, 2009) 7
Table 2.2: Seattle Ground Motions with POE of 10% in 50 Years (SAC, 1997)........................... 8
Table 2.3: Seattle Ground Motions with POE of 2% in 50 Years (SAC, 1997)............................. 8
Table 3.1: NBI Database Search Criteria.. 15
Table 3.2: NBI Item 43A - Kind of Material/Design Used on Oregon Bridges on Chosen Highways 15
Table 3.3: NBI Item 43B - Type of Design/Construction Used on Oregon Bridges on Chosen Highways 16
Table 3.4: Statistics of Three-Span NBI Code 202 Oregon Bridges on Chosen Highways......... 16
Table 3.5: Bridge Used In Three-Span Study (Oregon Bridge 07865A East)............................. 16
Table 3.6: Kind of Material/Design Used on Five-Span Oregon Bridges on Chosen Highways. 17
Table 3.7: Type of Design/Construction on Five-Span Oregon Bridges on Chosen Highways... 17
Table 3.8: Majority of Bridge Types on Oregon Bridges on Chosen Highways.......................... 17
Table 3.9: Statistics of Five-Span NBI Code 202 Oregon Bridges on Chosen Highways........... 18
Table 3.10: Bridge Used In Five-Span Study (Oregon Bridge 07628)... 18
Table 4.1: Element Types Used With Three-Span Model.. 22
Table 4.2: ElasticPPGap Material Values for Three-Span Abutment-Soil Model....................... 22
Table 4.3: Element Values for Three-Span Deck... 22
Table 4.4: Concrete04 Values for Confined Concrete Used With Three-Span Bridge................ 23
Table 4.5: Concrete01 Values for Cover Concrete Used With Three-Span Bridge..................... 24
Table 4.6: Hysteretic Steel Values Used with Five-Span Bridge... 24
Table 4.7: OpenSees Boundary Conditions for Three-Span Bridge... 25
Table 4.8: Estimated Stiffness Values for Three-Span Bridge... 26
Table 4.9: Calculated Periods of Vibration for Various Three-Span Bridge Models................... 27
Table 4.10: Maximum Displacements Using POE-of-10%-in-50-Years Group.......................... 29
Table 4.11: Maximum Displacements Using POE-of-2%-in-50-Years Group............................ 29
Table 4.12: Element Types Used With Five-Span Model.. 31
Table 4.13: ElasticPPGap Material Values for Five-Span Abutments... 31
Table 4.14: elasticBeamcolumn Element Values for Five-Span Deck... 31
Table 4.15: Concrete01 Values for Confined Concrete Used With Five-Span Bridge................ 32
Table 4.16: Concrete01 Values for Cover Concrete Used With Five-Span Bridge..................... 32
Table 4.17: Hysteretic Steel Values Used With Five-Span Bridge.. 33
Table 4.18: Estimated Stiffness Values for Five-Span Bridge... 34
Table 4.19: Calculated Periods of Vibration for Various Five-Span Bridge Models................... 34
Table 4.20: Maximum Displacements Using POE-of-10%-in-50-Years Group.......................... 36
Table 4.21: Maximum Displacements Using POE-of-2%-in-50-Years Group............................ 36
Table 5.1: Displacement Ductilities Using POE-of-10%-in-50-Years Group.............................. 43
Table 5.2: Displacement Ductilities Using POE-of-2%-in-50-Years Group................................ 43
Table 5.3: PSDM for Three-Span Bridge.. 43
Table 5.4: Displacement Ductilities Using POE-of-10%-in-50-Years Group.............................. 44
Table 5.5: Displacement Ductilities Using POE-of-2%-in-50-Years Group................................ 44
Table 5.6: PSDM for Five-Span Bridge.. 45

Table 6.1: FEMA Limit States 47
Table 6.2: Model Bridge Capacity Values 48
Table 6.3: Fragility Curves Values for Typical Three-Span Bridge 49
Table 6.4: Fragility Curves Values for Typical Three-Span Bridge and Reference Values 50
Table 6.5: Fragility Curve Values With and Without Abutments 51
Table 6.6: Fragility Curve Values with All Abutments and Longitudinal Abutments Only 52
Table 6.7: Fragility Medians Using POE-10%-in-50-Years Ground-Motion Suite 52
Table 6.8: Fragility Medians Using Reduced Data Set 53
Table 6.9: Fragility Medians after Ground Motion Rotation (θ=45°) Using POE-10%-in-50-Years Suite 55
Table 6.10: Fragility Medians after Steel Retrofit Using POE-10-in-50 Suite 57
Table 6.11: Fragility Curves Values for Typical Five-Span Bridge 58

LIST OF FIGURES

Figure 1.1: Analytical Fragility Curve Generation Using Nonlinear Time-History Analysis........ 6
Figure 2.1: Histogram of PGA Values of POE-2%-in-50-Years Suite 9
Figure 2.2: Histogram of PGA Values of POE-10%-in-50-Years Suite 9
Figure 2.3: Histogram of PGA Values of All SAC Ground-Motion Time Histories Used.......... 10
Figure 2.4: Displacement Spectrum (5% damping) – POE-2%-in-50-Years Suite..................... 11
Figure 2.5: Displacement Spectrum (5% damping) – POE-10%-in-50-Years Suite................... 11
Figure 2.6: Pseudo-Acceleration Spectrum (5% damping) – POE-2%-in-50-Years Suite 12
Figure 2.7: Pseudo-Acceleration Spectrum (5% damping) – POE-10%-in-50-Years Suite 13
Figure 3.1: Elevation View of Oregon Bridge 07865A (Taylor Street East, Lane County)......... 17
Figure 3.2: Elevation View of Oregon Bridge 07628 (Sutherlin Creek, Douglas County).......... 18
Figure 4.1: Typical Bridge Model 19
Figure 4.2: Ground-Motion Sample from POE-of-10% Group.. 20
Figure 4.3: Ground-Motion Sample from POE-of-2% Group.. 20
Figure 4.4: Concrete Member Reinforcement for Three-Span Bridge....................................... 21
Figure 4.5: OpenSees Material Types Used In Reinforced Concrete Models (from OpenSees 2009) 23
Figure 4.6: OpenSees Model for Three-Span Bridge 24
Figure 4.7: Comparison of Experimental and Modeled Hysteretic Behavior of Test Column 26
Figure 4.8: Mode Shapes of Typical Three-Span Bridge with no Soil-Abutment Stiffness Included.. 28
Figure 4.9: Concrete Member Reinforcement for Typical Five-Span Bridge............................ 30
Figure 4.10: OpenSees Model for Typical Five-Span Bridge 33
Figure 4.11: Mode Shapes of Typical Five-Span Bridge with no Soil-Abutment Stiffness Included.. 35
Figure 5.1: PSDM Illustration in Lognormal Space (Padgett, 2007) 41
Figure 5.2: PSDM Plot for Three-Span Bridge 44
Figure 5.3: PSDM Plot for Five-Span Bridge.. 45
Figure 6.1: Fragility Curves for Three-Span Bridge.. 49
Figure 6.2: Complete and Extensive Damage Fragility Curve for Three-Span Bridge without Abutments 51
Figure 6.3: Complete and Extensive Damage Fragility Curve for Three-Span Bridge Suite Change 53
Figure 6.4: Complete and Extensive Damage Fragility Curves for Three-Span Bridge without Abutments 54
Figure 6.5: Complete and Extensive Damage Fragility Curves for Three-Span Using Rotated Ground-Motion Suite 55
Figure 6.6: Slight and Moderate Damage Fragility Curves for Three-Span Using Retrofitted Columns 57
Figure 6.7: Extensive and Complete Damage Fragility Curves for Three-Span Using Retrofitted Columns 58
Figure 6.8: Fragility Curves for Five-Span Bridge.. 59

EXECUTIVE SUMMARY

The U.S. highway transportation network relies on the health and integrity of major infrastructure elements such as bridges. Frequently traveled parts of Oregon are within the seismically active Pacific Northwest, and many of the bridges were designed and built to lateral demands that were assumed to be less than the current expectation, a deficiency caused by our growing awareness of seismic hazard and our enhanced understanding of the non-linear response of bridges. This vulnerability to damage from earthquakes can result in not only immediate damage, but also in potentially lingering economic impacts caused by the disruption to traffic and freight mobility.

One of the key components in determining the impact of an earthquake on the transportation network is the bridge damage state model represented by fragility curves. A bridge fragility curve provides the probability that a bridge is damaged beyond a specified damage state under various levels of ground movement. Several methods of producing fragility curves were considered, specifically curves based upon actual failure data, expert opinion, and analytical models derived from the physics of the actual bridge system.

In order to fully define a bridge fragility curve, demands imposed upon the structure must be known or assumed. These demands are typically provided by using suites of ground-motion time histories, and may come from actual time histories from strong ground-motion records from the area of interest or synthetically produced. Two sets of ground motions were developed for the Seattle area by the SAC Joint Venture. The first having a probability of exceedance of 2% in 50 years, and the second having a probability of exceedance of 5% in 50 years. These sets are a combination of actual and synthetic time histories.

The other requirement to developing a structure's fragility curves is the ability to model the capacity of that structure. To do this, an inventory of a subset of Oregon bridges was made, from which a typical three-span and five-span bridge was identified using average attributes. Then, an OpenSees (Open System for Earthquake Engineering Simulation) model was made for both of these average bridges. Various assumptions were made during the modeling process, but most notable were the assumptions that the bridge deck would behave elastically and the columns would behave inelastically. Because of the expected inelastic behavior the columns were modeled using the OpenSees beamWithHinges element. This specialized element considers plasticity to be concentrated over specified hinge lengths at the element ends. Each ground motion was then applied to the two OpenSees models, from which the displacement response was determined for each column and from each ground motion the maximum PGA was determined. Since both capacity and demand distributions were assumed to be lognormal, for each ground motion a data pair was made relating the logarithm of the maximum PGA and the logarithm of the maximum column displacement seen by each structure in the OpenSees model. When these data pairs spanning all ground-motion records were combined into one data set for each average bridge, a best-fit line was determined by performing a regression analysis, resulting in the capacity model used in the fragility curves.

The probability of demand exceeding the capacity of the structure was then determined by using standard worksheet software, resulting in fragility curves for both typical structures under consideration.

Using analytical methods, fragility curves were constructed using the calculated median value and dispersion (standard deviation) values of the lognormal capacity distributions for the four damage-state conditions of slight, moderate, extensive, and complete levels of damage. These statistical values were compared to the median and dispersion values proposed by other researchers, in addition to those calculated using guidelines from the HAZUS Technical Manual.

As a result of this modeling and analysis effort, the relative fragility of the modeled typical three-span and five-span bridges was determined and quantified. Possible causes of the relatively high fragilities were also considered.

1.0 OVERVIEW OF BRIDGE FRAGILITY WORK

1.1 INTRODUCTION

Portland State University has developed a computer model of ODOT-identified freight routes of the western Oregon and Columbia River highway network using new Geographic Information System (GIS) software called REDARS2 (Risks from Earthquake Damage to Roadway Systems). The methodology and software was the result of 12 years of development with the primary financial sponsorship of the Federal Highway Administration and significant contributions from Caltrans. The Oregon study area was chosen to represent areas of relatively high seismic risk and strategic importance. The Oregon model was created by combining the structural, transportation, geotechnical and seismic attributes of the bridges, roadways and soils of the study area. This information was available on various databases, which were collected, interpreted and modified to the format recognized by the program. Using the REDARS2 model, bridge vulnerability and the associated impact to Oregon's economy can be assessed in different ways. Deterministic or probabilistic seismic risk analysis (SRA) can be performed on the Oregon network providing multilevel economic and structural damage assessments, as well as transportation functions such as post-earthquake travel time and detour-route assessments. As part of this scope, PSU has successfully performed both types of SRA to provide an initial assessment of bridge and highway network vulnerability to regional seismic activity.

Although three previous REDARS2 models have been constructed (in the New Madrid, Bay Area and Los Angeles seismic zones), the Oregon highway network model developed by PSU constitutes the first use of the program by anyone outside of the team that originally developed the software. The Oregon model encompasses a much larger area and assesses more bridges than ever attempted using this technology. Finally, the Oregon model is the first REDARS2 model to assess vertical settlement from liquefaction as part of the transportation network assessment.

In order to fully exploit the capabilities of REDARS2, proper fragility curves applicable to Oregon bridges needed to be developed. The following section provides a brief overview of bridge fragility work. Subsequent chapters describe the methods that were used in this study to develop fragility curves (also called fragility functions) for typical Oregon three-span and five-span continuous, reinforced-concrete bridges.

1.2 OVERVIEW OF FRAGILITY FUNCTIONS

One of the key issues in determining an earthquake's impact on the transportation network is to estimate damage to components of lifeline systems. Modeling the performance of structures as a function of a chosen ground-motion intensity measure can do this. Peak Ground Acceleration (PGA) or Spectral Acceleration (S_a) values are commonly used for intensity measures. The performance can be modeled using two methods. If discrete probabilities are associated with the intensity measure, then a damage probability matrix (Filliben et al., 2002) can be assembled. If a continuous relationship is used fragility curves can be formulated, which describes how likely a structure will meet or exceed a specified level of damage (limit state) given a specific ground motion intensity. Symbolically this is written as:

$$\text{Fragility} = \text{Probability}\,[\text{LS} \mid \text{IM} = im] \qquad \textbf{(1-1)}$$

where LS is the limit state or level of damage experienced by the structure, IM is the ground motion intensity measure (i.e., PGA or S_a), and *im* is a specific value of the intensity measure. Once a fragility function is generated, the user can predict the level of damage a system (or components, if fragility functions are available at the component level) may experience for a given intensity of earthquake.

Various methods can be used to construct structural fragility curves, with three being described here: empirical, expert-based and analytical methods.

1.2.1 EMPERICAL FRAGILITY CURVES

Empirical fragility curves are developed using statistical methods on post-earthquake inspection data. After the Northridge, CA (Jan. 17, 1994) and Loma Prieta, CA (Oct. 17, 1989) earthquakes, more effort was invested in the development of empirical fragility curves (Basoz et al., 1998, and Shinozuka et al., 2003). This was primarily due to more complete ground-motion data being available in addition to better bridge-damage data. Data from the Kobe, Japan (Jan. 17, 1995) earthquake has also been used to develop empirical fragility curves (Shinozuka et al., 2003).

The general methodology used to develop empirical fragility curves can be generalized as follows. First, bridges of interest are assigned to distinct classes according to common structural characteristics. Post-earthquake assessments are then performed on each of these bridges in order to determine bridge-specific damage states. Correlation studies are then used to determine relationships between ground-motion intensity measures and damage states. This also can be extended to include repair-cost considerations.

This method lends itself to look at bridges in a relatively broad sense. For example, the data may be categorized by something general such as R/C column or multi-span R/C bridge type. Because of the subjective nature of the input inspection data and the coarseness of the data, the uncertainties associated with this approach can be high.

1.2.2 EXPERT-BASED FRAGILITY FUNCTIONS

Through the SRA process, the probability of earthquake damage is synthesized from information from different fields like seismology, geology, engineering and economics (Wen et al., 2003). Any other information used during SRA is qualitative and can't easily be described using statistical means. Expert-based development of functions can be challenging since subjectivity introduces high levels of uncertainty.

A procedure to implement (Porter et al., 2007) expert-based functions can be outlined as follows. Note that only experts with professional experience in the design or post-earthquake observation of the component of interest should be used. Using a provided form, advice from the experts should be solicited about their judgment regarding a specific engineering demand parameter (EDP) at which a particular damage state may occur. Using this data, simple relations are used to estimate a median value of the EDP and dispersion (standard deviation). If the dispersion is uncharacteristically low, indicating possible overconfidence by the experts, then provisions are made to use a minimum value of 0.4 for the dispersion.

1.2.3 ANALYTICAL FRAGILITY FUNCTIONS

Analytical fragility curves are primarily used when sufficient actual bridge damage and ground-motion data aren't available to predict the performance of bridge structures. Much research has been devoted to this subject using various methodologies (Nielson, 2006; Saxena et al., 2000; Mander, 1999; Hwang et al., 2001). Bridge-damage states are related to the capacity of the structure, and ground shaking is linked to the demand of the structure. The magnitude of ground shaking is usually quantified by using a ground-motion intensity factor of Peak Ground Acceleration (PGA) or Spectral Acceleration (S_a). The probability of failure of a bridge or component can be described as the probability that the seismic demand (D) will exceed the capacity (C) of the bridge or component. This is usually written as:

$$P_f = P\left[\frac{C}{D} \le 1\right]$$

When this probability is modeled as a lognormal distribution, the fragility curve can be represented by a lognormal cumulative distribution function as follows:

$$P_f = \Phi\left[\frac{\ln\frac{D}{C}}{\sqrt{\beta_d^2+\beta_c^2}}\right] = \Phi\left[\frac{\ln D - \ln C}{\sqrt{\beta_d^2+\beta_c^2}}\right] \tag{1-2}$$

where D is the median value of the seismic demand in terms of an intensity parameter, C is the median value of the capacity defined for a particular damage state, and the β terms are the logarithmic standard deviations for the demand and capacity distributions. Equation 1-1 can be written in various forms as will be shown in Chapter 5.

Several methods have been researched and used to model the structural demand and capacity. Three common methods used are elastic spectral response, nonlinear static analysis, and nonlinear time-history analysis.

Using the elastic spectral response method to generate fragility curves is one of the simplest available; however, forces and displacements are determined using linear elastic analysis. The applicability of this method decreases with increasing nonlinear behavior that is typically expected from bridge columns exposed to extreme ground motion.

The nonlinear static analysis method is an improvement to the elastic spectral analysis method, and is also called the capacity spectrum method (CSM) or a pushover analysis. With this method, forces are applied to a structural model that can include nonlinear properties such as the yielding of steel members. Although this method attempts to take into account nonlinear behavior and doesn't have the computation overhead of the nonlinear time history (NLTH) method, the CSM should be considered as a coarser approximation when compared to the NLTH method.

The nonlinear time history method is a more reliable method for modeling capacity and demand. However, this approach can be very computationally expensive. The NLTH method was used in this study, and the implementation used will be discussed in more detail in Chapter 5. A basic graphic showing the NLTH method used in this study is included as Figure 1.1.

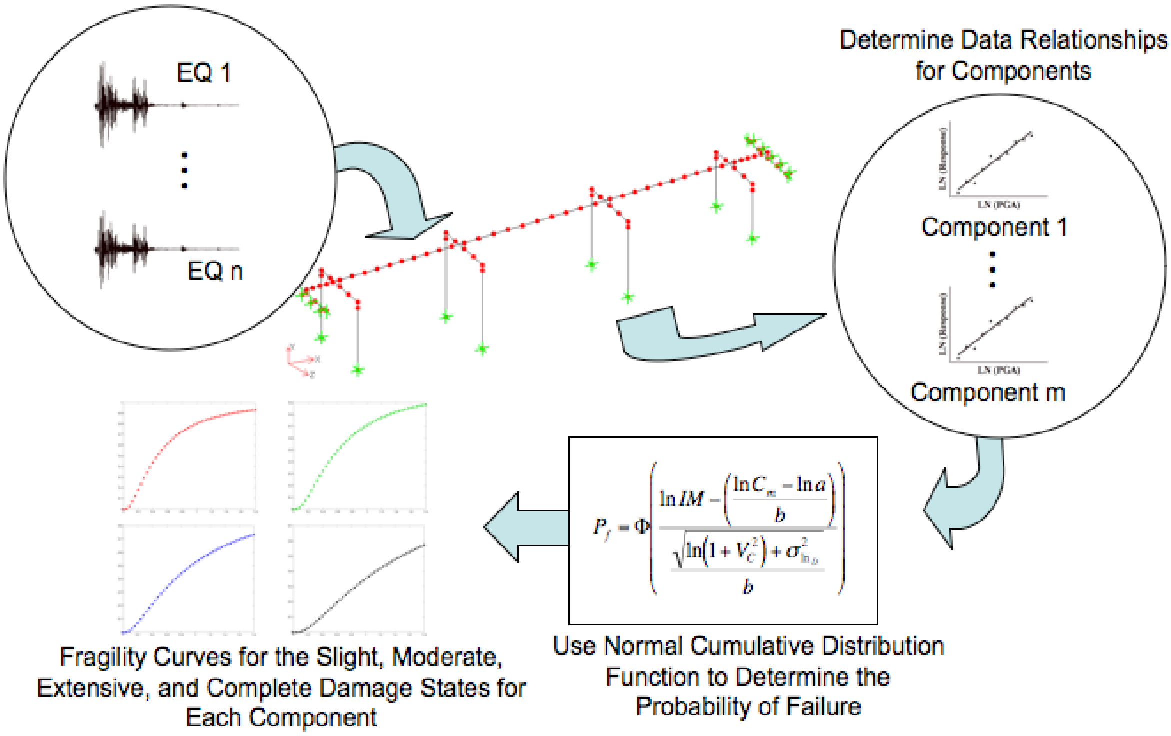
EQ 1
EQ n
Determine Data Relationships for Components
LN (Response)
LN (PGA)
Component 1
Component m
$P_f = \Phi\left(\frac{\ln IM - \left(\frac{\ln C_m - \ln a}{b}\right)}{\frac{\sqrt{\ln\left(1+V_C^2\right)+\sigma_{\ln_D}^2}}{b}}\right)$
Use Normal Cumulative Distribution Function to Determine the Probability of Failure
Fragility Curves for the Slight, Moderate, Extensive, and Complete Damage States for Each Component

Figure 1.1: Analytical Fragility Curve Generation Using Nonlinear Time-History Analysis

2.0 GROUND-MOTION SUMMARY

2.1 HISTORICAL EARTHQUAKES

Geologists have indicated that the question is not if a catastrophic earthquake will occur in Oregon, but when one will occur. Evidence indicates that off the Oregon coast, Cascadia subduction zone earthquakes of magnitude 8.0 or greater have occurred once every 300 to 600 years, most recently in late January of 1700 A.D (Oregon Coastal Management Program, 2007). Shallow crustal earthquakes also routinely occur throughout the western part of the state. One specific year, 1993, saw two notable earthquakes at Scotts Mills (5.6 magnitude) (Ludwin et al., 1996) and Klamath Falls (6.0 magnitude). These earthquakes provided a reminder of Oregon seismicity, with the resulting damage from these events being around $30 million despite the relatively low magnitude.

Referring to the magnitudes published by the United States Geological Survey, as seen in Table 2.1, one of the largest earthquakes in the United States was from the Cascadia subduction zone.

Table 2.1: Selected U.S. Earthquakes of General Historic Interest (USGS, 2009)

No.	Date	Location	Magnitude
1	March 28, 1964	Prince William Sound, Alaska	9.2
2	January 26, 1700	Cascadia Subduction Zone	9.0
3	February 4, 1965	Rat Islands, Alaska	8.7
4	March 9, 1957	Andreanof Islands, Alaska	8.6
5	November 10, 1938	Shumagin Islands, Alaska	8.2
6	April 1, 1946	Unimak Island, Alaska	8.1
7	December 16, 1811	New Madrid Region	8.1
8	September 10, 1899	Yakutat Bay, Alaska	8.0
9	February 7, 1812	New Madrid Region	8.0
10	November 3, 2002	Denali Fault, Alaska	7.9
11	June 10, 1996	Andreanof Islands, Alaska	7.9
12	May 7, 1986	Andreanof Islands, Alaska	7.9
13	September 4, 1899	Cape Yakataga, Alaska	7.9
14	April 3, 1868	Ka'u District, Hawaii	7.9
15	January 9, 1857	Fort Tejon, California	7.9

Evidence has been cited (Heaton et al., 1987) that suggests that the Cascadia subduction zone has characteristics found in other subduction zones that have experienced large shallow earthquakes. Examples are subduction zones in southern Chile, southwestern Japan and Columbia. Although these similarities may lead to the conclusion that there is a potential for large subduction earthquakes in the Cascadia subduction zone, a better state would be if there were direct evidence suggesting that the subduction zone is actually storing elastic energy along with evidence of prehistoric earthquakes. Possible evidence includes the lack of raised Holocene terraces in Oregon and Washington and extensive Holocene turbidites. An assumption could also be made that Cascadia zone earthquakes would resemble earthquakes of zones most similar (i.e., southern Chile, SW Japan and Colombia), and if so, then earthquakes ranging from magnitudes (M_w) 8.1 to 9.5 should be expected, resulting in relatively strong shaking and large and potentially destructive local tsunamis. Also, comparisons (Atwater et al., 1995) can be made between the Cascadia subduction zone and other subduction zones and from geodetic and heat-flow evidence to show that the Cascadia subduction zone is accumulating energy that could be released in future earthquakes.

2.2 PROPOSED GROUND MOTIONS IN THE PACIFIC NORTHWEST

To assess the vulnerability of the civil infrastructure to the associated seismic hazard of the state of Oregon, specific ground-motion time histories representative of the area were needed. Time histories, both naturally occurring and synthetic, produced from a previous study were used.

SAC (SAC, 1997) is a joint venture of the Structural Engineers Association of California (SEAOC), the Applied Technology Council (ATC), and California Universities for Research in Earthquake Engineering (CUREe). The SAC Joint Venture was formed in mid-1994 with the specific goal of investigating the damage to welded steel moment-frame buildings in the 1994 Northridge earthquake, and developing repair techniques and new design approaches to minimize damage to steel moment-frame buildings in future earthquakes. The purpose of Task 5.4.1 of the SAC project was to provide response spectra and time histories for use in case studies and trial applications in the SAC Phase 2 Steel Project. The ground motions from Task 5.4.1 developed for the Seattle area were prepared in two sets, resulting in a ground-motion suite. The first set has a probability of exceedance (POE) of 10% in 50 years, shown in Table 2.2. The second set of motions has a probability of exceedance of 2% in 50 years, shown in Table 2.3. In these tables, two orthogonal horizontal directions are shown for each time history.

Table 2.2: Seattle Ground Motions with POE of 10% in 50 Years (SAC, 1997)

Location	Magnitude	Duration (secs)	PGA Horizontal dir1 (g)	PGA Horizontal dir2 (g)
Long Beach, Vernon CMD Bldg.	6.5	39.08	0.174	0.135
Morgan Hill, 1984, Gilroy	6.2	59.98	0.386	0.662
West. Washington, Olympia, 1949	6.5	79.98	0.383	0.352
West. Washington, Seattle Army B., 1949	6.5	66.68	0.295	0.388
North Palm Springs, 1986	6	59.98	0.587	0.599
Puget Sound, Wa., Olympia, 1949	7.1	81.82	0.752	0.596
Puget Sound, Wa., Federal OFC B., 1949	7.1	74.08	0.369	0.303
Eastern Wa., Tacoma County, 1949	7.1	59.98	0.290	0.574
Llolleo, Chile 1985	8	99.975	0.697	0.670
Vinadel Mar, Chile, 1985	8	99.975	0.541	0.384

Table 2.3: Seattle Ground Motions with POE of 2% in 50 Years (SAC, 1997)

Location	Magnitude	Duration (secs)	PGA Horizontal dir1 (g)	PGA Horizontal dir2 (g)
1992 Mendocino	7.1	59.98	0.755	0.485
1992 Erzincan	6.7	20.775	0.605	0.539
1949 Olympia	6.5	79.98	0.895	0.821
1965 Seattle	7.1	81.82	1.755	1.390
1985 Valpariso	8	99.975	1.636	1.573
1985 Valpariso	8	99.975	1.270	0.901
Deep Interplate (simulation)	7.9	79.98	0.796	0.646

Location	**Magnitude**	**Duration (secs)**	**PGA Horizontal dir1 (g)**	**PGA Horizontal dir2 (g)**
1978 Miyagi-oki	7.4	79.98	0.606	0.783
Shallow Interplate (simulation)	7.9	79.98	0.563	0.534
Shallow Interplate (simulation)	7.9	79.98	0.578	0.749

The distribution of PGA values for the individual suites are shown in Figure 2.1 and Figure 2.2. The values range from a minimum of 0.485 g to a maximum of 1.755 g when using the POE-2%-in-50-years suite and range from a minimum of 0.135 g to a maximum of 0.752 g when using the POE-10%-in-50-years suite.

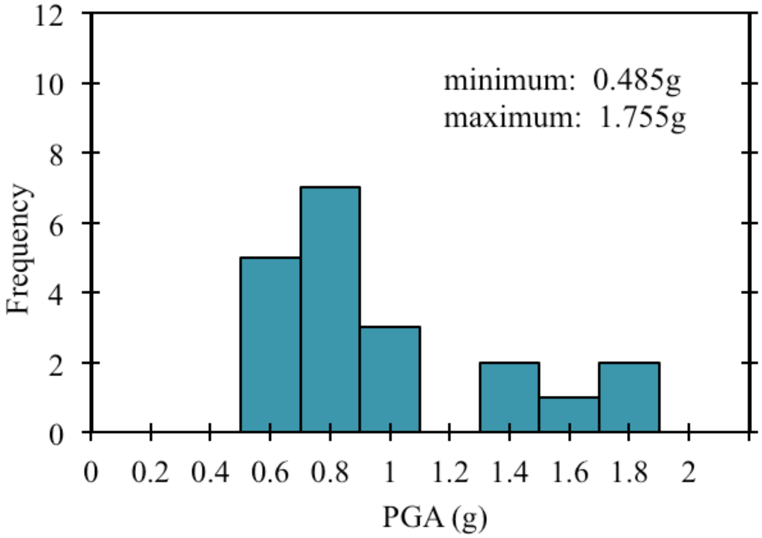

Figure 2.1: Histogram of PGA Values of POE-2%-in-50-Years Suite

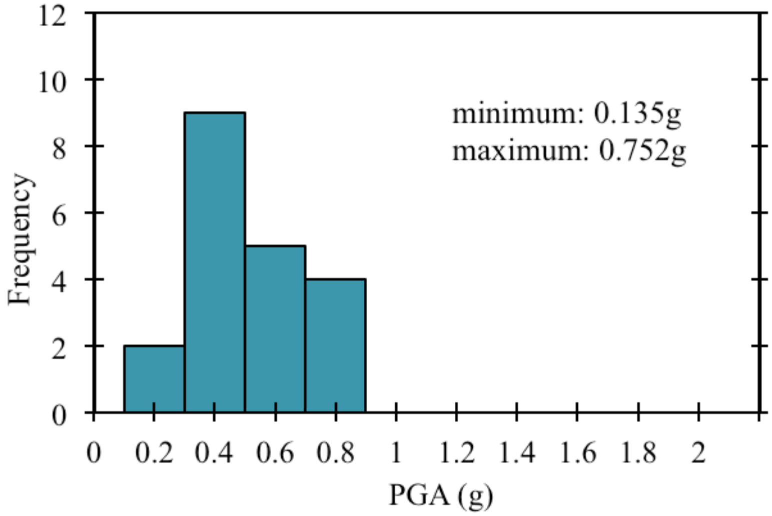

Figure 2.2: Histogram of PGA Values of POE-10%-in-50-Years Suite

As can be seen, the PGA distribution for the 2%-in-50-years suite has some ground motions at the higher end of the distribution in the 1.4 g to 1.8 g range, whereas this high level of acceleration is not seen in the other suite. The distribution of PGA values for both suites combined is shown in Figure 2.3. The suite is skewed to the left, giving emphasis to accelerations less than 1g; however, the PGA values have a considerable range from 0.135 g to 1.755 g.

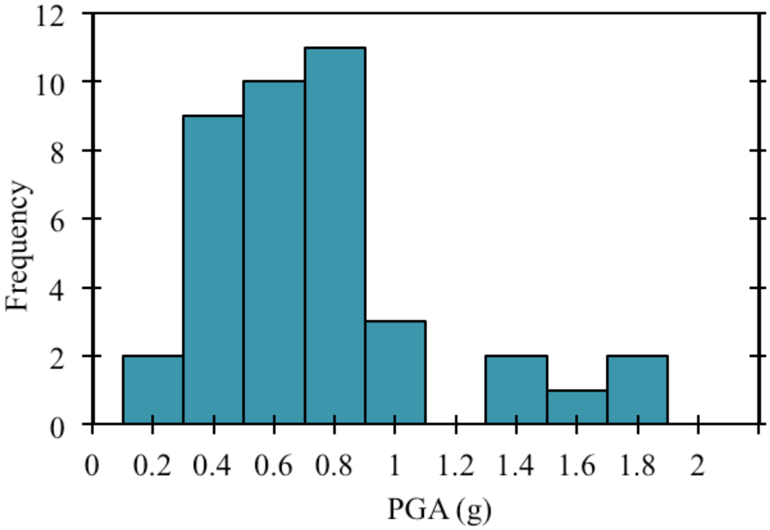

Figure 2.3: Histogram of PGA Values of All SAC Ground-Motion Time Histories Used

This combined suite is in contrast to the earthquake records used by other researchers (Nielson, 2005 and Hwang et al., 2001). For example, the two groups of ground motions used by Nielson have geometric mean PGA values ranging from 0.06 g to 0.66 g and 0.022 g to 0.764 g, with both groups skewed to the left emphasizing the lower accelerations.

In order to predict reasonable responses to the SAC ground-motion suites, the acceleration time histories were integrated resulting in the distance traveled of a simple single degree of freedom (SDOF) system. Using analysis techniques (Chopra, 2007) that rely on a recurrence formulation derived from exact solutions of the equation of motion, the displacement spectrums of the two suites of ground motions were determined and are shown in Figure 2.4 and Figure 2.5.

Two specific periods, with the corresponding ranges of displacement, are noted on the two displacement spectrums. These chosen periods correspond to specific mode shapes of vibration for specific models. The mode shapes, and the model variations considered in this study, are discussed in detail in Chapter 4.

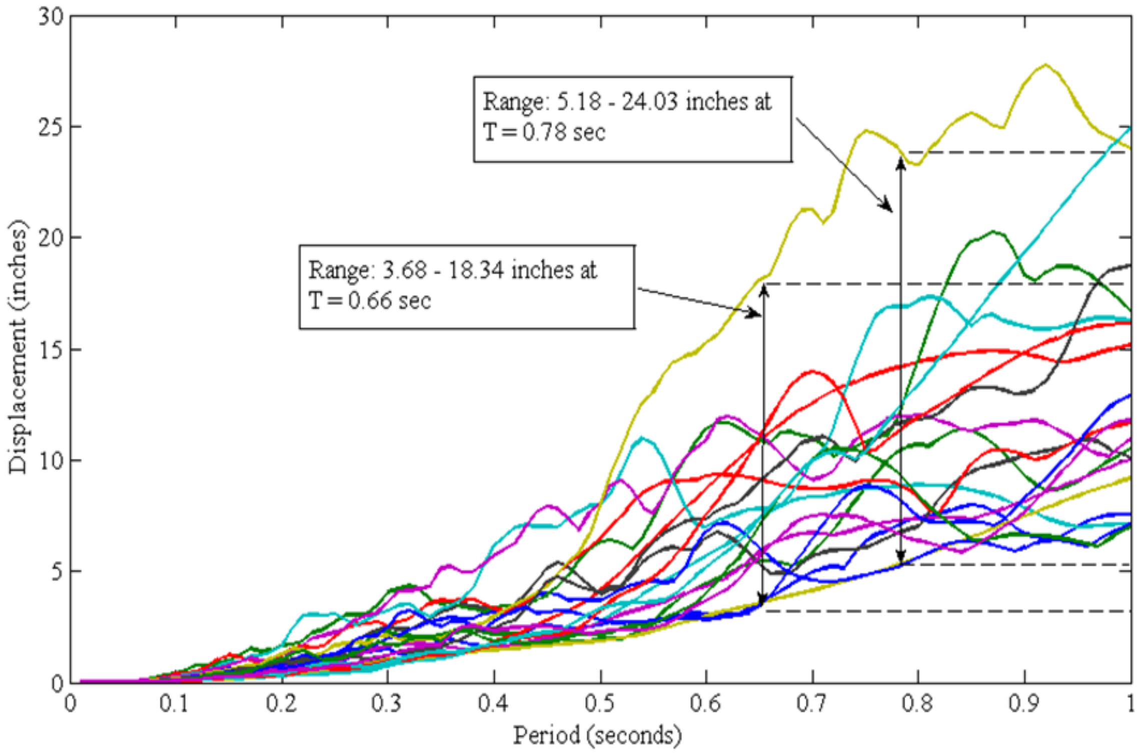

Figure 2.4: Displacement Spectrum (5% damping) – POE-2%-in-50-Years Suite

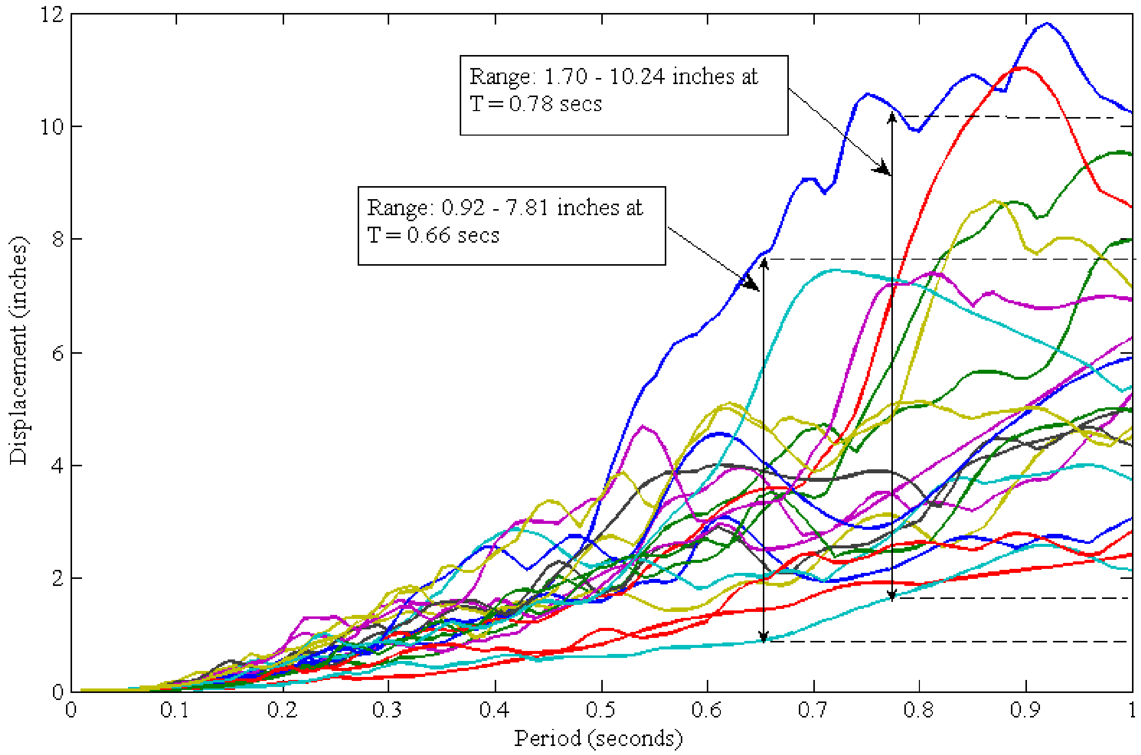

Figure 2.5: Displacement Spectrum (5% damping) – POE-10%-in-50-Years Suite

Referring to the 2% exceedance displacement spectrum (Figure 2.3), for a SDOF structure with a fundamental period of T=0.66 secs, the maximum expected displacement should be around 18 inches. Referring to the 10% exceedance displacement spectrum (Figure 2.2), for a SDOF structure with a fundamental period of T=0.66 secs, the maximum expected displacement should be around eight inches. The maximum displacement from the 2% exceedance portion of the ground-motion suite is significantly larger than that expected from the 10% exceedance portion, which should be expected since the maximum PGA values are significantly larger with the maximum PGA value of almost 1.8g. These expected displacement values will be compared to the displacements found using the OpenSees (Open System for Earthquake Engineering Simulation 2010) models in Chapter 4. Both of the ground-motion suites described in this section were used in the modeling process unless otherwise noted.

The pseudo-acceleration spectrums for the SDOF structure using the two suites were determined using:

$$A = \left(\frac{2\pi}{T}\right)^2 D \left(\frac{1g}{386.4\frac{in}{sec^2}}\right) \qquad \textbf{(2-1)}$$

where A is the pseudo-acceleration of the system, T is the period of vibration and D is the displacement from Figure 2.4 and Figure 2.5. The pseudo-acceleration spectrums for the two suites are shown in Figure 2.6 and Figure 2.7.

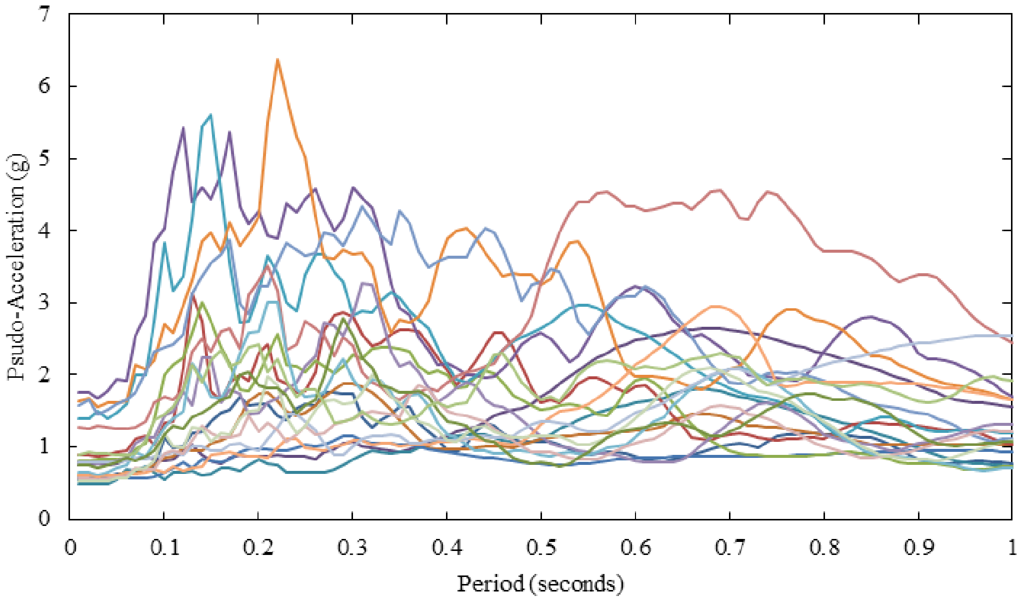

Figure 2.6: Pseudo-Acceleration Spectrum (5% damping) – POE-2%-in-50-Years Suite

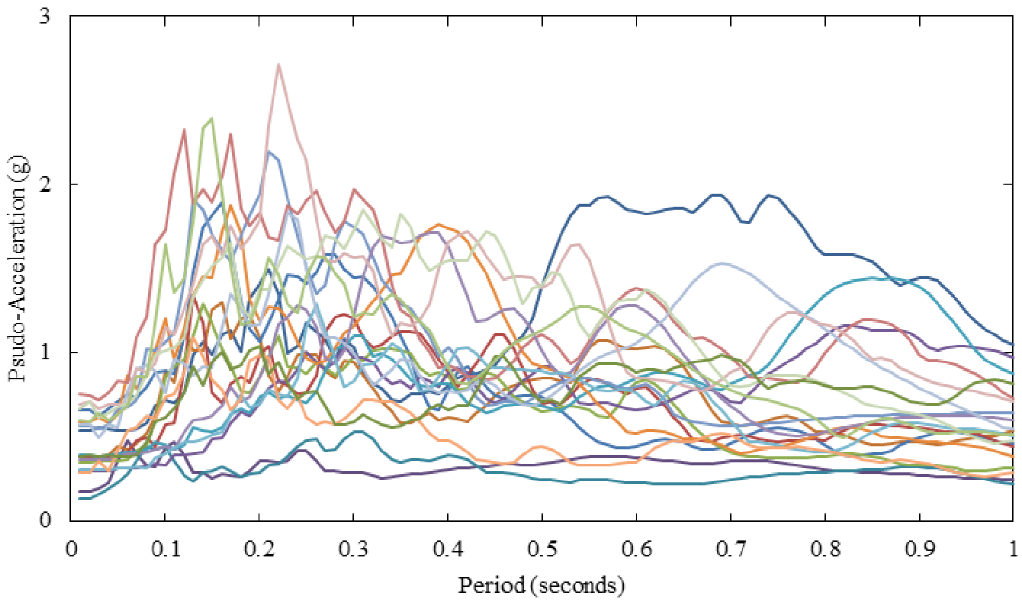

Figure 2.7: Pseudo-Acceleration Spectrum (5% damping) – POE-10%-in-50-Years Suite

When using the POE-2%-in-50-years suite with a SDOF system, Figure 2.6 shows the higher pseudo-accelerations occur when the period of the system is between around 0.1 and 0.3 seconds with a maximum value of 6.4 g at 0.22 seconds. In this range the maximum equivalent static force on the SDOF would be expected to occur, resulting in the maximum moment at the base support.

When using the POE-10%-in-50-years suite with a SDOF system, Figure 2.7 shows the higher pseudo-accelerations again occur when the period of the system is between around 0.1 and 0.3 seconds with a maximum value of 2.7 g at 0.22 seconds. In this range the maximum equivalent static force on the SDOF would be expected to occur, resulting in the maximum moment at the base support.

3.0 BRIDGE INVENTORY

3.1 NATIONAL BRIDGE INVENTORY

In 1967, there was a sudden collapse of the Silver Bridge, a pin-connected link suspension bridge over the Ohio River at Point Pleasant, WV, with the loss of 46 lives. As a result, the Federal Highway Act of 1968 initiated a national bridge inspection program that recognized the need for periodic and consistent bridge inspections. A direct result was the initiation of the National Bridge Inspection Standards (NBIS) in 1971. These standards currently require that every bridge on public roads be inspected at least every two years (FHWA, 2004).

To facilitate the inspection process, a coding guide (FHWA, 1995) was prepared for use by inspection authorities in recording and coding the information that make up the National Bridge Inventory (NBI) database. This study made use of the coding guide and the NBI in order to obtain dimensional information about Oregon bridges, such as longest span length and structure width. When using the NBI, care should be taken to use the proper units as specified by the coding guide.

3.2 DETERMINATION OF TYPICAL THREE-SPAN BRIDGE

NBI database data were manipulated so that only three-span structures that meet the criteria given in Table 3.1 were considered.

Table 3.1: NBI Database Search Criteria

NBI Item	Value
5C	Designated Level of Service = 1 (Mainline)
7	Facility Carried By Structure = I-5, I-84, I-205, OR-99W, US-26, and US-30
27	Year Built ≤ 1969

The resulting list of bridges was then sorted according to NBI Items No. 43A and 43B. Item No. 43A provides the kind of material/design used for the structure, and item No. 43B provides the type of construction used on the structure.

The quantity and percentage of Oregon bridges carrying I-5 for several materials and construction methods used are shown in Table 3.2 and Table 3.3.

Table 3.2: NBI Item 43A - Kind of Material/Design Used on Oregon Bridges on Chosen Highways

NBI Code	Description	Quantity	Percentage
1	Concrete	8	3.0
2	Concrete Continuous	193	73.1
3	Steel	4	1.5
4	Steel Continuous	19	7.2

NBI Code	Description	Quantity	Percentage
5	Pre-Stressed Concrete	37	14.0
6	Pre-Stressed Concrete Continuous	1	0.4
7	Timber	2	0.8

Table 3.3: NBI Item 43B - Type of Design/Construction Used on Oregon Bridges on Chosen Highways

NBI Code	Description	Quantity	Percentage
01	Slab	42	22.5
02	Stringer/Multi-beam or Girder	124	66.3
03	Girder and Floorbeam System	2	1.1
05	Box Beam or Girders - Multiple	19	10.2

The continuous concrete bridge, with over 73%, was found to be the most common bridge type along the defined Oregon highways. The most common construction type was then found to be multi-beam or girder, with over 66% of the bridges using this construction type.

To determine the dimensions of the three-span model bridge, the average and standard deviation values for bridge width and longest span were calculated from Oregon three-span bridges along the defined Oregon highways. Table 3.4 shows that the average three-span bridge has an average deck width of almost 58 feet, and the longest span has an average length of slightly over 58 feet.

Table 3.4: Statistics of Three-Span NBI Code 202 Oregon Bridges on Chosen Highways

Dimension	Average (ft)	Std Deviation (ft)
Width	57.3	23.7
Longest Span (S2)	50.7	15.0
Overall Length	126.8	42.6

The three-span bridge 07865A, having dimensions close to these average values, was chosen from the NBI database to be a typical three-span bridge. Table 3.5 gives the dimensions for the typical three-span bridge that was modeled, and an elevation view is shown in Figure 3.1.

Table 3.5: Bridge Used In Three-Span Study (Oregon Bridge 07865A East)

Dimension	Value (ft)
Width	33.3
Main Span (S2) Length	48.0
Secondary Span (S1/S3) Length	36.0
Total Structure Length	120.0

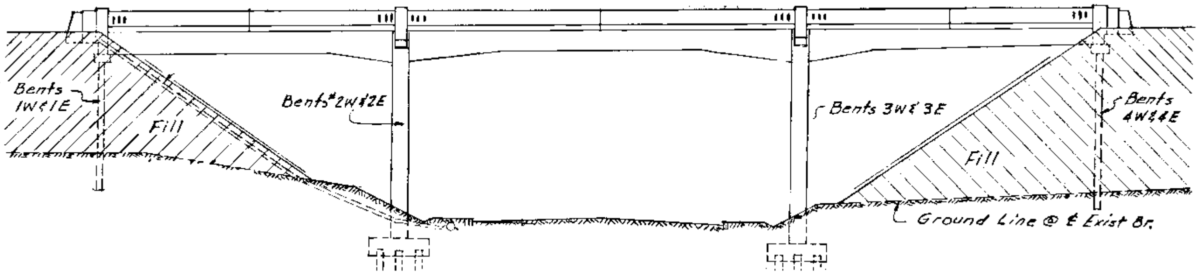

Figure 3.1: Elevation View of Oregon Bridge 07865A (Taylor Street East, Lane County)

3.3 DETERMINATION OF TYPICAL FIVE-SPAN BRIDGE

A similar methodology was used to determine which five-span bridges would be included in the study. The same set of highways was considered when gathering data from the NBI database: I-5, I-84, I-205, OR-99W, US-26, and US-30 highways. Table 3.6 through Table 3.10 provide data for five-span bridges from these highways.

Table 3.6: Kind of Material/Design Used on Five-Span Oregon Bridges on Chosen Highways

Segment 43A NBI Code	Description	Quantity	Percentage
2	Concrete Continuous	46	59.7
3	Steel	6	7.8
4	Steel Continuous	5	6.5
5	Pre-Stressed Concrete	11	14.3
6	Pre-Stressed Concrete Continuous	4	5.2
7	Timber	5	6.5

Table 3.7: Type of Design/Construction on Five-Span Oregon Bridges on Chosen Highways

Segment 43B NBI Code	Description	Quantity	Percentage
01	Slab	1	1.3
02	Stringer/Multi-beam or Girder	65	84.4
05	Box Beam or Girders - Multiple	5	6.5
06	Box Beam or Girders - Single or Spread	1	1.3
07	Frame	2	2.6
09	Truss - Deck	2	2.6
11	Arch - Deck	1	1.3

The continuous concrete bridge, with almost 60%, was found to be the most common five-span bridge type along the chosen highways in Oregon. The most common construction type is multi-beam or girder, with over 84% of the bridges using this construction type.

When considering only continuous concrete designed bridges, most of the bridges of this design are girder type, as shown in Table 3.8.

Table 3.8: Majority of Bridge Types on Oregon Bridges on Chosen Highways

Segment 43 (43A+43B) NBI Code	Description	Quantity	Percentage
202	Concrete Continuous - String/Multi-beam or Girder	42	54.5
502	Prestressed Concrete - Stringer/Multi-beam or Girder	11	14.3

702	Timber - Stringer/Multi-beam or Girder	5	6.5

To determine the dimensions of the five-span model bridge, the average and standard deviation values for bridge width and longest span were used from Oregon five-span bridges along the chosen highways. Table 3.9 shows that the average five-span bridge has an average deck width of almost 37 feet, and an average structure length of slightly over 246 feet.

Table 3.9: Statistics of Five-Span NBI Code 202 Oregon Bridges on Chosen Highways

Dimension	Average (ft)	Std Deviation (ft)
Width	40.5	16.2
Longest Span	62.2	11.8
Total Structure Length	246.1	38.1

The five-span bridge 07628, having a span and overall length dimensions within one standard deviation, was chosen from the NBI database to be the typical five-span bridge. Bridge 07628 has a webwall that wasn't modeled. This can be justified since there is another Oregon bridge (07628A) that has similar dimensions and characteristics, but wasn't designed with the webwall. Table 3.10 gives the dimensions for the typical five-span bridge that was modeled, and an elevation view is shown in Figure 3.2.

Table 3.10: Bridge Used In Five-Span Study (Oregon Bridge 07628)

Dimension	Value (ft)
Width	35.1
Main Span (S3) Length	69.9
Secondary Span (S2/S4) Length	60.0
Total Structure Length	222.1

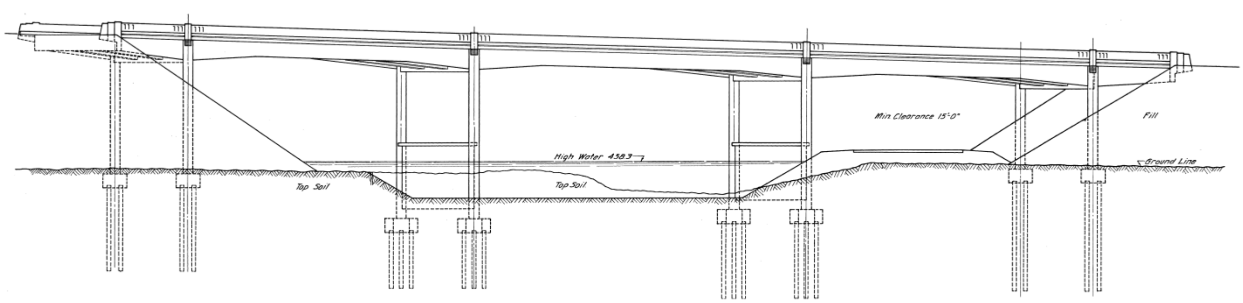

Figure 3.2: Elevation View of Oregon Bridge 07628 (Sutherlin Creek, Douglas County)

4.0 THREE-DIMENSIONAL MODELS OF TYPICAL BRIDGES

The method used to generate fragility curves in this study relies on analytical models of the structures being considered. The modeling process can become very complicated and cumbersome, leading to the necessity of simplifying assumptions. For example, the choice of modeling in two dimensions or three dimensions can greatly impact the modeling process. However, choosing if the longitudinal direction or transverse direction controls the response of the structure can be difficult to determine. By minimizing these assumptions and modeling three dimensionally, the dominant direction will be accounted for, in addition to possible combination of the responses in the two directions.

The highway bridges being considered are of a continuous concrete design with integral bent caps and two columns per bent. The bridges all are constructed using a series of typical bridge components. The first component is the superstructure made up of girders/beams supporting the deck and wearing surface. Any parapets used could also be included with the superstructure. The superstructure in the modeling process was consolidated into an aggregate, and will be referred to as the deck. The components of a typical bridge are shown in Figure 4.1. The second primary set of components is used to support the superstructure and include the abutments and bents (columns and bent caps). As mentioned previously, the bridges being modeled all have integral bent caps.

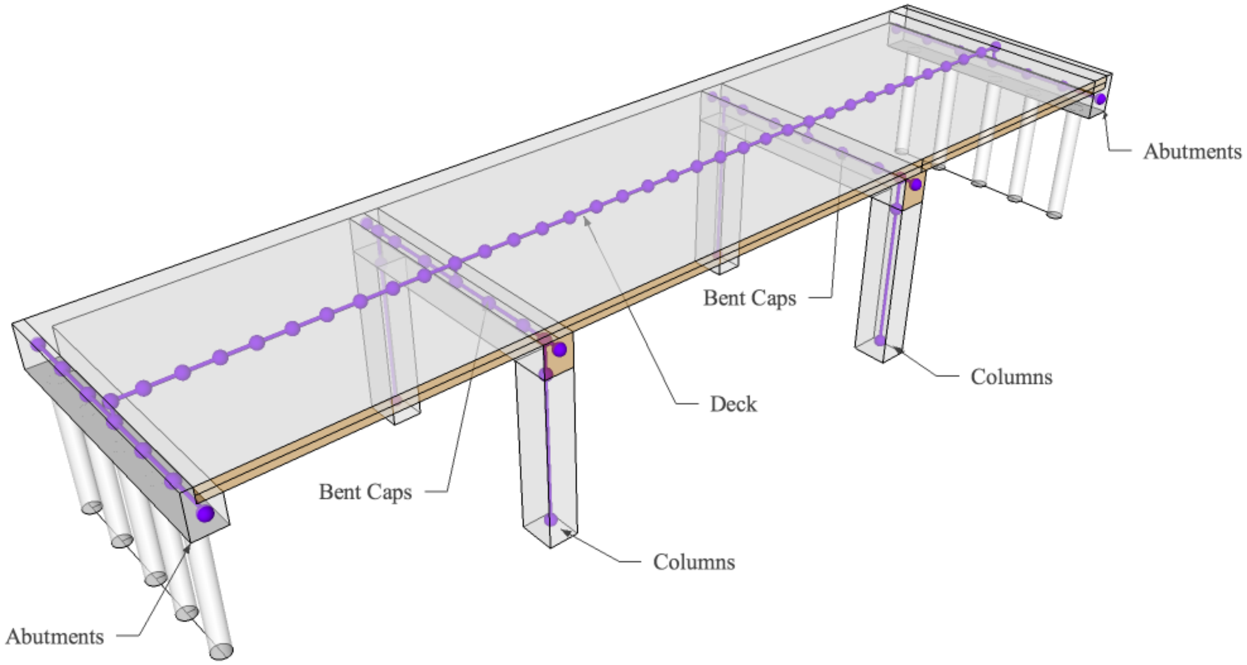

Figure 4.1: Typical Bridge Model

In the following sections, the analytical models for the two types of bridges will be presented. Nonlinearities were taken into account when modeling some of the bridge components. Five percent Rayleigh damping was used in all models, and was calculated using the first mode as calculated by the eigenvalue analysis.

Examples of the seismic loads being considered are two ground-motion records showing two extremes of the PGA spectrum. The first, with a peak PGA of 0.135 g and a probability of exceedance of 10%, was recorded at Long Beach, CA (SAC, 2010) and is shown in Figure 4.2. The time-history analyses conducted using records from the POE-of-10% group used a time step of five milliseconds in the OpenSees model.

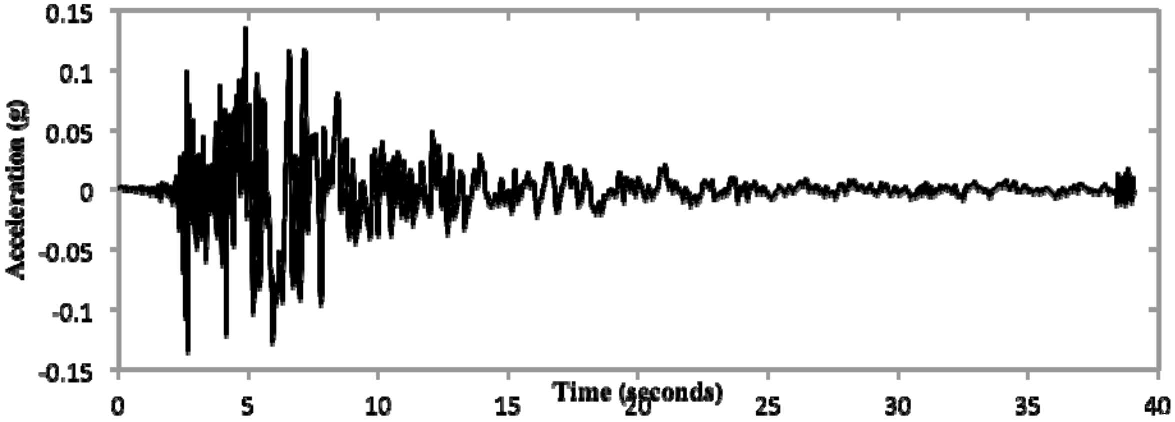

Figure 4.2: Ground-Motion Sample from POE-of-10% Group

The second ground-motion record, with a peak PGA of 1.637 g and a probability of exceedance of 2%, was recorded at Valparaiso, Chile, in 1985 (SAC, 2010) and is shown in Figure 4.3. This record also has a much longer duration, at almost 100 seconds.

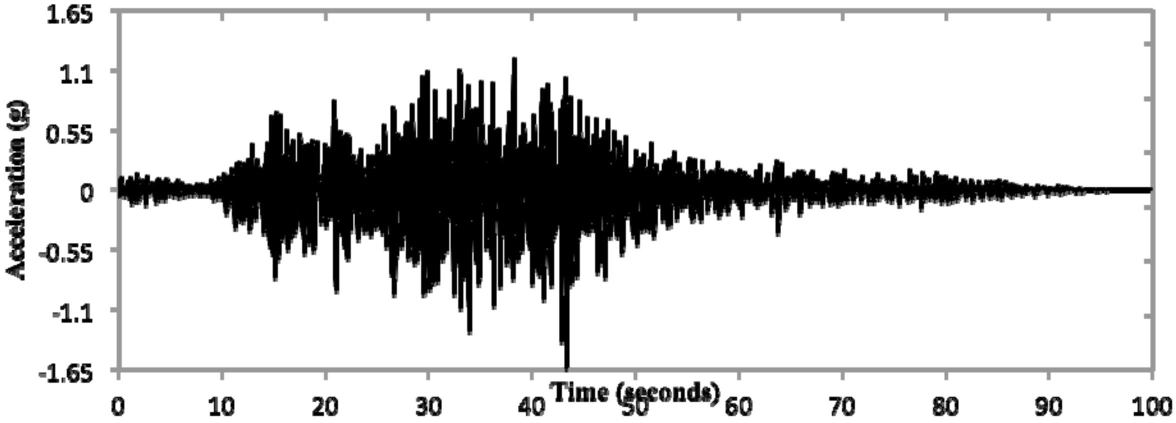

Figure 4.3: Ground-Motion Sample from POE-of-2% Group

The time-history analyses conducted using records from the POE-of-10% group started with a time step of two milliseconds. This time step was reduced as necessary in order to accommodate numerical convergence problems. Having the script used by OpenSees to automatically change the time step, in addition to the specific numerical method used for a given time step, was found to be the most convenient.

4.1 TYPICAL THREE-SPAN BRIDGE

4.1.1 BRIDGE LAYOUT

Oregon Bridge 07865A East was used as the template for the typical three-span bridge to be used in this study, and an elevation view is shown in Figure 3.1. This bridge has three spans that are 36, 48 and 36 feet long, for a total structure length of 120 feet, with the width of each span being almost 34 feet. This bridge has a continuous concrete deck with the bents being integral. The heights of the four columns range from 19.8 feet to 22.0 feet.

The dual-column bent caps for this bridge are made up of a 16-inch-wide-by-60-inch-deep reinforced concrete bent beam supported by two 24-inch-by-24-inch rectangular reinforced concrete columns. The bent beam uses three #10 bars at the top and a combination of three #9 and three #10 bars at the bottom of the beam. The reinforcement details are shown in Figure 4.4. The abutments used with this bridge are seat type abutments with pile supports. From the bridge plans, the abutments were assumed to use a 3.5-foot-high back wall, combined with seven piles.

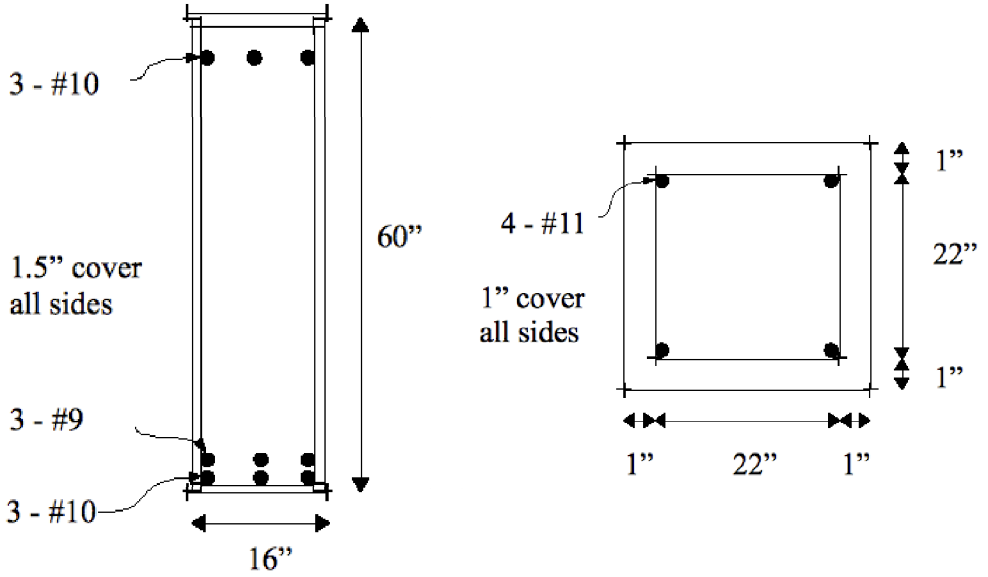

(a) Bents 2 / 3 (b) Columns

Figure 4.4: Concrete Member Reinforcement for Three-Span Bridge

4.1.2 OPENSEES MODEL

The typical three-span bridge was modeled using the OpenSees application. In order to take into account nonlinearities, several different element types were used when modeling some of the bridge components. An overview of the element and material types are shown in Table 4.1.

Table 4.1: Element Types Used With Three-Span Model

Component	Material	Element
Abutments (Bents 1/4)	Elastic properties	elasticBeamColumn
Soil Interaction	ElasticPPGap	zeroLength
Deck	Elastic properties	elasticBeamColumn
Bent Caps (Bents 2/3)	FiberSection, Concrete01, Hysteretic Steel	dispBeamColumn
Columns	FiberSection, Concrete01, Concrete04, Hysteretic Steel	beamWithHinges

The abutment-soil interaction was modeled as a combination of linear springs. The OpenSees zeroLength element was used in order to have only axial forces being applied to the abutment from the soil, with no bending. The ElasticPPGap material was used to allow the use of compressive loads only, and also to allow an initial gap to be present between the deck and the abutment. The material values used to define the gap material were derived from accepted design guidelines (Caltrans, 2006) and are provided in Table 4.2.

Table 4.2: ElasticPPGap Material Values for Three-Span Abutment-Soil Model

Description	Value
Stiffness of transverse spring	381.8 kips/in
Maximum compressive strength of transverse spring	-334.1 kips
Initial gap of transverse spring	-0.50 in
Total stiffness of longitudinal springs	381.8 kips/in
Total maximum compressive strength of longitudinal springs	-334.1 kips
Initial gap of longitudinal spring	-0.75 in

The superstructure deck was assumed to be level with no skew relative to the abutment. The column base locations were moved slightly vertically to maintain appropriate column heights and a level deck. The deck was assumed to behave elastically and therefore was modeled using the elasticBeamColumn element. The element was defined using the values found in Table 4.3.

Table 4.3: Element Values for Three-Span Deck

Description	Value
Cross Sectional Area	4436.25 in2
Elastic Modulus (E)	3733.4 ksi
Shear Modulus (G)	1500.0 ksi
Torsional Moment of Inertia (J)	61.509×10^6 in^4
Second Moment of Area about the local y Axis (I_y)	6.3344×10^7 in^4
Second Moment of Area about the local z Axis (I_z)	4.2778×10^5 in^4

Concrete and steel OpenSees material types were used to model the reinforced concrete portions of the bridges. The Concrete01 material accounts for compression of the concrete, but doesn't allow for any tension load and was used for the cover concrete. The Concrete04 material was used for the confined concrete since the material will predict the crushing strength as a function of the crushing strain using the Mander model. The columns were modeled using both Concrete01 and Concrete04 materials, while the bent caps only used the Concrete01 material. In order to prevent bending of the bent caps in the model about the global vertical axis, another element was introduced with large EI values that restricted bending only about the vertical axis. This approximates the behavior of the bent cap being integral to the superstructure.

The hysteretic material was used to model the reinforcement steel of all reinforced concrete members. The general behavior provided by these OpenSees material types is shown in Figure 4.5. When possible, material property values were found from Oregon Department of Transportation (ODOT) drawings of the bridges used in this study, such as maximum compressive strength of the concrete and yielding stress of the reinforcing steel. To model the stress-strain relationship of the column-confined concrete of the columns, an analytical model (Mander et al., 1988) was used. The specific values used to define the materials are given in tables Table 4.4 through Table 4.6.

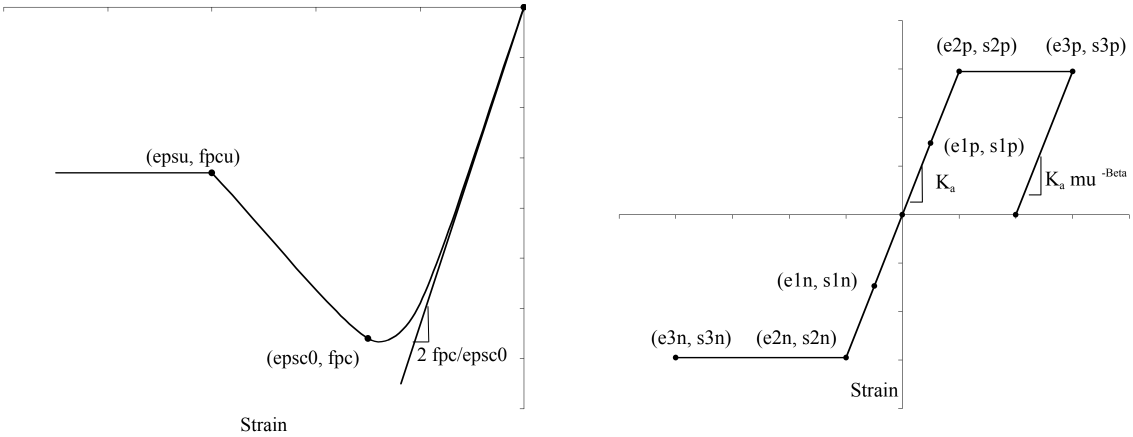

(a) General Concrete01 Material

(b) General Hysteretic Material

Figure 4.5: OpenSees Material Types Used In Reinforced Concrete Models (from OpenSees 2009)

Table 4.4: Concrete04 Values for Confined Concrete Used With Three-Span Bridge

Property	Description	Value
fpc	maximum concrete compressive strength	-4.464 ksi
epsc0	concrete strain at maximum strength	-0.002433 in./in.
epsU	concrete strain at crushing strength	-0.010 in./in.
	Elastic modulus of concrete	3733.4 ksi
	ratio of confined concrete strength to unconfined strength	1.04

Table 4.5: Concrete01 Values for Cover Concrete Used With Three-Span Bridge

Property	**Description**	**Value**
fpc	maximum concrete compressive strength	-4.29 ksi
epsc0	concrete strain at maximum strength	-0.002023 in./in.
fpcu	concrete crushing strength	0.0 ksi
epsU	concrete strain at crushing strength (AASHTO, 2009)	-0.005 in./in.

Table 4.6: Hysteretic Steel Values Used with Five-Span Bridge

Property	**Description**	**Value**
s2p	stress at second point of the envelope in the positive direction (yield stress)	40 ksi
e2p	strain at second point of the envelope in the positive direction (yield strain)	0.0013793
s3p	stress at third point of the envelope in the positive direction	40 ksi
e3p	strain at third point of the envelope in the positive direction	0.20

There was a small increase (4 %) when comparing the confined strength to the unconfined strength of the concrete. These values are a result of the Mander model, and are fully expected since the level of transverse reinforcement for the columns is relatively poor, with the #4 transverse bars spaced at 12 inches. This spacing is in contrast to transverse spacing using current design guidelines, which can be in the range of three to four inches.

The hysteretic material used to model the steel in the columns has the ability to use pinching factors and to model damage due to energy and ductility. The default values provided by OpenSees were used in this case. The typical bridge, modeled using OpenSees, is shown in Figure 4.6.

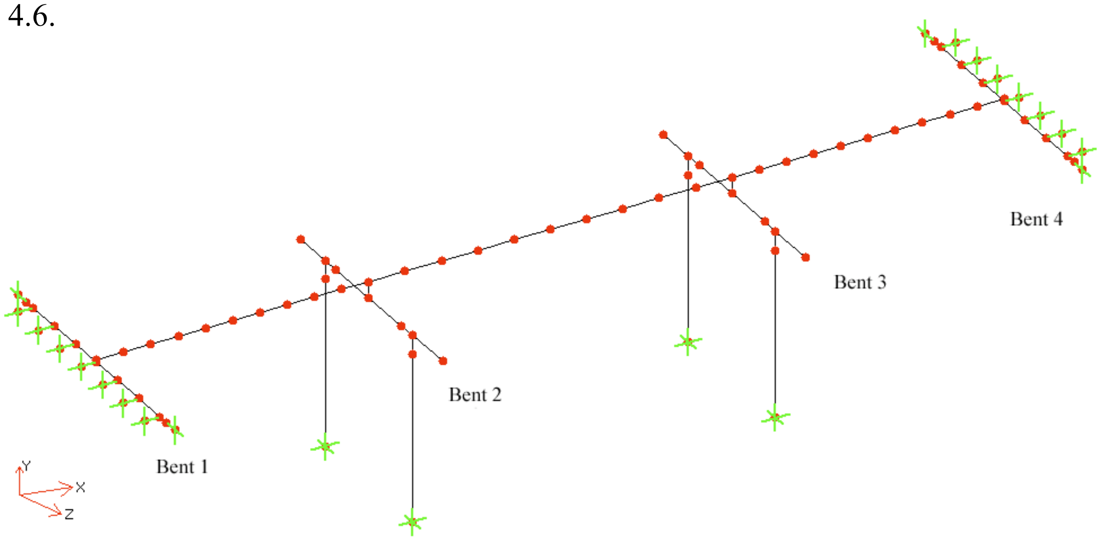

Figure 4.6: OpenSees Model for Three-Span Bridge

The boundary conditions applied to the OpenSees model, as indicated in Figure 4.6, are described in Table 4.7. The nodes representing the soil portion of the soil-abutment connection were fixed except to allow movement with the abutment in the direction normal to the connection. For example, the longitudinal soil node was allowed to move in the transverse direction to ensure the soil nodes and bent nodes were always aligned. This resulted in a normal force being applied to the bent, with no load due to soil friction being modeled.

Table 4.7: OpenSees Boundary Conditions for Three-Span Bridge

Model Element	Boundary Condition
Column Bases	Fixed in all directions
Bents 1/4	Fixed in vertical direction
Longitudinal Soil-Abutment Connections	Base of element (soil) fixed in all directions except transverse; tied to move with Bent 1 in transverse direction
Transverse Soil-Abutment Connections	Base of element (soil) fixed in all directions except longitudinal; tied to move with Bent 1 in longitudinal direction
All nodes fixed in the transverse and longitudinal directions	Ground motions were applied to these nodes

4.1.2.1 MODEL VERIFICATION

In order to verify the proper usage of these concrete and hysteretic material types, several simple verification tests were used. The first verification test was performed by making an OpenSees model of a fixed-base RC column and subjecting it to a lateral force at the top of the column. The modeled column was identical to a column from the typical three-span bridge column, with the base being fixed and the top being free with no restraints. The column was subjected to a concentric axial load of 150 kips. While the column was being loaded by a lateral force, the overturning moment at the base was being recorded. The moment from the OpenSees model was determined to be 3727.6 kip/inch when the reinforcing steel being loaded in tension was just starting to yield. The same scenario was then considered, but using standard analytical techniques. The following equations were used:

$$a = \frac{P}{0.85 f'_c b} \qquad \textbf{(4-1)}$$

$$M = 0.85 f'_c ab(\bar{y} - \frac{a}{2}) + A'_s f_y (d - d') \qquad \textbf{(4-2)}$$

where a is the depth of the equivalent rectangular stress block, P is the axial load, f'_c is the compressive strength of the concrete, M is the overturning moment, b is the width of the column, d is the depth of the beam measured from the extreme compression fiber to the centroid of the steel area in tension, and d′ is the distance from the extreme compression fiber to the centroid of the steel area in compression.

When equations 4-1 and 4-2 are solved, the overturning moment, M, is found to be 3866.7 kip/inch. Comparing the two estimates of the overturning moment shows a 3.6 % difference between the analytical and numerical methods.

The second test involved modeling a simple reinforced concrete column using information from the National Science Foundation Pacific Earthquake Engineering Research Center (PEER, 2009) structural performance database. Using the design data of the nosh96n1 square column, an OpenSees model was constructed and subjected to a cyclic load. This particular column was the smallest column available in the database, and closest to the actual column size of the modeled three-span bridge. The experimental column and OpenSees model had the following characteristics:

0.625 in long. bars (#5), qty (4)	0.25 in. bars transverse reinforcement
1 inch cover, 11 in x 11 in column	9 inch transverse spacing

A comparison of the experimental test results and the numerical OpenSees model is shown in Figure 4.7. Based upon this comparison, an argument could easily be made that the OpenSees model is a reasonable representation of the column and, therefore, similar efforts to model bridge columns should yield reasonable models.

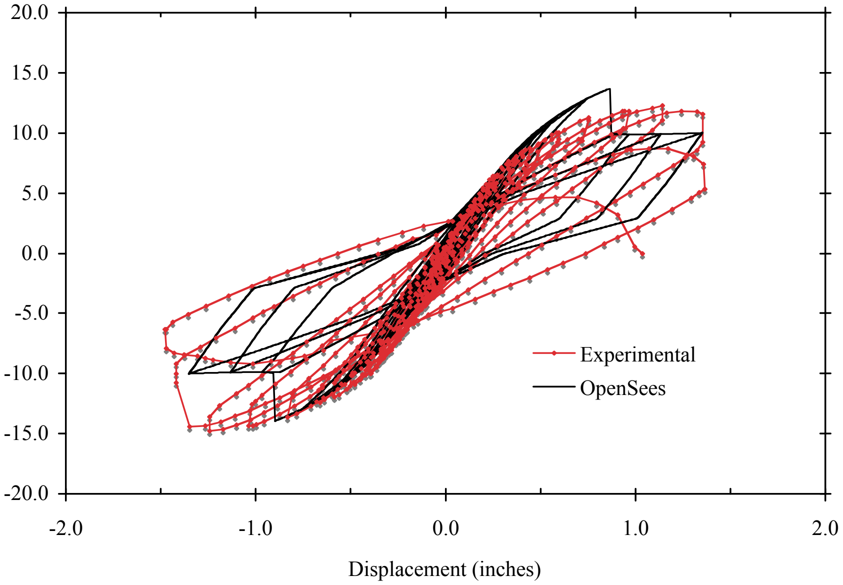

Figure 4.7: Comparison of Experimental and Modeled Hysteretic Behavior of Test Column

The OpenSees model for the test column used an assumed value of 1.05 for the ratio of confined concrete strength to unconfined strength.

Another simple, but effective, method of model verification is to ensure that the period of vibration predicted by the OpenSees model is reasonably close to the period of a simple, single degree of freedom system having the same mass and stiffness. The values used in this calculation were: E = 3733 ksi, I_{col} = 27,648 in^4 and weight of superstructure = 708.7 kips (mass = 708.7/386.4 = 1.834 kips-sec^2/in.). The stiffness of a fixed-fixed column was idealized to be $k_{col} = \frac{12EI}{L^3}$. The stiffness associated with two columns for each bent was calculated and are shown in Table 4.8

Table 4.8: Estimated Stiffness Values for Three-Span Bridge

Location	Bent Stiffness (kips/in)
Bent 2	143.6
Bent 3	174.3
Total	317.9

The period of vibration can be calculated for the three-span bridge, in both the transverse and longitudinal directions, and with the soil-abutment interaction included and not included. As an example, for the case where the soil-abutment stiffness is not included, and for the longitudinal direction, the period of a simple SDOF system can be calculated to be:

$$T = 2\pi\sqrt{\frac{m}{k}} = 2\pi\sqrt{\frac{1.834\,\frac{kips \cdot \sec^2}{in}}{317.9\,\frac{kips}{in}}} = 0.477 \text{ seconds}$$

Similar calculations yield the data shown below in Table 4.9 for both directions of displacement.

Table 4.9: Calculated Periods of Vibration for Various Three-Span Bridge Models

Periods (seconds)	Soil-Abutment Stiffness Included	Soil-Abutment Stiffness Not Included
Longitudinal	0.322	0.477
Transverse	0.322	0.477

The periods are identical for the three-span bridge for both directions since the abutment stiffness is the same in both directions, and the stiffness for the columns are also the same in both directions. Using the OpenSees model with the soil-abutment stiffness included, the period of vibration with a longitudinal motion was found to be 0.262 seconds. With the soil-abutment stiffness removed, the period of vibration with a longitudinal motion was found to be 0.484 seconds. The calculated approximations agree relatively well with the OpenSees numerical model.

4.1.3 MODEL RESPONSE

Using the provided dimensions from ODOT drawings and OpenSees material and element types, a numerical model was constructed with the geometry shown in Figure 4.6. Ground motions were applied to the soil nodes of the soil-abutment connections and to the bases of the columns. An eigenvalue analysis of this model, using OpenSees, has a fundamental period of 0.76 seconds with the associated motion being a twisting motion around the center of the structure. Mode shapes for the three-span bridge, and with no soil-abutment stiffness included, are shown in Figure 4.8. The second mode has a period of 0.66 seconds and the third mode has a period of 0.48 seconds and has a longitudinal motion, with good agreement with the simple SDOF system described in the previous section.

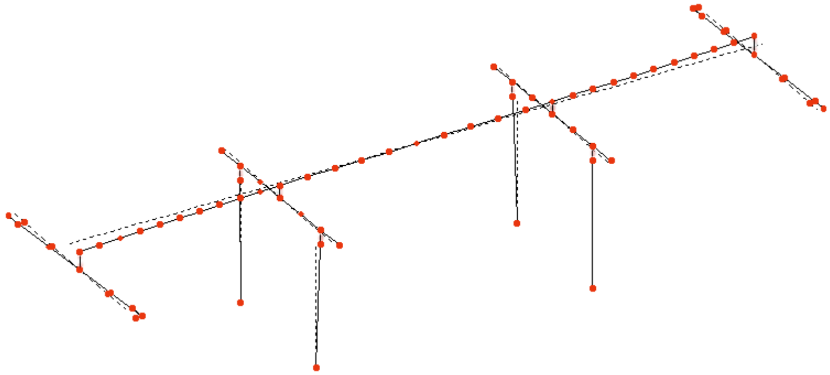

(a) Mode 1 with period of 0.76 seconds (rotating motion near the bridge center)

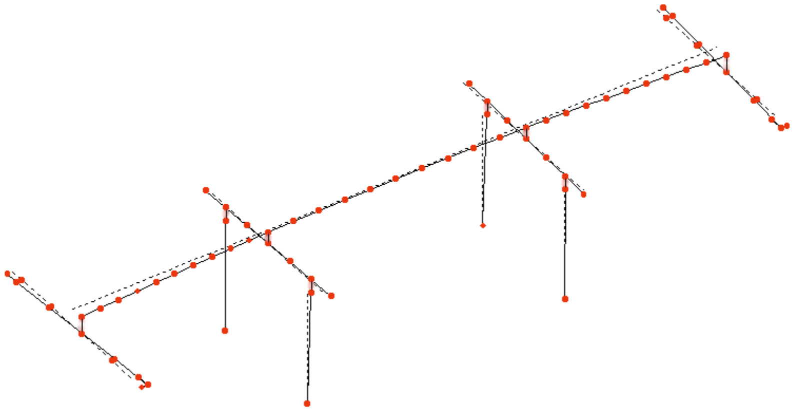

(b) Mode 2 with period of 0.66 seconds (bowing motion about bridge center)

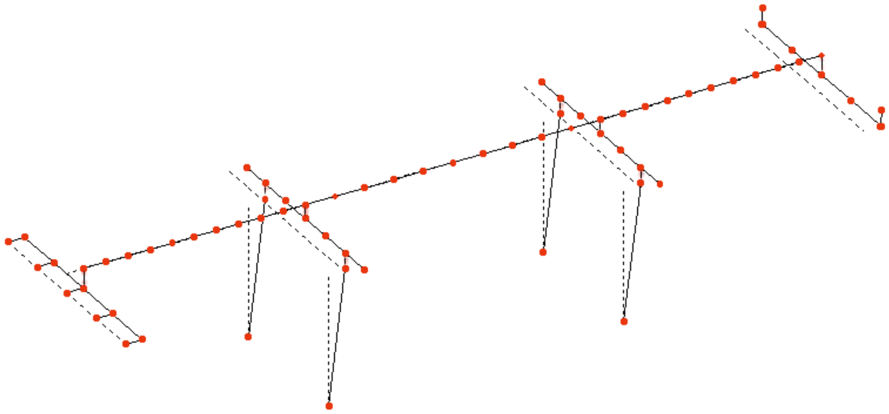

(c) Mode 3 with period of 0.48 seconds (longitudinal motion)

Figure 4.8: Mode Shapes of Typical Three-Span Bridge with no Soil-Abutment Stiffness Included

Using the ground-motion records listed in tables 2.2 and 2.3, and the previously defined OpenSees model, multiple time history analyses were run until completion. The ground-motion records (SAC, 2010) are provided as orthogonal pairs. The ground motions were oriented along the longitudinal (x) direction and transverse (z) direction of the bridge model. Each pair was used with two runs, one in the horizontal x-z orientation, and then the records were reversed and rerun in the z-x direction. This resulted in a total of 40 runs with the three-span model.

Maximum column displacements resulting from these 40 runs are provided in Table 4.10 and Table 4.11.

Table 4.10: Maximum Displacements Using POE-of-10%-in-50-Years Group

Ground-Motion Record	PGA dir1 (g)	PGA dir2 (g)	Orientation 1		Orientation 2	
			Long. Disp. (in)	Trans. Disp. (in)	Long. Disp. (in)	Trans. Disp. (in)
Long Beach, Vernon CMD Bldg.	0.174	0.135	1.7	1.1	1.7	1.4
Morgan Hill, 1984, Gilroy	0.386	0.662	3.3	2.7	2.7	3.1
West. Washington, Olympia, 1949	0.383	0.352	2.7	2.0	2.5	2.9
West. Washington, Seattle Army B., 1949	0.295	0.388	5.4	5.9	4.5	5.4
North Palm Springs, 1986	0.587	0.599	3.3	3.6	2.6	2.2
Puget Sound, Wa., Olympia, 1949	0.752	0.596	4.7	3.3	4.1	5.9
Puget Sound, Wa., Federal OFC B., 1949	0.369	0.303	3.4	3.2	3.0	4.2
Eastern Wa., Tacoma County, 1949	0.290	0.574	3.8	5.9	5.1	2.3
Llolleo, Chile 1985	0.697	0.670	4.0	4.0	4.2	5.0
Vinadel Mar, Chile, 1985	0.541	0.384	6.3	5.1	7.4	8.9

Table 4.11: Maximum Displacements Using POE-of-2%-in-50-Years Group

Ground-Motion Record	PGA dir1 (g)	PGA dir2 (g)	Orientation 1		Orientation 2	
			Long. Disp. (in)	Trans. Disp. (in)	Long. Disp. (in)	Trans. Disp. (in)
1992 Mendocino	0.755	0.485	10.0	5.2	9.7	13.0
1992 Erzincan	0.605	0.539	7.8	6.0	5.8	7.2
1949 Olympia	0.895	0.821	6.8	4.9	6.0	8.1
1965 Seattle	1.755	1.390	15.3	8.4	9.5	13.5
1985 Valpariso	1.636	1.573	10.8	8.8	10.3	13.2
1985 Valpariso	1.270	0.901	21.2	14.7	13.2	22.6
Deep Interplate (simulation)	0.796	0.646	9.0	6.5	8.3	8.2
1978 Miyagi-oki	0.606	0.783	13.6	23.7	23.9	15.5
Shallow Interplate (simulation)	0.563	0.534	6.0	6.6	6.4	5.6
Shallow Interplate (simulation)	0.578	0.749	6.2	8.0	7.4	5.7

The maximum displacement found in Table 4.6 is 8.9 inches for the structure being loaded by the group of ground motions having a POE of 10% in 50 years. This compares favorably to the 10.2 inches predicted by the response spectrum envelope from Figure 2.5 for a structure having a fundamental period of 0.76 seconds.

The maximum displacement found in Table 4.7 is 23.9 inches for the structure being loaded by the group of ground motions having a POE of 2% in 50 years. This compares favorably to the 24.0 inches predicted by the response spectrum envelope from Figure 2.4 for a structure having a fundamental period of 0.76 seconds.

These displacement values are used in subsequent sections to calculate displacement ductilities, and then ultimately build fragility curves.

4.2 TYPICAL FIVE-SPAN BRIDGE

4.2.1 BRIDGE LAYOUT

Oregon Bridge 07628 was used as the template for the typical five-span bridge to be used in this study, and an elevation view is shown in Figure 3.2. This bridge has five spans that are 16, 60, 70, 60 and 16 feet long, for a total structure length of 220 feet, with the width of each span being 30 feet. This bridge has a continuous concrete deck with the bents being integral. The heights of the eight columns range from 22.6 feet to 36.4 feet, with the shortest at bent 5 and the longest at bent 3.

The dual-column bents for this bridge are made up of a 15-inch-wide-by-62-inch-deep reinforced concrete bent beam supported by two 24-inch-by-24-inch rectangular reinforced concrete columns. The as-designed bent beam uses three layers of three 1½ inch^2 bars at the bottom of the beam. The model is simplified by using one layer of larger (4 ½ inch^2) bars at the center of gravity of the second layer. The reinforcement as modeled is shown in Figure 4.9.

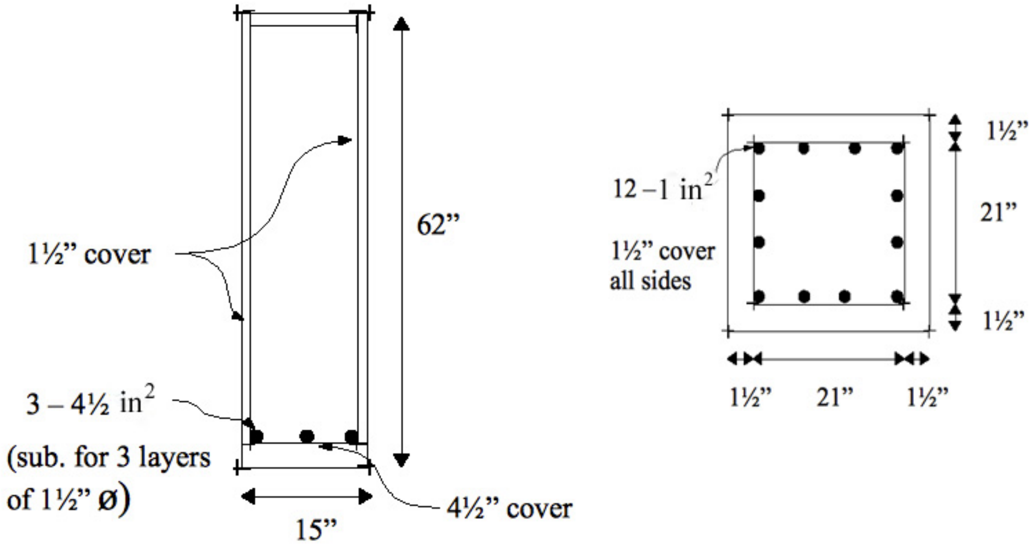

Figure 4.9: Concrete Member Reinforcement for Typical Five-Span Bridge

4.2.2 OPENSEES MODEL

The typical five-span bridge was modeled using the OpenSees application.

In order to take into account nonlinearities, several different element types were used when modeling some of the bridge components. An overview of the element and material types are shown in

Table 4.12.

Table 4.12: Element Types Used With Five-Span Model

Component	Material	Element
Abutments (Bents 1/6)	Elastic properties	elasticBeamColumn
Soil Interaction	ElasticPPGap	zeroLength
Deck	Elastic properties	elasticBeamColumn
Bent Caps (Bents 2/3/4/5)	FiberSection, Concrete01, Hysteretic Steel	dispBeamColumn
Columns	FiberSection, Concrete01, Concrete04, Hysteretic Steel	beamWithHinges

The soil-abutment interaction was modeled as a combination of linear springs. The ElasticPPGap material was used to allow the use of compressive loads only. In this model there was no gap between the abutments and deck. The material values used to define the gap material were derived from accepted design guidelines (Caltrans, 2006) and are provided in Table 4.13.

Table 4.13: ElasticPPGap Material Values for Five-Span Abutments

Description	Value
Stiffness of transverse spring	40 kips/in
Maximum compressive strength of transverse spring	-10 kips
Initial gap of transverse spring	0 in
Total stiffness of longitudinal springs	327.3 kips/in
Total maximum compressive strength of longitudinal springs	-245.5 kips
Initial gap of longitudinal spring	0 in

The guidelines also suggest using a nominal transverse spring stiffness equal to 50% of the transverse stiffness of the adjacent bent. In the five-span bridge case, approximations of the adjacent stiffness are 31 kips/inch (Bent 2) and 62 kips/inch (Bent 5). The value used (40 kips/inch) can be considered near to an average of the two bent stiffnesses.

As a comparison, another model for a four-span bridge (Hwang et al., 2001) with a total length of 234 feet and width of almost 60 feet was designed to have more piers supporting the abutment and a higher back wall (6 feet) when compared to the Oregon typical five-span bridge. This resulted in a transverse stiffness that is over nine times the stiffness of the modeled Oregon five-span bridge, and a longitudinal stiffness that is four times the stiffness of the Oregon bridge.

The superstructure deck was assumed to be level with no skew relative to the abutment. The column base locations were moved slightly vertically to maintain appropriate column heights and a level deck. The deck was assumed to behave elastically and therefore was modeled using the elasticBeamColumn element. The element was defined using the values found in Table 4.14.

Table 4.14: elasticBeamcolumn Element Values for Five-Span Deck

Description	Value
Cross Sectional Area	4746 in^2
Elastic Modulus (E)	3274 ksi

Description	Value
Shear Modulus (G)	1500 ksi
Torsional Moment of Inertia (J)	38.38×10^6 in^4
Second Moment of Area about the local y Axis (I_y)	2.537×10^6 in^4
Second Moment of Area about the local z Axis (I_z)	6.230×10^7 in^4

Concrete and steel OpenSees material types were used to model the reinforced concrete portions of the bridges. The Concrete01 material accounts for compression of the concrete, but doesn't allow for any tension load and was used for the cover concrete. The values used to define the concrete and reinforcing steel are shown below in tables Table 4.15 and Table 4.16, and were used only for the five-span bridge model. The 28-day compressive strength specified by ODOT drawings was given as -3.3 ksi. To account for the time-related strength development property of concrete, the modeled compressive strength (AASHTO, 2009) was increased by 30% to -4.259 ksi. This is the compressive strength used for the cover concrete. To model the stress-strain relationship of the confined column concrete, an analytical model (Mander et al., 1988) was used to determine the confined concrete maximum strength and the cover strain at maximum strength. Typical values for the ultimate compressive strain (AASHTO, 2009) range from 0.008 to 0.025, but the lowest value was chosen because of the relatively poor amount of transverse confinement reinforcement present in the modeled five-span bridge. Also because of the amount of transverse confinement, the Mander model predicts a modest strength increase of the confined concrete (1.7 %) when compared to the cover concrete.

Table 4.15: Concrete01 Values for Confined Concrete Used With Five-Span Bridge

Description	Value
maximum concrete compressive strength	-4.333 ksi
concrete strain at maximum strength	-0.0021999 in/in
concrete crushing strength	0 ksi
concrete strain at crushing strength (AASHTO, 2009)	-0.008 in/in

Table 4.16: Concrete01 Values for Cover Concrete Used With Five-Span Bridge

Description	Value
maximum concrete compressive strength	-4.259 ksi
concrete strain at maximum strength	-0.002023 in/in
concrete crushing strength	0 ksi
concrete strain at crushing strength (AASHTO, 2009)	-0.005 in/in

The hysteretic steel material was used to model the reinforcement steel of all reinforced concrete members. The general behavior provided by these OpenSees material types are shown in figures 4.1 and 4.2. When possible, material property values were found from ODOT drawings of the bridges used in this study, such as maximum compressive strength of the concrete and yielding stress of the reinforcing steel. To model the stress-strain relationship of the column confined concrete of the columns, an analytical model (Mander et al., 1988) was used. The specific values used to define the hysteretic material are given in

Table 4.17. The typical bridge, modeled using OpenSees, is shown in Figure 4.10.

Table 4.17: Hysteretic Steel Values Used With Five-Span Bridge

Description	Value
yield stress	40 ksi
yield strain	0.0013793
ultimate strain	0.20

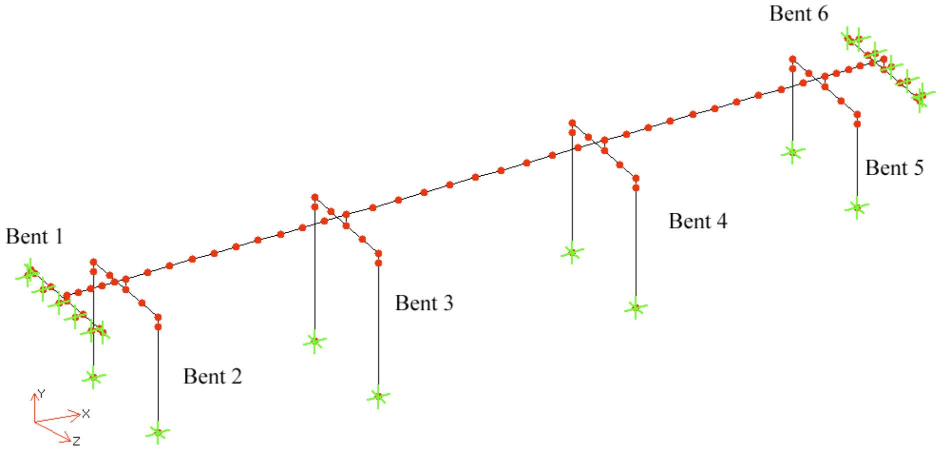

Figure 4.10: OpenSees Model for Typical Five-Span Bridge

4.2.2.1 MODEL VERIFICATION

The same verifications that were performed on the three-span model (Section 4.1.2.1) were also performed on the five-span model. A typical five-span modeled column was subjected to a concentric axial load of 170 kips. While the column was being loaded by a lateral force, the overturning moment at the base was being recorded. The moment from the OpenSees model was determined to be 2,933 in·kips when the reinforcing steel being loaded in tension was just starting to yield. The same scenario was then considered, but using standard analytical techniques. When equations 4-1 and 4-2 were solved, the overturning moment was found to be 3,048 in·kips. Comparing the two estimates of the overturning moment shows a 3.8 % difference between the analytical and numerical methods.

Another simple, but effective, method of model verification is to ensure that the period of vibration predicted by the OpenSees model is reasonably close to the period of a simple, single degree of freedom system having the same mass and stiffness. The values used in this calculation were: E = 4300 ksi, I_{col} = 27,648 in^4, Weight of superstructure = 1187.3 kips (mass = 1187.3/386.4 = 3.0728 kips-sec^2/in.). The stiffness of a fixed-fixed column was idealized to be $k_{col} = \frac{12EI}{L^3}$. The stiffness associated with two columns for each bent was calculated and are shown in

Table 4.18.

Table 4.18: Estimated Stiffness Values for Five-Span Bridge

Location	Bent Stiffness (kips/in)
Bent 2	68.5
Bent 3	34.0
Bent 4	47.9
Bent 5	141.8
Total	292.2

The period of vibration can be calculated for the five-span bridge, in both the transverse and longitudinal directions, and with the soil-abutment interaction both being included and not included. As an example, for the case where the soil-abutment stiffness is not included, and for the longitudinal direction, the period of a simple SDOF system can be calculated to be:

$$T = 2\pi\sqrt{\frac{m}{k}} = 2\pi\sqrt{\frac{3.0728\,\frac{kips\cdot\sec^2}{in}}{292.2\,\frac{kips}{in}}} = 0.644\text{ seconds}$$

Similar calculations yield the data shown below in Table 4.19 for both directions of displacement.

Table 4.19: Calculated Periods of Vibration for Various Five-Span Bridge Models

Periods (seconds)	Soil-Abutment Stiffness Included	Soil-Abutment Stiffness Not Included
Longitudinal	0.442	0.644
Transverse	0.604	0.444

Using the OpenSees model with the soil-abutment stiffness included, the period of vibration with a longitudinal motion was found to be 0.363 seconds. With the soil-abutment stiffness removed, the period of vibration with a longitudinal motion was found to be 0.660 seconds. The calculated approximations agree relatively well with the OpenSees numerical model.

4.2.3 MODEL RESPONSE

Using the provided dimensions from ODOT drawings and OpenSees material and element types, a numerical model was constructed with the geometry shown in Figure 4.10. Ground motions were applied to the soil nodes of the soil-abutment connections and to the bases of the columns. An eigenvalue analysis of this model, using OpenSees, shows a fundamental period of 0.72 seconds with the associated motion being a twisting motion near bent 5. Mode shapes for the five-span bridge, and with no soil-abutment stiffness included, are shown in Figure 4.11. The second mode has a period of 0.66 seconds with a longitudinal motion, with good agreement with the simple SDOF system described in the previous section. The third mode has a period of 0.48 seconds.

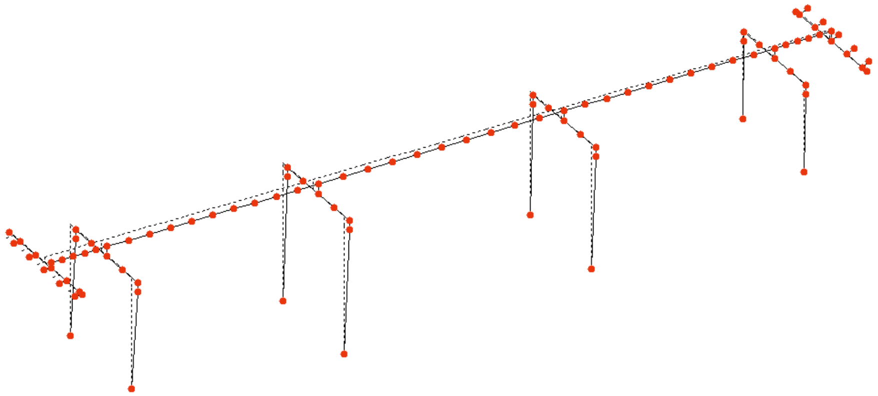

(a) Mode 1 With Period of 0.72 seconds With Twisting Motion Near Bent 5

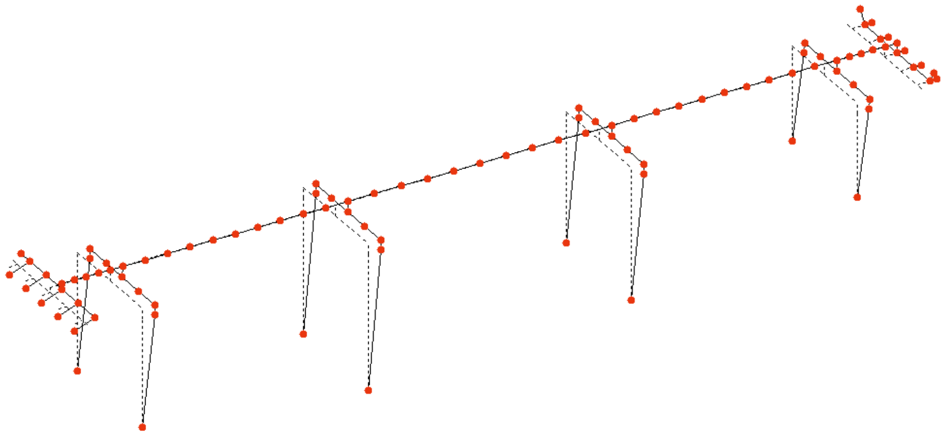

(b) Mode 2 With Period of 0.66 seconds With Longitudinal Motion

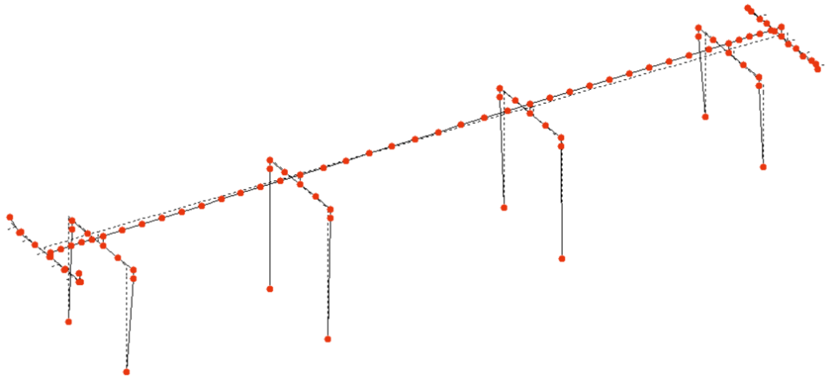

(c) Mode 3 With Period of 0.53 seconds With Rotating Motion Near Center

Figure 4.11: Mode Shapes of Typical Five-Span Bridge with no Soil-Abutment Stiffness Included

Using the ground-motion records listed in tables 2.2 and 2.3, and the previously defined OpenSees model, multiple time-history analyses were run until completion. The ground-motion records (SAC, 2010) are provided as orthogonal pairs. The ground motions were oriented along the longitudinal (x) direction and transverse (z) direction of the bridge model. Each pair was used with one run, one in the horizontal x-z orientation. This resulted in a total of 20 runs with the five-span model. Maximum column displacements resulting from these 20 runs are provided in tables 4.18 and 4.19.

The maximum displacement found in Table 4.20 is 10.9 inches for the structure being loaded by the group of ground motions having a POE of 10% in 50 years. This compares favorably to the 8.0 inches predicted by the response spectrum envelope from Figure 2.5 for a structure having a fundamental period of 0.72 seconds.

Table 4.20: Maximum Displacements Using POE-of-10%-in-50-Years Group

Ground-Motion Record	PGA dir1 (g)	PGA dir2 (g)	Orientation 1	
			Long. Disp. (in)	Trans. Disp. (in)
Long Beach, Vernon CMD Bldg.	0.174	0.135	1.0	3.1
Morgan Hill, 1984, Gilroy	0.386	0.662	2.7	5.1
West. Washington, Olympia, 1949	0.383	0.352	2.4	5.3
West. Washington, Seattle Army B., 1949	0.295	0.388	4.5	7.1
North Palm Springs, 1986	0.587	0.599	1.5	10.9
Puget Sound, Wa., Olympia, 1949	0.752	0.596	5.6	5.6
Puget Sound, Wa., Federal OFC B., 1949	0.369	0.303	3.6	3.7
Eastern Wa., Tacoma County, 1949	0.290	0.574	0.9	6.2
Llolleo, Chile 1985	0.697	0.670	3.4	10.1
Vinadel Mar, Chile, 1985	0.541	0.384	9.5	3.9

Table 4.21: Maximum Displacements Using POE-of-2%-in-50-Years Group

Ground-Motion Record	PGA dir1 (g)	PGA dir2 (g)	Orientation 1	
			Long. Disp. (in)	Trans. Disp. (in)
1992 Mendocino	0.755	0.485	15.3	12.0
1992 Erzincan	0.605	0.539	11.3	41.3
1949 Olympia	0.895	0.821	7.1	14.2
1965 Seattle	1.755	1.390	19.5	17.3
1985 Valpariso	1.636	1.573	8.6	16.1
1985 Valpariso	1.270	0.901	17.1	14.3
Deep Interplate (simulation)	0.796	0.646	18.6	7.9
1978 Miyagi-oki	0.606	0.783	14.0	19.6
Shallow Interplate (simulation)	0.563	0.534	7.9	18.7
Shallow Interplate (simulation)	0.578	0.749	6.0	14.8

The maximum displacement found in Table 4.21 is 41.3 inches for the structure being loaded by the group of ground motions having a POE of 2% in 50 years. When reviewing the data associated with run, material failure was found to have occurred. If this outlying data point is ignored, then the maximum displacement was 19.6 inches. This compares favorably to the 21 inches predicted by the response spectrum envelope from Figure 2.4 for a structure having a fundamental period of 0.72 seconds.

These displacement values are used in subsequent sections to calculate displacement ductilities, and then to ultimately build fragility curves.

5.0 PROBABALISTIC SEISMIC DEMAND ANALYSIS

5.1 PROBABALISTIC SEISMIC DEMAND

Within the framework of predicting the risk of damage to Oregon bridges, being able to quantify the seismic demand seen by those structures is fundamental to the effort to define fragility curves. A simple mathematical description of this loss estimation is provided by the following equation (Ellingwood et al, 2005):

$$P[Loss] = \sum_{s}\sum_{LS}\sum_{d} P[Loss \mid D = d] \ P[D = d \mid LS] \ P[LS \mid IM = s] \ P[IM = s] \qquad \textbf{(5-1)}$$

where *Loss* is an appropriate metric such as number of deaths or injuries, damage expenses or lost opportunity costs. The last term *P[IM = s]* represents a relevant measure of the hazard Intensity Measure (IM) such as Peak Ground Acceleration (PGA) or Spectral Acceleration (S_a). Given that the structure experiences a hazard of intensity *s*, the third term *P[LS | IM = s]* represents the probability that the structure exceeds a particular limit state given a certain Intensity Measure. If a specified limit state is exceeded, the second term *P[D = d | LS]* represents the probability that the structure will sustain a damage state of *d*. If the structure sustains a damage state *d*, then the first term *P[Loss | D = d]* represents the probability that the structure will sustain a given level of loss. The product of these individual terms result in the probability the structure will sustain a given level of loss. The term *P[LS | IM = s]* in Eq. (5-1) allows the seismic demand to be defined and can be thought of as a fragility term because the ability of the structure to withstand ground motions of a specified intensity is represented. The LS represent a specified structural limit state which is a measure of the structural response (e.g., displacement or curvature ductility), and is referred to as an engineering demand parameter (EDP).

The two parts of the fragility concept are capacity and demand where the damage states of a structure can be considered to be related to structural capacity (C) and the ground-motion intensity is a representation of structural demand (D). The probability of failure, P_f, can then be written as:

$$P_f = P\left\lfloor \frac{C}{D} \leq 1 \right\rfloor \qquad \textbf{(5-2)}$$

which gives the probability that the structural demand will exceed the structural capacity. Since both capacity and demand distributions are assumed to be lognormal (Wen, 2003), P_f can be expressed (Melchers, 1999) using the standard normal distribution function Φ():

$$
\begin{aligned}
P_f &= \Phi(-\beta) \\
&= \Phi\left(\frac{-\ln\left(\dfrac{\mu_C}{\mu_D}\dfrac{\sqrt{1+V_D^2}}{\sqrt{1+V_C^2}}\right)}{\sqrt{\ln\left[\left(1+V_C^2\right)\left(1+V_D^2\right)\right]}}\right) \\
&= \Phi\left(\frac{-\ln\left(\dfrac{C_m}{D_m}\right)}{\sqrt{\ln\left[\left(1+V_C^2\right)\left(1+V_D^2\right)\right]}}\right) \\
&= \Phi\left(\frac{\ln\left(\dfrac{D_m}{C_m}\right)}{\sqrt{\ln\left(1+V_C^2\right)+\ln\left(1+V_D^2\right)}}\right)
\end{aligned}
\qquad \textbf{(5-3)}
$$

where μ_C and μ_D are the means of the capacity and demand distributions, V_C and V_D are the coefficients of variation (COV) of the capacity and demand distributions, and C_m and D_m are the median values of the capacity and demand distributions. Using the fact that for a lognormal distribution $\sigma_{\ln X}^2 = \ln\left(1+V_X^2\right)$, Eq. (5-3) can be further simplified:

$$
P_f = \Phi\left(\frac{\ln\left(\dfrac{D_m}{C_m}\right)}{\sqrt{\ln\left(1+V_C^2\right)+\sigma_{\ln_D}^2}}\right) \qquad \textbf{(5-4)}
$$

where $\sigma_{\ln_D}$ is the standard deviation of the lognormal demand distribution.

The median demand can be represented by a power model (Cornell et al., 2002) such that

$$
D_m = a(S_a)^b \qquad \textbf{(5-5)}
$$

Assuming that this can be extended to include other intensity measures, a more general expression will be used:

$$
D_m = a(IM)^b \qquad \textbf{(5-6)}
$$

Since two ground-motion records were used for each simulation, the geometric average of the PGA for each of the two records was used when specifying the IM. Research has shown that the dispersion of displacement data relative to spectral acceleration, in lognormal space, is less than the dispersion of displacement data relative to PGA, also in lognormal space (Hwang et al., 2001). However, spectral acceleration is considered a structural parameter and is not directly related to ground shaking, and since PGA is easily derived from ground-motion records it was the only IM used in this study.

Transforming Equation 5-6 into lognormal space yields:

$$\ln D_m = b \cdot \ln IM + \ln a \qquad \textbf{(5-7)}$$

An illustration from Padgett (2007) showing the transformation into lognormal space is shown in Figure 5.1.

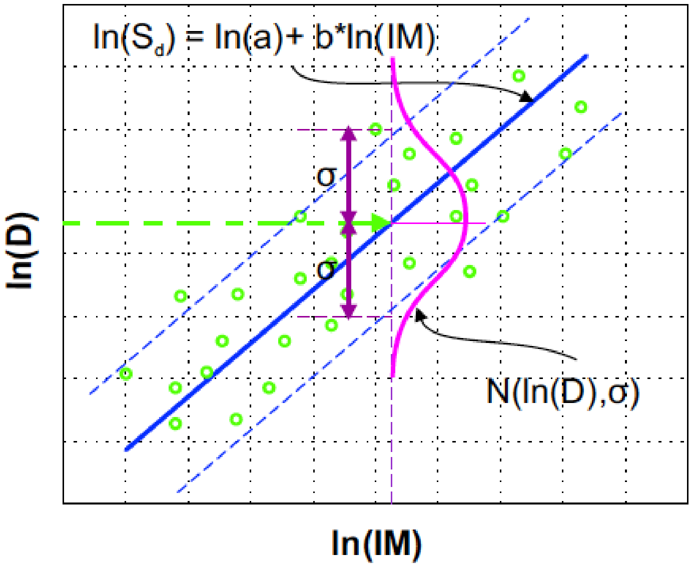

Figure 5.1: PSDM Illustration in Lognormal Space (Padgett, 2007)

The chart shows data from the nonlinear analyses being plotted in the ln (*D*) vs. ln (*IM*) space. A regression analysis yields the equation of the desired line: ln *a* + *b* ln *IM*. Additionally, the standard deviation of the transformed data is also shown; this is the standard deviation used in Equation 5-4.

Using Equation (5-6) in Equation (5-4), another expression for the failure probability P_f can be derived:

$$P_f = \Phi\left[\frac{\ln\left(\frac{D_m}{C_m}\right)}{\sqrt{\ln(1+V_c^2)+\sigma_{\ln_D}^2}}\right] = \Phi\left[\frac{\ln D_m - \ln C_m}{\sqrt{\ln(1+V_c^2)+\sigma_{\ln_D}^2}}\right]$$

$$= \Phi\left[\frac{\ln\left(aIM^{b}\right) - \ln C_m}{\sqrt{\ln(1+V_c^2) + \sigma_{\ln_D}^2}}\right] = \Phi\left[\frac{\ln a + b\ln IM - \ln C_m}{\sqrt{\ln(1+V_c^2) + \sigma_{\ln_D}^2}}\right]$$

$$= \Phi\left[\frac{\ln IM - \left(\frac{\ln C_m - \ln a}{b}\right)}{\frac{\sqrt{\ln(1-V_c^2)+\sigma_{\ln_D}^2}}{b}}\right] \tag{5-8}$$

Rewriting Equation 5-8 in the form used in Equation 1-2:

$$P_f = \Phi\left[\frac{\ln IM - \ln\left(e^{\frac{\ln C_m - \ln a}{b}}\right)}{\frac{\sqrt{\ln(1-V_c^2)+\sigma_{\ln_D}^2}}{b}}\right] \tag{5-9}$$

Since Equation 1-2 is the form of an equation that represents a lognormal cumulative distribution function, the second term of Equation 5-9, $e^{\frac{\ln C_m - \ln a}{b}}$, is the median of the lognormal capacity distribution and the bottom term, $\frac{\sqrt{\ln(1+V_c^2)+\sigma_{\ln_D}^2}}{b}$, is a measure of the dispersion.

The primary failure location of the bridges considered was expected to be the columns. Therefore, the only engineering demand parameter that was considered was the column displacement ductility.

Displacement ductility demand was used to evaluate the extent of loading of the columns and is defined as:

$$\mu_\Delta = \frac{\Delta_{max}}{\Delta_{yield}} \tag{5-10}$$

where Δ_{max} is the maximum displacement throughout a given time history and Δ_{yield} is the displacement of the column at first yield of the outermost longitudinal reinforcement steel.

5.2 PSDM FOR TYPICAL THREE-SPAN BRIDGE

The displacement of a column resulting in the yielding of the outermost steel reinforcement for the three-span bridge was around 0.8 inches. This value was determined by doing a pushover analysis of the actual bridge model. Using Equation 5-10, the displacement ductilities were determined and are shown in tables 5.1 and 5.2.

Table 5.1: Displacement Ductilities Using POE-of-10%-in-50-Years Group

Ground-Motion Record	**PGA dir1 (g)**	**PGA dir2 (g)**	**Displacement Ductility, μ_Δ Orientation 1**	**Displacement Ductility, μ_Δ Orientation 2**
Long Beach, Vernon CMD Bldg.	0.174	0.135	2.17	2.08
Morgan Hill, 1984, Gilroy	0.386	0.662	4.12	3.82
West. Washington, Olympia, 1949	0.383	0.352	3.37	3.65
West. Washington, Seattle Army B., 1949	0.295	0.388	7.31	6.70
North Palm Springs, 1986	0.587	0.599	4.52	3.21
Puget Sound, Wa., Olympia, 1949	0.752	0.596	5.87	7.34
Puget Sound, Wa., Federal OFC B., 1949	0.369	0.303	4.19	5.18
Eastern Wa., Tacoma County, 1949	0.290	0.574	7.42	6.33
Llolleo, Chile 1985	0.697	0.670	5.04	6.25
Vinadel Mar, Chile, 1985	0.541	0.384	7.86	11.07

Table 5.2: Displacement Ductilities Using POE-of-2%-in-50-Years Group

Ground-Motion Record	**PGA dir1 (g)**	**PGA dir2 (g)**	**Displacement Ductility, μ_Δ Orientation 1**	**Displacement Ductility, μ_Δ Orientation 2**
1992 Mendocino	0.755	0.485	12.5	16.2
1992 Erzincan	0.605	0.539	9.71	9.04
1949 Olympia	0.895	0.821	8.55	10.1
1965 Seattle	1.755	1.390	19.2	16.9
1985 Valpariso	1.636	1.573	13.4	16.4
1985 Valpariso	1.270	0.901	26.5	28.3
Deep Interplate (simulation)	0.796	0.646	11.2	10.4
1978 Miyagi-oki	0.606	0.783	29.6	29.8
Shallow Interplate (simulation)	0.563	0.534	8.19	8.05
Shallow Interplate (simulation)	0.578	0.749	9.93	9.26

Using the methodology described in Section 5.1, the probability seismic demand model (PSDM) was found and is shown below in Figure 5.2. The defining parameters are provided in Table 5.3.

The dispersion found during this analysis is comparable to that found from other researchers (Nielson, 2005 and Padgett, 2007) using this method.

Table 5.3: PSDM for Three-Span Bridge

PSDM	**Dispersion $\sigma_{\ln D_m}$**
$\ln D_m = 0.914 \cdot \ln IM + 2.577$	0.643

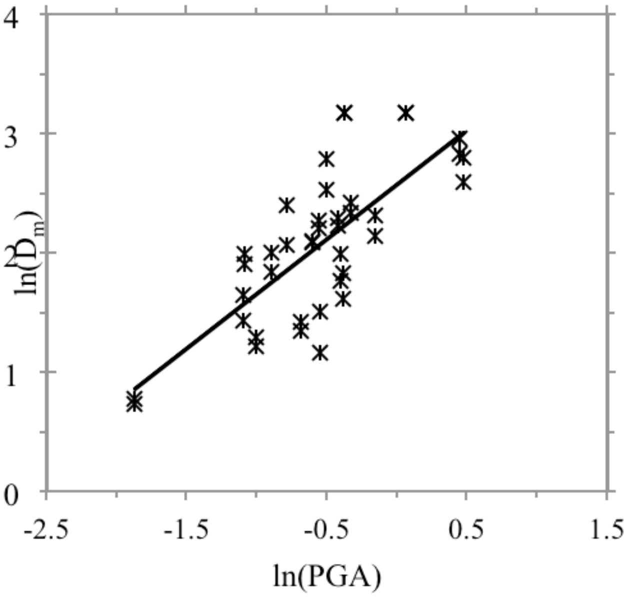

Figure 5.2: PSDM Plot for Three-Span Bridge

5.3 PSDM FOR TYPICAL FIVE-SPAN BRIDGE

The displacement of shortest column resulting in the yielding of the outermost steel reinforcement for the five-span bridge column was around 2.0 inches. This value was determined by doing a pushover analysis of the actual bridge model. Using Equation 5-10, the displacement ductilities were determined and are shown in tables 5.4 and 5.5.

Table 5.4: Displacement Ductilities Using POE-of-10%-in-50-Years Group

Ground-Motion Record	PGA dir1 (g)	PGA dir2 (g)	Displacement Ductility μ_Δ
Long Beach, Vernon CMD Bldg.	0.174	0.135	1.55
Morgan Hill, 1984, Gilroy	0.386	0.662	2.55
West. Washington, Olympia, 1949	0.383	0.352	2.65
West. Washington, Seattle Army B., 1949	0.295	0.388	3.55
North Palm Springs, 1986	0.587	0.599	5.45
Puget Sound, Wa., Olympia, 1949	0.752	0.596	2.80
Puget Sound, Wa., Federal OFC B., 1949	0.369	0.303	1.85
Eastern Wa., Tacoma County, 1949	0.290	0.574	3.10
Llolleo, Chile 1985	0.697	0.670	5.05
Vinadel Mar, Chile, 1985	0.541	0.384	4.75

Table 5.5: Displacement Ductilities Using POE-of-2%-in-50-Years Group

Ground-Motion Record	PGA dir1 (g)	PGA dir2 (g)	Displacement Ductility μ_Δ
1992 Mendocino	0.755	0.485	7.65
1992 Erzincan	0.605	0.539	20.7

Ground-Motion Record	PGA dir1 (g)	PGA dir2 (g)	Displacement Ductility μ_Δ
1949 Olympia	0.895	0.821	7.10
1965 Seattle	1.755	1.390	9.75
1985 Valpariso	1.636	1.573	8.05
1985 Valpariso	1.270	0.901	8.55
Deep Interplate (simulation)	0.796	0.646	9.30
1978 Miyagi-oki	0.606	0.783	9.80
Shallow Interplate (simulation)	0.563	0.534	9.35
Shallow Interplate (simulation)	0.578	0.749	7.40

Using the methodology described in Section 5.1, the PSDM was found and is shown below in Figure 5.3. The defining parameters are provided in Table 5.6. The dispersion found during this analysis is larger comparable to that found from other researchers (Nielson, 2005 and Padgett, 2007) using this method.

Table 5.6: PSDM for Five-Span Bridge

PSDM	Dispersion $\sigma_{\ln Dm}$
$\ln D_m = 0.850 \cdot \ln IM + 2.131$	0.670

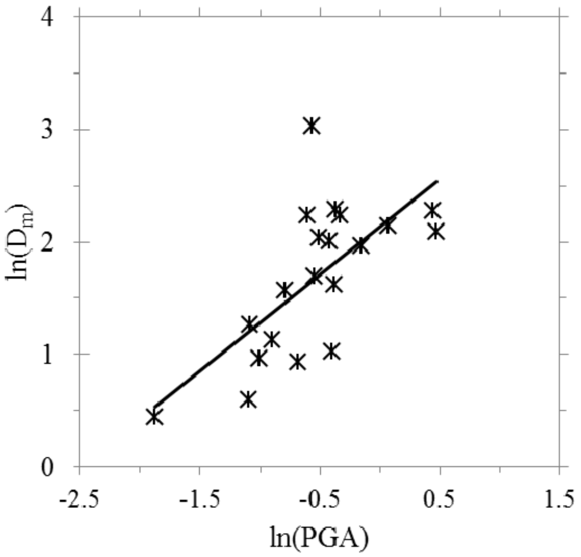

Figure 5.3: PSDM Plot for Five-Span Bridge

6.0 SEISMIC FRAGILITY ANALYSIS OF BRIDGES

6.1 LIMIT STATES

The capacity limit states (C_m) used in Equation (5-8) are conceptually the same qualitative limit states used in the FEMA loss assessment package HAZUS-MH MR3 (FEMA, 2003). Descriptions of these limit states are given in Table 6.1:

Table 6.1: FEMA Limit States

Slight/Minor	Minor cracking and spalling to the abutment, cracks in shear keys at abutments, minor spalling and cracks at hinges, minor spalling at the column (damage requires no more than cosmetic repair) or minor cracking to the deck
Moderate	Any column experiencing moderate (shear cracks) cracking and spalling (column structurally still sound), moderate movement of the abutment (<2"), extensive cracking and spalling of shear keys, any connection having cracked shear keys or bent bolts, keeper bar failure without unseating, rocker bearing failure or moderate settlement of the approach.
Extensive	Any column degrading without collapse – shear failure - (column structurally unsafe), significant residual movement at connections, or major settlement approach, vertical offset of the abutment, differential settlement at connections, shear key failure at abutments.
Complete	Any column collapsing and connection losing all bearing support, which may lead to imminent deck collapse, tilting of substructure due to foundation failure.

But the real need is to have quantitative values which can be used in the generation of fragility curves. Other researchers dealing with the modeling of reinforced concrete bridges in the Central and Southeastern United States (CSUS) have recognized that the detailing for the typical reinforced concrete column will produce poor confinement due to the widely spaced transverse steel and also due to lap splices being located where a plastic hinge is expected to occur. From research related to the CSUS, Hwang et al. (2000) proposed quantitative limit states that roughly correspond to the limit states in Table 5.1. The median displacement ductilities of 1.0, 1.2, 1.76, and 4.76 were suggested, which correspond to yielding, cracking, spalling and reinforcement buckling, respectively. The values used to model bridge capacity are shown in Table 6.2.

Once the median displacement ductilities (C*m*) are available, then the amount of variability, or dispersion, of the capacity distribution needs to be estimated. The coefficient of variation (COV), when working with a single variable, is defined to be the ratio of the standard deviation to the mean of the distribution. Generally, a lower COV corresponds to a lower dispersion of the variable. Since the COV for the capacity distribution is unknown, an assumption was made about its value. Nielson (2007) assumed that the COV for the slight and moderate damage states was 0.25, which corresponds to a relatively lower variation. The COV for the extensive and complete damage states had a value of 0.5, which corresponds to a higher level of variation. Instead of a jump in values, a more gradual increase of variability was used so that the COV for the slight, moderate, extensive and complete damage states was 0.25, 0.33, 0.42, and 0.5. Bridge capacity values used are shown in Table 6.2. The increased variability is assumed since the higher damage states correspond to more nonlinear behavior of the bridge components, and the ability to model actual behavior of the bridges becomes more difficult at the higher levels of damage.

Table 6.2: Model Bridge Capacity Values

Damage State	Median Capacity Displacement Ductility	Coefficient of Variation
Slight	1.0	0.25
Moderate	1.2	0.33
Extensive	1.76	0.42
Complete	4.76	0.50

Research has shown that natural, physical processes can frequently be represented using lognormal distributions. Typical values of the standard deviation, s*, of these natural processes can range from s*= 1.2 to 3.0 (Eckhard et al., 2001). The following equation relating the coefficient of variation and the lognormal standard deviation can be used:

$$s^* = e^{\sqrt{\ln(1+COV^2)}}$$

Using the assumed standard deviation values, the COV is found to range from 0.18 to 1.53, and the assumed COV values used in this study fall within the lower portion of this range.

6.2 FRAGILITY CURVE GENERATION

At this point of the discussion, all of the elements needed to calculate fragility curves are available. These are:

- A method to predict the median of the lognormal demand distribution in terms of the chosen intensity measure. In the current research, this takes the form of the PSDM.
- Quantitative values of the median value of the capacity lognormal distribution. As mentioned previously, these values are assumed to be 1.0, 1.2, 1.76, and 4.73, which correspond to yielding, cracking, spalling and reinforcement buckling, respectively.
- An estimate of the dispersion of the capacity distribution: The COV is used to estimate the dispersion, $\beta = \sqrt{\ln(1 + COV^2)}$.
- An estimate of the dispersion of the demand distribution. The standard deviation of the displacement ductility values in the lognormal space was taken to be a measure of the dispersion.
- A mathematical model which links the above elements. This function is served by Equation 5-9.

Once these values are known, any standard spreadsheet software package can plot the fragility curve associated with the calculated demand median and dispersion.

6.3 THREE-SPAN BRIDGE FRAGILITY CURVES

Using Equation 5-9, the following median and dispersion values were calculated for the three-span bridge and are provided in Table 6.3 and Figure 6.1.

Table 6.3: Fragility Curves Values for Typical Three-Span Bridge

Damage State	Median	Dispersion
Slight	0.06	0.64
Moderate	0.07	0.68
Extensive	0.11	0.73
Complete	0.33	0.78

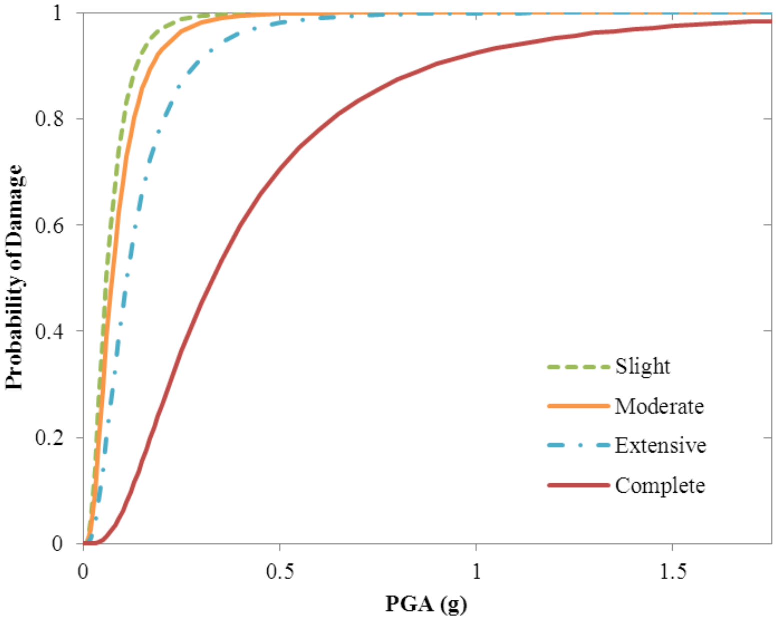

Figure 6.1: Fragility Curves for Three-Span Bridge

For a comparison, the fragility curves specified in HAZUS (2003) were calculated. The fragility curves currently being used in HAZUS were developed using a nonlinear static analysis method described in Section 1.2.3. This method attempts to take into account nonlinear behavior and doesn't have the computational overhead of the nonlinear time-history method, but should be considered a coarser approximation.

The procedure found in HAZUS was followed to modify the fragility medians for a "standard bridge" for local conditions. The location was chosen to be Portland, OR, and from the USGS website, the spectral acceleration values were determined to be S_1=0.339 g and S_s=0.963 g. All values from the USGS website were based upon the 2003 NEHRP design provisions. The USGS specifies the short-period spectral acceleration at 0.2 seconds, but the HAZUS procedure requires the spectral acceleration at 0.3 seconds. The following equation is provided by HAZUS to convert: $S_a(0.3) = S_s/1.1 = 0.963/1.1 = 0.876$ g.

To allow for local soil conditions, these spectral accelerations were modified by the soil amplification factors, F_A and F_V. The spectral acceleration values then become $S_a(0.3)=1.00565$ g and $S_a(1.0)=0.584$ g.

Several other modifications were also made. The K_{shape} factor is the modifier that converts cases for short periods to an equivalent spectral amplitude at T=1.0 second and K_{3D} accommodates the three-dimensional movement of the deck. K_{shape} and K_{3D} were found to be 1.451 and 1.110, respectively. K_{skew} has a value of unity because no deck skew was modeled.

The median values for the "standard bridge" type 202 are:

$$a_2 = 0.62g;\ a_3 = 0.79g;\ a_4 = 1.05g;\ a_5 = 1.38g$$

The final step is to modify these median values to reflect the local structural and soil conditions using the following equations:

$$A_2 = K_{shape} a_2 = 0.871\,g \tag{6-1}$$

$$A_3 = K_{skew} K_{3D} a_3 = 0.999\,g \tag{6-2}$$

$$A_4 = K_{skew} K_{3D} a_4 = 1.221\,g \tag{6-3}$$

$$A_5 = K_{skew} K_{3D} a_5 = 1.665\,g \tag{6-4}$$

where A_i is the modified median value for the slight, moderate, extensive and complete damage states. HAZUS specifies the reference median values, $a_2 – a_5$, to be 0.60 g, 0.90 g, 1.10 g, and 1.50 g, respectively, for a continuous concrete, pre-1990, non-CA, conventionally built bridge. HAZUS also specifies a dispersion of 0.6 for all damage states to be used for bridges.

The median values and dispersions for the four damage states from the three-span bridge model, from HAZUS, and Nielson (2007) are shown below in Table 6.4.

Table 6.4: Fragility Curves Values for Typical Three-Span Bridge and Reference Values

Damage State	**3-Span Model**		**Nielson**		**HAZUS**	
	Median	Dispersion	Median	Dispersion	Median	Dispersion
Slight	0.06	0.64	0.16	0.7	0.87	0.6
Moderate	0.07	0.68	0.53	0.7	1.00	0.6
Extensive	0.11	0.73	0.75	0.7	1.22	0.6
Complete	0.33	0.78	1.01	0.7	1.67	0.6

As can be seen, the medians from the model are significantly lower than both Nielson and HAZUS. However, the dispersion of the model is similar to the other two sources. For simplicity, the dispersion of the model could be distilled to an average value of 0.7.

6.3.1 EFFECT OF ABUTMENTS

The three-span model used the ElasticPPGap OpenSees material type, which allowed a gap between the abutment and deck to be specified. When the gap is modified to a large value, this effectively removes any effect from the abutments. The median and dispersion values from this model are shown in Table 6.5, and the fragility curves for the extensive and complete damage states are shown in Figure 6.2.

Table 6.5: Fragility Curve Values With and Without Abutments

Damage State	**With Abutments**		**Without Abutments**		**Median Percent Difference**
	Median	Dispersion	Median	Dispersion	
Slight	0.06	0.64	0.02	0.74	-66.7
Moderate	0.07	0.68	0.03	0.79	-57.1
Extensive	0.11	0.73	0.05	0.84	-54.5
Complete	0.33	0.78	0.18	0.90	-45.5

From this data, the impact of just the abutments on the damage state of the structure, as a whole, can be seen. The median values, for all damage states, were decreased by 45% or more showing a large increase in bridge fragility with no abutments.

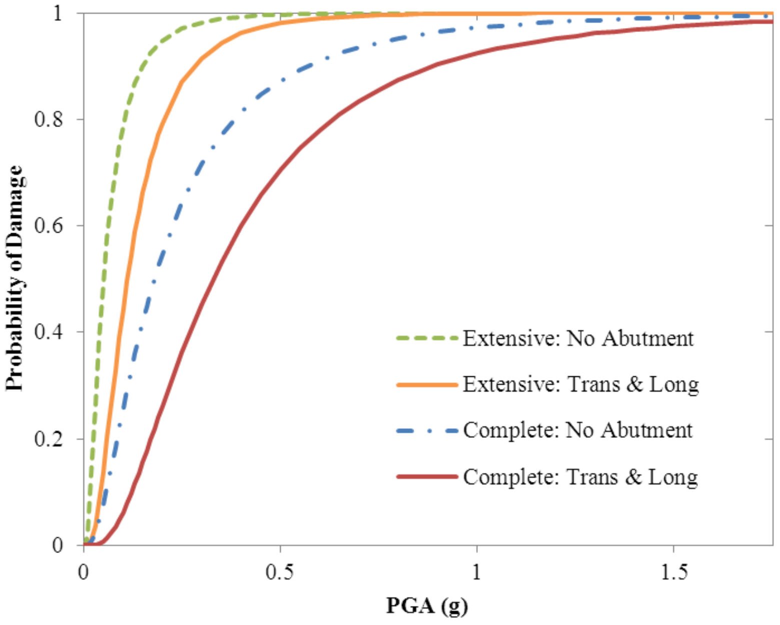

Figure 6.2: Complete and Extensive Damage Fragility Curve for Three-Span Bridge without Abutments

When the only effect is in the longitudinal direction, the median values are again changed. The median and dispersion values are shown in Table 6.6.

Table 6.6: Fragility Curve Values with All Abutments and Longitudinal Abutments Only

Damage State	**With Abutments**		**With Long. Abutment Only**		**Median Percent Difference**
	Median	Dispersion	Median	Dispersion	
Slight	0.06	0.64	0.03	0.70	-50.0
Moderate	0.07	0.68	0.04	0.74	-42.9
Extensive	0.11	0.73	0.07	0.79	-36.4
Complete	0.33	0.78	0.21	0.84	-36.4

When comparing the data from tables 6.4 and 6.5, the largest impact came from introducing the transverse soil-abutment interaction, with the longitudinal soil-abutment interaction being less significant but still useful in reducing bridge movement. For example, when using only the longitudinal soil-abutment interaction, the median value for the complete damage state increased by 18.8%. By using both the longitudinal and transverse interactions, the median value for the complete damage state increased by over 83% compared to when no soil-abutment interactions were modeled.

6.3.2 EFFECT OF GROUND-MOTION SUITE CHANGE

The original three-span model was evaluated using the entire ground-motion suite described in Section 2.2. That model was then modified such that only the ground motions from the POE-10%-in-50-years suite were used. The median and dispersion values from this new model are shown in Table 6.7, and the fragility curves for the extensive and complete damage states are shown in Figure 6.3.

Table 6.7: Fragility Medians Using POE-10%-in-50-Years Ground-Motion Suite

Damage State	**Complete Suite**		**POE-10-in-50 suite only**	
	Median	Dispersion	Median	Dispersion
Slight	0.06	0.64	0.02	0.90
Moderate	0.07	0.68	0.03	0.98
Extensive	0.11	0.73	0.06	1.07
Complete	0.33	0.78	0.39	1.17

The POE-10%-in-50-years ground-motion suite is centered near 0.4 g with a maximum of 0.68 g, whereas the full suite is centered near 0.6 g with a maximum of 1.76 g. With this downwards shift of ground-motion acceleration, the columns are displaced less, leading to the lower median values. Also, with the smaller column displacements comes a smaller dispersion.

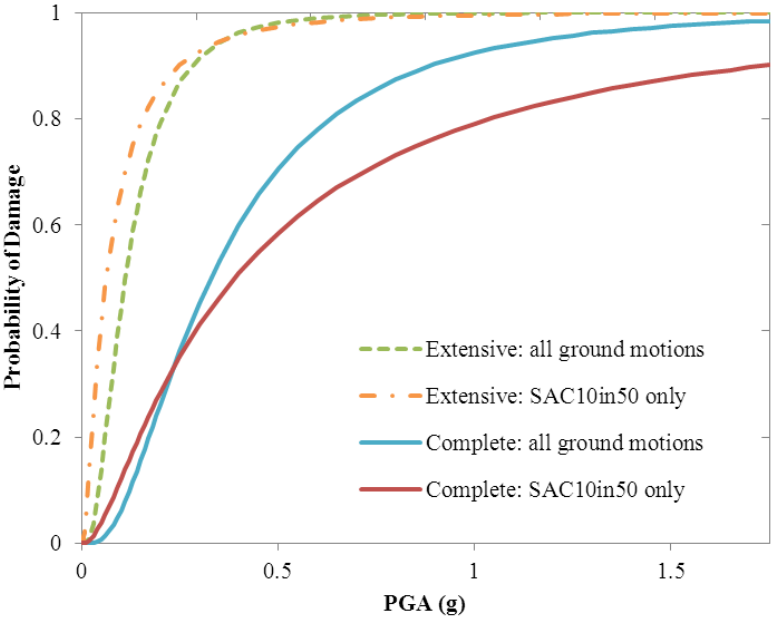

Figure 6.3: Complete and Extensive Damage Fragility Curve for Three-Span Bridge Suite Change

6.3.3 EFFECT OF DECREASING THE NUMBER OF RUNS

The original three-span model was evaluated using the entire ground-motion suite described in Section 2.2, with each ground-motion pair being applied in two orientations: the longitudinal and transverse directions, and then reversed to be applied in the transverse and longitudinal directions, resulting in a total of 40 runs. The data from this larger data set was then simplified to just include the runs which used the ground motions in first orientation, resulting in data from 20 runs being evaluated. The motivation in doing this was to justify using a reduced ground-motion suite, thus reducing computational time in half.

The median and dispersion values from this new, smaller data set are shown in Table 6.8, and the fragility curves for the extensive and complete damage states are shown in Figure 6.4.

Table 6.8: Fragility Medians Using Reduced Data Set

Damage State	Complete Suite		Reduced Data Set	
	Median	Dispersion	Median	Dispersion
Slight	0.06	0.64	0.05	0.65
Moderate	0.07	0.68	0.07	0.69
Extensive	0.11	0.73	0.11	0.74
Complete	0.33	0.78	0.33	0.79

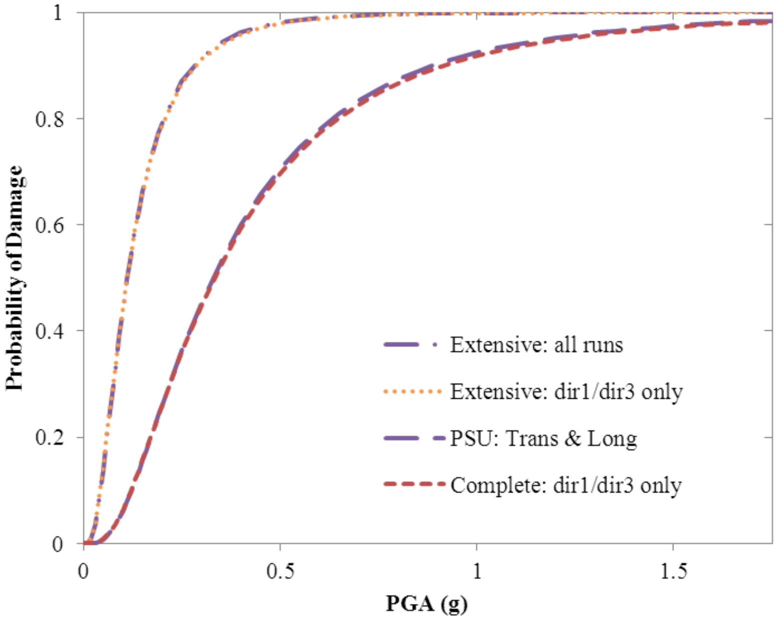

Figure 6.4: Complete and Extensive Damage Fragility Curves for Three-Span Bridge without Abutments

The results show that there is very little practical difference when comparing the results using the full data set to the smaller 20-run data set. Therefore, future models using the SAC ground-motion suite will only be applied in just one bi-directional orientation, without the ground-motion reversal.

6.3.4 EFFECT OF GROUND-MOTION ORIENTATION

The fragility curves presented in Section 6.3 were based upon ground motions being applied to the columns and abutments in the transverse and longitudinal directions. The ground-motion records were then modified using a transformation so that the direction of the ground motions were rotated 45°. The simple transformation used was:

$$\begin{bmatrix} x' \\ y' \end{bmatrix} = \begin{vmatrix} \cos\theta & -\sin\theta \\ \sin\theta & \cos\theta \end{vmatrix} \begin{vmatrix} x \\ y \end{vmatrix}$$

where x and y are the transverse and longitudinal acceleration components, θ is the ground-motion rotation angle, and x´ and y´ are the transformed values.

The POE-10%-in-50-years ground-motion suite was modified using this transformation for $\theta = 45°$. The median and dispersion values using the rotated ground motions are shown in Table 6.9, and the fragility curves for the extensive and complete damage states are shown in Figure 6.5.

For practical purposes, there was little effect on how the three-span bridge model reacted to rotated ground motions.

Table 6.9: Fragility Medians after Ground-Motion Rotation (θ=45°) Using POE-10%-in-50-Years Suite

Damage State	Without Rotation		With 45° Rotation	
	Median	Dispersion	Median	Dispersion
Slight	0.02	0.90	0.03	0.81
Moderate	0.03	0.98	0.04	0.89
Extensive	0.06	1.07	0.07	0.97
Complete	0.39	1.17	0.38	1.05

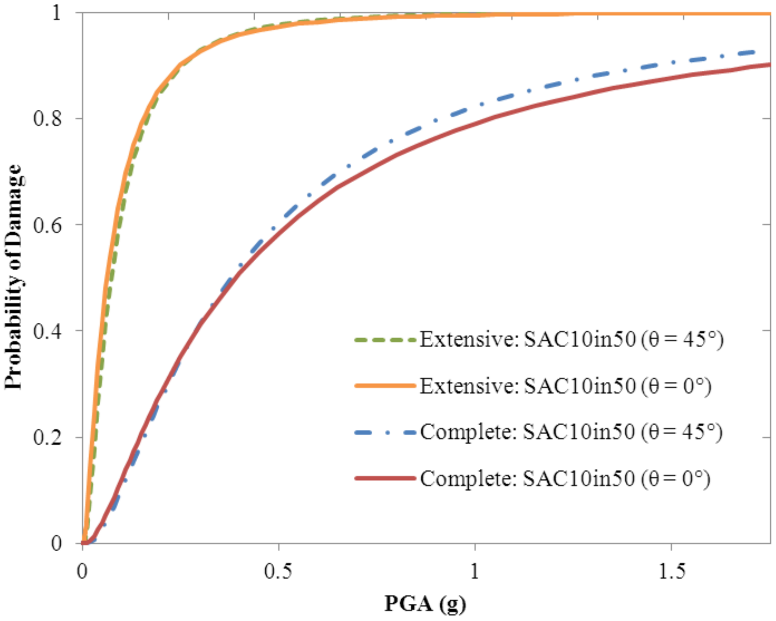

Figure 6.5: Complete and Extensive Damage Fragility Curves for Three-Span Using Rotated Ground-Motion Suite

6.3.5 EFFECT OF CONCRETE CONFINEMENT RETROFIT

The most common retrofit method used in California (Caltrans, 2010) is to encase the column with a steel jacket. The intent of this retrofit technique is to increase the confinement, which results in improving the flexural ductility of the column. The use of steel jacketing was originally developed for circular columns, but has been extended to include columns with square and rectangular cross sections (FHWA, 2006). Two steel plates are rolled to a radius equal to the column radius, or the diagonal of a square column, plus 0.5 to 1.0 inches for clearance. For a rectangular column, an oval jacket is used. After the vertical seams are welded, the gap between the column and the steel jacket is filled with grout. When working with rectangular columns with the larger space between the jacket and column, small aggregate is added to the grout. To prevent the jacket from bearing on the supporting member, such as the footing, at large drift angles a vertical gap of about two inches is usually used between the end of the jacket and the member. This technique is effective to increase confinement performance, but does not occur until the radial expansion of the concrete column induces circumferential stresses in the steel shell.

The minimum steel shell thickness can be estimated by using:

$$t \geq \frac{f_l D}{58} \text{ (in)} \tag{6-5}$$

where f_l is the confinement stress and D is the diameter of the column. f_l is assumed to be approximately 300 psi which is the value used (Chai et al., 1991) during the development of this method. The minimum steel jacket thickness was calculated to be 0.18 inches, suitable for the typical three-span bridge.

The value of f'_{cc} , the ultimate confined concrete stress capacity, can be related to shell thickness (Caltrans, 2010):

$$f'_{cc} = f'_c \left[-1.254 + 2.254\sqrt{1 + \frac{15.88 t f_s}{D f'_c}} - \frac{4 t f_s}{D f'_c}\right] \tag{6-6}$$

where f'_c is the ultimate unconfined concrete stress capacity and f_s is the stress induced in the steel jacket. Using 4.290 ksi for the unconfined strength, and 36 ksi for the stress induced in the steel jacket, f'_{cc} was found to be 6.448 ksi.

By equating the strain energy in the confined concrete to the strain energy in the confining steel jacket, the ultimate strains in the concrete based on the ultimate achievable strains in the confining steel can be found (Mander et al., 1988). Applying this principle to a circular steel shell of constant thickness results in the ultimate concrete strain capacity (Caltrans, 2010):

$$\varepsilon_{cu} = 0.004 + \frac{5.6 t f_{ys} \varepsilon_{su}}{D f'_{cc}} \tag{6-7}$$

where f_{ys} is the yield stress in the steel shell, ε_{su} is the ultimate strain in the steel shell, D is the diameter of the steel shell, and f'_{cc} is the ultimate confined concrete stress capacity. The ultimate strain capacity was found to be 0.022 in/in.

Using full-scale laboratory tests (Priestley et al., 1994a and Priestley et al., 1994b), the performance of as-built and retrofitted columns were tested. The columns were subjected to both lateral and axial loads. The as-built columns all displayed limited-ductile shear failures, followed by the rapid reduction of strength and stiffness. When retrofitted with steel jackets, the columns displayed an improved ductility, with capacities greater than or equal to $\mu_\Delta = 8$. Also, the failure mode changed from predominantly shear failure for the as-built columns to predominately flexural deformation for the retrofitted columns.

Using these new concrete capacity values, the three-span OpenSees model was again used with the ground motions from the POE-of-10%-in-50-years group.

The increased capacity from the steel jacket retrofit was then reflected in different capacity median, C_m, values used in Equation 5-9. The new values used were 3.1, 5.2, 7.2, and 8.3 for the slight, moderate, extreme and complete damage states, respectively. These were derived from the curvature ductility values used in Padgett 2007.

Using Equation 5-9 and the results from the OpenSees model, new fragility median and dispersion values were calculated. These are provided in Table 6.10. The new fragility curves are shown in figures Figure 6.6 and Figure 6.7.

Table 6.10: Fragility Medians after Steel Retrofit Using POE-10-in-50 Suite

Damage State	**Without Retrofit**		**With Retrofit**	
	Median	Dispersion	Median	Dispersion
Slight	0.02	0.90	0.11	0.83
Moderate	0.03	0.98	0.26	0.90
Extensive	0.06	1.07	0.45	0.98
Complete	0.39	1.17	0.57	1.07

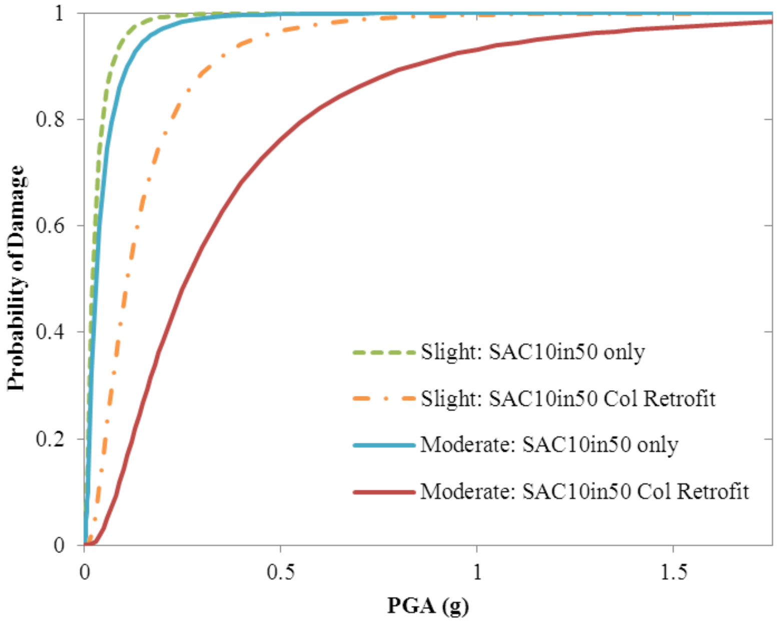

Figure 6.6: Slight and Moderate Damage Fragility Curves for Three-Span Using Retrofitted Columns

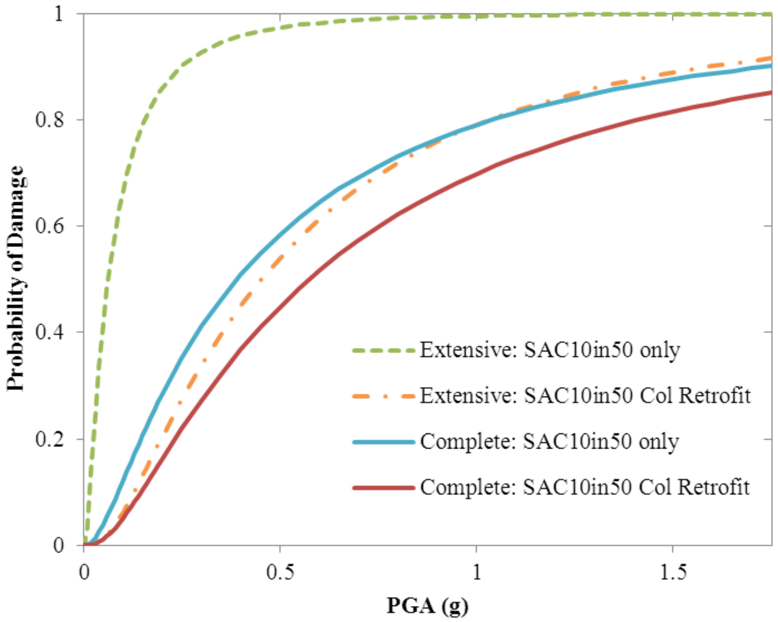

Figure 6.7: Extensive and Complete Damage Fragility Curves for Three-Span Using Retrofitted Columns

The medians for the slight, moderate and extensive damage states experienced the greatest improvement when using retrofitted columns, with improvements ranging from five times to almost nine times. The dispersion values decreased slightly, which were expected since the displacements experienced by the columns decreased with the retrofit jackets.

6.4 FIVE-SPAN BRIDGE FRAGILITY CURVES

The original five-span model was evaluated using the entire ground-motion suite described in Section 2.2, with each ground-motion pair being applied in the manner described in Section 6.3.3. This resulted in a total of 20 runs with the model resulting in column displacement data. Using this data and Equation 5-9, the following median and dispersion values were calculated for the five-span bridge and are provided in Table 6.11. The fragility curves are shown in Figure 6.8.

Table 6.11: Fragility Curves Values for Typical Five-Span Bridge

Damage State	Median	Dispersion
Slight	0.08	0.70
Moderate	0.10	0.74
Extensive	0.16	0.79
Complete	0.51	0.84

These median values indicate that the five-span bridge is somewhat less fragile when compared to the three-span bridge model (reduced data set in Table 6.6). The dispersions are very similar, so comparison of the fragility curves is appropriate.

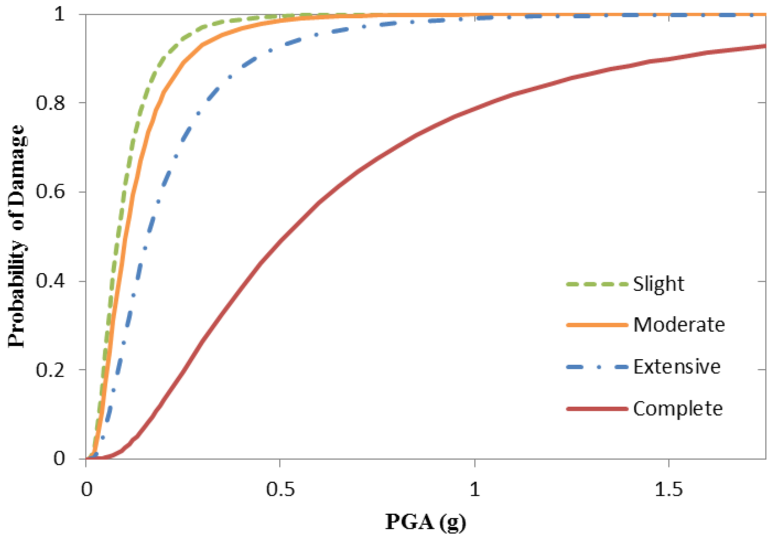

Figure 6.8: Fragility Curves for Five-Span Bridge

7.0 DISCUSSION AND CONCLUSIONS

All bridges in Oregon vary in length, width, materials, site conditions and general design. This means that each bridge may react differently when exposed to a given earthquake. Prior to the 1970s, minimal consideration was given to seismic loads in the Northwest. Because of increased awareness, bridges designed after the 1980s have a lower risk of experiencing damage from a moderate to large earthquake compared to those bridges designed before 1980. However, much of the interstate highway system in the Pacific Northwest was designed in the mid- to late 1960s. Therefore, there are a large number of bridges that have minimal seismic resistance.

As stated in Chapter 5, ground-motion intensity was used in this study as a representation of structural demand. Two sets of ground motions were used which were developed for the Seattle area by the SAC Joint Venture. The suites are a combination of actual and synthetic ground motions, in which the first is a collection of ground motions having a probability of exceedance (POE) of 2% in 50 years and the second having a POE of 10% in 50 years. Using the two separate suites allowed the development of distinct fragility curves based upon suite. By assuming that each suite was equally important, the combined effects of both suites were also used to develop aggregate fragility curves. This study determined that the ground-motion suite, with overall PGA values ranging from 0.13 g to 1.7g, had a significant effect on the developed fragility curves.

The two parts of the fragility concept are capacity and demand, where the damage states of a structure can be considered to be related to structural capacity and the ground-motion intensity is a representation of structural demand. Numerous researchers have investigated the use of fragility curves to describe the vulnerability to seismic loading. This study used the more precise but more costly method, in terms of computation time, of nonlinear time-history analysis.

The other requisite to developing fragility curves of a structure is the ability to model the capacity of that structure. To do this, an inventory of a subset of Oregon bridges was made, from which a typical three-span and five-span bridge was identified using average attributes. Using these attributes, the two bridge types were modeled as spine models, focusing only on Oregon bridges designed prior to 1960. The continuous concrete bridge type was found to be the most common type for both three-span and five-span bridges. The intent was to quantify the vulnerability of these older, but common, Oregon bridge types. The bridges were then analyzed using the research-oriented finite element program called OpenSees.

The finite element models assumed that the bridge deck would behave elastically, and the columns would behave inelastically. Because of the expected inelastic behavior the columns were modeled using the OpenSees beamWithHinges element. This specialized element considers plasticity to be concentrated over specified hinge lengths at the element ends. In this study, the plastic hinge position was assumed to be located at 10% of the column lengths, which agrees well to available predictive equations.

The abutment-soil interaction was modeled using a gap element which allows for the specification of a gap between the abutment and soil. When a sufficient amount of movement is experienced, a linear spring then applies a compressive load to the abutment. With the original model, which included both longitudinal and transverse abutment-soil interactions, the fragility medians for the typical three-span bridge were found to be 0.06 g, 0.07 g, 0.11 g, and 0.33 g for the slight, moderate, extensive and complete damage states, respectively. For the five-span typical bridge, the fragility medians were found to be near 0.08 g, 0.10 g, 0.16 g, and 0.51 g for the slight, moderate, extensive and complete damage states, respectively. When compared to predicted values from other researchers, these median values are very low, for both types of bridges. This can be predicted by looking at the relative sizes of the columns typically considered from other studies. In these studies, a common circular column diameter was 36 inches, which translates to an area moment of inertia of 82,406 in^4. For both Oregon typical bridges, the square columns had a side length of 24 inches, which translates to an area moment of inertia of 27,648 in^4. Given two equal bridges, but with the first with the larger moment of inertia for its columns, and the second bridge with the smaller inertia for its columns, the first bridge would have an initial stiffness of about three times of the second. If the two bridges weren't equal, where the first bridge had four columns per bent and the second still had the original three columns per bent, then the first bridge would have an initial stiffness of about five times of the second. In both of these cases, the bridge with the larger columns would displace less, especially before extensive cracking occurred, and would therefore experience less damage if subjected to a given ground motion. The smaller displacements would translate to larger fragility medians.

If the columns for the typical Oregon bridges were made larger, with the accordingly larger moment of inertia, what would be the impact? This can be estimated by calculating the period of a single degree of freedom system with the same mass as the three-span bridge, but with an increase of stiffness by a factor of five. This calculation results in a reduction of period of about 55%, or a period of 0.35 seconds. Using the response spectrums from Section 2, the maximum displacements would be estimated to decrease by about 79%. The fragility medians, when using the estimated reduced displacements, were found to be 0.32 g, 0.40 g, 0.61, and 1.83 g for the slight, moderate, extensive and complete damage states, respectively. Thus, the estimated reduction in displacements yields significantly larger fragility medians. When compared to results from Nielson (2007) and HAZUS, there is still disagreement. In all cases except for the complete damage state, the modified three-span medians were less (50-60%) than those predicted by HAZUS. For the complete damage state, the modified median was almost 10% greater than that predicted by HAZUS. For all damage states, the modified medians were closer to HAZUS values compared to the non-modified medians. But, in general, HAZUS still underestimates the fragility for the bridges considered in this study.

Several iterations were run where the three-span model was modified with the soil-abutment influence removed in both the longitudinal and transverse directions, and then removed only in the transverse direction. When all soil-abutment interaction was removed, the fragility medians were decreased, in most cases, by at least 50%. This means that the likelihood of damage was significantly increased. For example, at a ground motion PGA of 0.25 g, the probability of complete damage is 36 % when taking into account the effect of the soil-abutment interaction in both directions, and 64 % without taking into account the interaction. When the transverse soil-abutment interaction was removed, the fragility medians were decreased, in most cases, by at least 36 %. This illustrates that the transverse soil-abutment interaction had the most influence on the degree of bridge damage. This also indicates the importance of abutment wing-walls (or other methods such as shear keys) for restricting transverse movement to improve the resiliency of bridges that are exposed to seismic loads.

Several other changes were made to how the original three-span bridge model was analyzed. The first was to determine the effect of individual ground-motion suites. The full suite included actual and synthetic ground motions that have probabilities of exceedance of both 2% and 10% in 50 years. The second suite only included ground motions having a POE of 10% in 50 years. Using Peak Ground Acceleration (PGA) as the measure of demand usually results in a larger spread in the displacement data set, or data dispersion. This means that a larger data set is necessary in order to reduce its dispersion. This is confirmed by the model results, since the dispersion values for all damage states significantly increased by at least 40%. The fragility medians decreased, except the median for the complete damage state, which increased by 18%. However, since the smaller suite resulted in a larger set of dispersions, either the suite size should be increased, or another measure of demand should be considered, such as spectral acceleration.

A second change was to decrease the number of runs applied to the three-span model. The original test scheme used the ground motions applied in the longitudinal and transverse directions, and then reversed to be applied in the transverse and longitudinal directions. To reduce the number of runs, the set of runs which used the reverse ground motions were not used in the analysis. The result of this was that both the dispersions and fragility medians, for all damage states, were changed very little. For future modeling, the extra runs can be removed, resulting in a large time savings.

The third change was to vary the orientation of the ground motions applied to the three-span model. The original model called for the ground motions to be applied in the longitudinal and transverse directions. This was changed so that the ground motions were applied at an angle 45° from the longitudinal axis. This change, however, produced very little impact upon the fragility medians.

A single change was made to the three-span model itself, which was to model a column retrofit. The retrofit consisted of a circular steel jacket mounted along the length of the column. The space between the steel jacket and the existing column was assumed to be filled with a small aggregate and grout. The intent of this retrofit is to improve the ductility of the column by increasing the confinement experienced by the concrete. This increase of confinement is modeled by increasing the maximum strength of the concrete. In addition to the model change, the displacement ductility at which damage occurs is also assumed to increase. These two changes resulted in a significant increase of fragility medians. The fragility medians increased, at least by a factor of 4.5, for the slight, moderate and extensive damage states. The median increased by 46% for the complete damage state. The largest increase in fragility median occurs with the moderate damage state. This corresponds with the largest increase in C_m value (the assumed median value of the capacity distribution), which also occurs with the moderate damage state. Therefore, the results are highly dependent upon the improvement of ductility resulting from the physical retrofit, which was reflected by the larger C_m values.

The final stage of this study was to model a typical Oregon five-span bridge. The same methodology used with the three-span model was used with the five-span bridge. The fragility medians found were similar in scale as those found for the three-span bridge. All of the medians are relatively low, with the medians for the slight, moderate and extensive damage states being almost 50% greater than of those for the three-span bridge. Although the medians were larger, the fact that they are relatively low still points to the relative fragility of the typical five-span bridge.

In general, the results of this study show that the typical three-span and five-span bridges found in Oregon are relatively fragile structures. The results from other researchers and HAZUS underestimate bride fragility in these types of bridges. HAZUS deviates from the methods used in this study in two important aspects. The first is that a static analysis procedure was used when modeling the bridges, versus a time-dependent procedure. The second is that multiple bridge types are aggregated into more generalized and all-encompassing bridge classes. This will make the HAZUS results less applicable to specific bridge subclasses.

Other numerical models used for other U.S. regions have used relatively large column cross sections, which will dramatically change the magnitude of displacements seen by the columns, directly affecting the fragility medians. Also, other models have included soil interactions at the column bases in addition to including bearings in the model. Previous research has found that changing parameters relating to the coefficient of friction values for elastomeric pads and the initial stiffness of foundations may have minimal impact (Padgett, 2007) on the behavior of a multi-span continuous concrete bridge. This may also imply that disregarding these design features may also have minimal impact.

Several assumptions made during this study could potentially impact the fragility results. The first set of assumptions all pertain to the values used when calculating the probability of failure (Equation 5-9). The median values of the capacity distribution (C_m) were all derived using results from previous research. Although this previous research involved actual test specimens, for both non-retrofitted and retrofitted columns, the tests consisted of relatively small numbers of specimens. The amount of deviation, and whether the results pertain directly to the columns found in the typical Oregon bridge, is unknown. Additionally, the coefficient of variation (COV) for the capacity distribution was also assumed. Although the COV values used in this study ranged from 0.25 to 0.50, which lie within reasonable bounds for physical processes, the values were still somewhat arbitrary.

The final point to be stressed is to highlight the relative fragility of the bridges considered in this study. Retrofitting the columns with a steel jacket to increase concrete confinement significantly improved the performance of the columns. Without the retrofit measure, the columns were very susceptible to damage, experiencing slight to extensive damage at very low levels of ground motion.

8.0 FUTURE WORK

The ability to model specific types of Oregon bridges was the primary outcome of this study. Some extensions of this work would be very beneficial and are summarized below.

1. The major assumption was regarding the hysteretic behavior of the sections typical to Oregon. The primary response used in the current study was displacement ductility demand of the structure columns. In order to calibrate and fully evaluate the model, several large-scale tests should be conducted to obtain actual response data of a typical column. These results could also be compared to another column retrofitted.

2. Numerous assumptions were made when defining the OpenSees models. The values used to define the hysteretic behavior of the reinforcing steel were designed to result in very simple behavior of the steel. Studies should be performed to vary the hysteretic behavior of the steel, in addition to other properties used in the model.

3. While each major portion of this study was implemented with either *tcl* or *MATLAB* scripts, the scripts currently must be executed individually. These individual scripts should be combined in a manner such that incorporation into the Oregon transportation seismic hazard model, that is currently being developed, is possible.

4. The models in this study assumed that the ground motion was directly applied to the abutments and column bases. Soil and liquefaction effects should be incorporated into the models, which would result in a more realistic representation of demand on the structures.

5. The run time of each OpenSees model, using a given pair of ground motion records, was on the magnitude of several hours to a day. The models should be simplified, possibly by reducing the number of nonlinear elements used, in order to reduce run times.

6. Other types of bridges (e.g., steel, pre-stressed R/C, curved superstructure) should be modeled and investigated. This could also include more modern designs currently being used in Oregon.

7. Data from the Loma Prieta and Northridge earthquakes imply that high bridge skew has an effect on damage levels (Basoz et al., 1998). Bridge skew is accounted for in the HAZUS-HM technical manual by using modification factors applied to fragility medians. The current model should be modified to account for bridge skew, and the model output could then be compared to the effect of the HAZUS modification factors.

8. The OpenSees models should be extended to include the use of various types of bearings.

9. The uncertainty of specific material parameters (e.g., steel strength) was ignored in the current models. There have been studies that show that these parameters hold to various distributions with known means and deviations. This information should be integrated into the OpenSees models.

9.0 REFERENCES

AASHTO (2009). *AASHTO LRFD Bridge Design Specifications*. American Association of State Highway and Transportations Officieals, Washington, D.C.

Atwater, B.F., Nelson, A.R., Clague, J.J., Carver, G.A., Yamaguchi, D.K., Bobrowsky, P.T., Bourgeois, J., Darienzo, M.E., Grant, W.C., Hemphill-Haley, E., Kelsey, H.M., Jacoby, G.C., Nishenko, S.P., Palmer, S.P., Peterson, C.D., and Reinhart, M.A. (1995). "Summary of coastal geologic evidence for past great earthquakes at the Cascadia subduction zone." *Earthquake Spectra*, 11, 1-18.

Basoz N. and Kiremidjian A. (1998), "Evaluation of Bridge Damage Data from the Loma Prieta and Northridge, California Earthquakes". *Report MCEER-98-0004*, University at Buffalo, State University at New York.

Caltrans (2006). *Caltrans Seismic Design Criteria*. California Department of Transportation, Sacramento, CA, Version 1.4.

Caltrans (2010). *Earthquake Retrofit Guidelines for Bridges Memo to Designers 20-4.* California Department of Transportations, Sacramento, CA.

Chai, Y.H., Priestley, M.J.N., and Seible, F., 1991, *Flexural Retrofit of Circular Reinforced Concrete Bridge Columns by Steel Jackets*," Report Number SSRP-91/06, Department of Applied Mechanics and Engineering Sciences, University of California, San Diego.

Chopra, A. K. (2007). *Dynamics of Structures*, 167-170. Pearson, third edition.

Cornell, A. C., Jalayer, F., Hamburger, R. O., and Foutch, D. A. (2002). "Probabilistic Basis for 2000 SAC Federal Emergency Management Agency Steel Moment Frame Guidelines." *Journal of Structural Engineering*, 128(4), 526–533.

Ellingwood, B. R. and Wen, Y.-K. (2005). "Risk-Benefit-Based Design Decisions for Low-Probability/High Consequence Earthquake Events in Mid-America." *Progress in Structural Engineering and Materials*, 7(2), 56–70.

FEMA (2003). *HAZUS-MH MR3: Technical Manual*, Vol. Earthquake Model. Federal Emergency Management Agency, Washington DC.

FHWA (1995). *Recording and Coding Guide for the Structure Inventory and Appraisal of the Nation's Bridges: Report No. FHWA-PD-96-001*, Federal Highway Administration, Washington DC.

FHWA (1995). *Seismic Retrofitting Manual for Highway Bridges*, FHWA-RD-94-052. Office of Engineering and Highway Operations R&D, Federal Highway Administration, McLean, VA.

FHWA (2004). “Nation Bridge Inspection Standards.” *Title 23 Code of Federal Regulations, Highways, Section 650.311*, http://ecfr.gpoaccess.gov (accessed October 12, 2010).

FHWA (2006). *Seismic Retrofitting Manual for Highway Structures: Part I - Bridges*, FHWA-HRT-06-032. Office of Engineering and Highway Operations R&D, Federal Highway Administration, McLean, VA.

Filliben J. J., Gurley K., Pinelli, J. P. and Simiu E. “Fragility Curves, damage matrices, and wind induced loss estimation”. *Proceedings from the Third International Conference on Computer Simulation in Risk Analysis and Hazard Mitigation*, June 19-21, 2002, Sintra, Portugal, 119-126.

Heaton, T. H. and Hartzell, S. H. (1987). “Earthquake Hazards on the Cascadia Subduction Zone.” *Science*, 236, 162-168.

Hwang, H., Liu, J.B., and Chiu, Y.H. (2000). “Seismic Fragility Analysis of Highway Bridges.” Report No. MAEC RR-4, Center for Earthquake Research Information.

Hwang, H., Liu, J.B., and Chiu, Y.H. (2001). “Seismic Fragility Analysis of Highway Bridges.” Report No. MAEC RR-4, Mid-America Earthquake Center.

Limpert E., Stahel W. and Abbt M. (2001). “Log-normal Distributions across the Sciences: Keys and Clues.” *BioScience*, 51(5), 341-352.

Ludwin, R.S., A.I. Qamar, S.D. Malone, R.S. Crosson, S. Moran, G,C. Thomas, and W.P. Steele. 1996, *Scotts Mills Earthquake Summary*, http://www.pnsn.org/SEIS/EQ_Special/ScottsMills/scottsmills.html (accessed December 30, 2010).

Mander, J. B., Priestley M. J. N., Park R. (1988). “Theoretical Stress-Strain Model for Confined Concrete.” *Journal of Structural Engineering*, 114(8), 1804-1826.

Mander, J. B. (1999). Fragility Curve Development for Assessing the Seismic Vulnerability of Highway Bridges, Research Progress and Accomplishments: 1997–1999, Multidisciplinary Center for Earthquake Engineering Research, Buffalo, NY.

Mander, J. B., Kim, D. K., Chen, S. S., and Premus, G. J. (1996). “Response of Steel Bridge Bearings to the Reversed Cyclic Loading.” *Report No. NCEER 96-0014*, NCEER.

Melchers, R. E. (1999). *Structural Reliability Analysis and Prediction*. John Wiley & Sons Ltd., West Sussex, England, second edition.

Nielson, B. (2005). “Analytical Fragility Curves for Highway Bridges in Moderate Seismic Zones,” PhD thesis, Georgia Institute of Technology.

Nowak, A. S. and Collins, K. R. (2000). *Reliability of Structures*. McGraw-Hill Company, Boston, MA.

Open System for Earthquake Engineering Simulation, *The Open System for Earthquake Engineering Simulation Online*, http://opensees.berkeley.edu/ (accessed December 30, 2010).

Oregon Coastal Management Program, *Types of Coastal Hazards*, http://www.oregon.gov/LCD/OCMP/ShorHaz_HazType.shtml (accessed December 30, 2010).

Pacific Earthquake Engineering Research Center, *Structural Performance Database*, http://www.ce.washington.edu/~peera1/ (accessed December 30, 2010).

Padgett, J. (2007). "Seismic Vulnerability Assessment of Retrofitted Bridges Using Probabilistic Methods," PhD thesis, Georgia Institute of Technology.

Porter, K., Kennedy R. and Bachman R. (2007). "Creating Fragility Functions for Performance-Based Earthquake Engineering." *Earthquake Spectra*, 23, 471-489.

Priestley, M. J. N., Seible, F., Xiao, Y., and Verma, R. (1994a). "Steel Jacket Retrofitting of Reinforced Concrete Bridge Columns for Enhanced Shear Strength-Part 1: Theoretical Considerations and Test Design." *ACI Structural Journal*, 91(4), 394–405.

Priestley, M. J. N., Seible, F., Xiao, Y., and Verma, R. (1994b). "Steel Jacket Retrofitting of Reinforced Concrete Bridge Columns for Enhanced Shear Strength-Part 2: Test Results and Comparison with Theory." *ACI Structural Journal*, 91(5), 537–551.

SAC, *Develop Suite of Time Histories – SAC Venture Steel Project Phase 2 Task 5.4.1*, http://nisee.berkeley.edu/data/strong_motion/sacsteel/draftreport.html (accessed December 30, 2010).

Saxena, V., Deodatis G., Shinozuka M., Feng M. Q. (2000). Development of Fragility Curves for Multi-Span Reinforced Concrete Bridges. Proceedings of the International Conference on Monte Carlo Simulation. Principality of Monaco.

United States Geological Survey, *Historic United States Earthquakes Online,* http://earthquake.usgs.gov/regional/states/historical_mag.php/ (accessed: December 30, 2010).

Wen Y. K., Ellingwood B. R., Veneziano D., and Bracci J. (2003), "Uncertainty Modeling in Earthquake Engineering". *MAE Center Project FD-2 Report*, Mid-America Earthquake Center, University of Illinois at Urbana-Champagne.

Werner S. D., Taylor C. E., Cho S., Lavoie J-P., Huyck C., Eitzel C., Chung H. and R.T. Eguchi R. T. (2006), "REDARS 2 Methodology and Software for Seismic Risk Analysis of Highway Systems". *Report MCEER-06-SP08*, University at Buffalo, State University at New York.

10.0 APPENDICES

The OpenSees tcl files used in this study were separated into three broad categories. The first was the geometry file, which defines the geometry, boundary conditions, and nodal masses used in the model. The second file defines all of the gravity loads being applied to each node. The third file applies the ground motion to the appropriate nodes.

10.1 OPENSEES SCRIPT FOR THREE-SPAN GEOMETRY

```
source units.tcl;

#
# Define the properties of a generic elastic rigid element.
# These values are only used for the abutment elements.  RigidLink elements
# are used elsewhere, but eigenvalues couldn't be found when using them for
# the abutments.  The reason is unknown, but the large values should work for
# the abutments.
#
set ge_A 1.E8;
set ge_E 1.e10;
set ge_G 1.e10;
set ge_J 1.e10;
set ge_Iy 1.e10;
set ge_Iz 1.e10;

set S1 432.0; # length of span 1
set S2 576.0; # length of span 2
set S3 432.0; # length of span 3

#
# Bent 1 Nodes/Masses
#
node  100    0.000  277.850    0.000;
node  101    0.000  277.850   99.750;
node  102    0.000  277.850  199.500;
node  103    0.000  277.850  299.250;
node  104    0.000  277.850  399.000;
mass  100   0.0120710 0.0120710 0.0120710 0.0 0.0 0.0;
 set mass100 0.0120710
mass  101   0.0241420 0.0241420 0.0241420 0.0 0.0 0.0;
 set mass101 0.0241420;
mass  102   0.0241420 0.0241420 0.0241420 0.0 0.0 0.0;
 set mass102 0.0241420;
mass  103   0.0241420 0.0241420 0.0241420 0.0 0.0 0.0;
```

```
 set mass103 0.0241420;
mass  104   0.0120710 0.0120710 0.0120710 0.0 0.0 0.0;
 set mass104 0.0120710
fix 100 0 1 0 0 0 0;
fix 101 0 1 0 0 0 0;
fix 102 0 1 0 0 0 0;
fix 103 0 1 0 0 0 0;
fix 104 0 1 0 0 0 0;
equalDOF 100 1 1;
equalDOF 100 2 3;
equalDOF 101 3 3;
equalDOF 102 4 3;
equalDOF 103 5 3;
equalDOF 104 6 3;
equalDOF 104 7 1;

#
# A1 Longitudinal Nodes used with zeroLength elements
#
node 2    0.000  277.850    0.000;
node 3    0.000  277.850   99.750;
node 4    0.000  277.850  199.500;
node 5    0.000  277.850  299.250;
node 6    0.000  277.850  399.000;
fix 2 1 1 0 1 1 1;
fix 3 1 1 0 1 1 1;
fix 4 1 1 0 1 1 1;
fix 5 1 1 0 1 1 1;
fix 6 1 1 0 1 1 1;

#
# A1 Transverse Nodes used with zeroLength elements
#
node    1    0.000  277.850    0.000;
node    7    0.000  277.850  399.000
fix 1 0 1 1 1 1 1;
fix 7 0 1 1 1 1 1;

#
# B2 Bent Nodes/Masses
#
node  200  432.000  290.250    0.000;
node  201  432.000  290.250   63.500;
node  202  432.000  290.250  131.500;
node  203  432.000  290.250  199.500;
node  204  432.000  290.250  267.500;
node  205  432.000  290.250  335.500;
node  206  432.000  290.250  399.000;
mass  200   0.0067724 0.0067724 0.0067724 0.0 0.0 0.0;
 set mass200 0.0067724;
mass  201   0.0140248 0.0140248 0.0140248 0.0 0.0 0.0;
```

```
 set mass201 0.0140248;
mass  202   0.0145047 0.0145047 0.0145047 0.0 0.0 0.0;
 set mass202 0.0145047;
mass  203   0.0145047 0.0145047 0.0145047 0.0 0.0 0.0;
 set mass203 0.0145047;
mass  204   0.0145047 0.0145047 0.0145047 0.0 0.0 0.0;
 set mass204 0.0145047;
mass  205   0.0140248 0.0140248 0.0140248 0.0 0.0 0.0;
 set mass205 0.0140248;
mass  206   0.0067724 0.0067724 0.0067724 0.0 0.0 0.0;
 set mass206 0.0067724;

#
# B3 Bent Nodes/Masses
#
node  300 1008.000  290.250    0.000;
node  301 1008.000  290.250   63.500;
node  302 1008.000  290.250  131.500;
node  303 1008.000  290.250  199.500;
node  304 1008.000  290.250  267.500;
node  305 1008.000  290.250  335.500;
node  306 1008.000  290.250  399.000;
mass  300   0.0067724 0.0067724 0.0067724 0.0 0.0 0.0;
 set mass300 0.0067724;
mass  301   0.0140248 0.0140248 0.0140248 0.0 0.0 0.0;
 set mass301 0.0140248;
mass  302   0.0145047 0.0145047 0.0145047 0.0 0.0 0.0;
 set mass302 0.0145047;
mass  303   0.0145047 0.0145047 0.0145047 0.0 0.0 0.0;
 set mass303 0.0145047;
mass  304   0.0145047 0.0145047 0.0145047 0.0 0.0 0.0;
 set mass304 0.0145047;
mass  305   0.0140248 0.0140248 0.0140248 0.0 0.0 0.0;
 set mass305 0.0140248;
mass  306   0.0067724 0.0067724 0.0067724 0.0 0.0 0.0;
 set mass306 0.0067724;

#
# Bent 4 Nodes/Masses
#
node  400 1440.000  277.850    0.000;
node  401 1440.000  277.850   99.750;
node  402 1440.000  277.850  199.500;
node  403 1440.000  277.850  299.250;
node  404 1440.000  277.850  399.000;
mass  400    0.012071 0.0120710 0.0120710 0.0 0.0 0.0;
 set mass400 0.0120710;
mass  401    0.024142 0.0241420 0.0241420 0.0 0.0 0.0;
 set mass401 0.0241420;
mass  402    0.024142 0.0241420 0.0241420 0.0 0.0 0.0;
 set mass402 0.0241420;
```

```
mass  403    0.024142 0.0241420 0.0241420 0.0 0.0 0.0;
 set mass403 0.0241420;
mass  404    0.012071 0.0120710 0.0120710 0.0 0.0 0.0;
 set mass404 0.0120710;
fix 400 0 1 0 0 0 0;
fix 401 0 1 0 0 0 0;
fix 402 0 1 0 0 0 0;
fix 403 0 1 0 0 0 0;
fix 404 0 1 0 0 0 0;
equalDOF 400 501 1;
equalDOF 400 502 3;
equalDOF 401 503 3;
equalDOF 402 504 3;
equalDOF 403 505 3;
equalDOF 404 506 3;
equalDOF 404 507 1;

#
# A4 Longitudinal Nodes used with zeroLength elements
#
node 502 1440.000  277.850    0.000;
node 503 1440.000  277.850   99.750;
node 504 1440.000  277.850  199.500;
node 505 1440.000  277.850  299.250;
node 506 1440.000  277.850  399.000;
fix 502 1 1 0 1 1 1;
fix 503 1 1 0 1 1 1;
fix 504 1 1 0 1 1 1;
fix 505 1 1 0 1 1 1;
fix 506 1 1 0 1 1 1;

#
# A4 Transverse Nodes used with zeroLength elements
#
node  501 1440.000  277.850    0.000;
node  507 1440.000  277.850  399.000;
fix 501 0 1 1 1 1 1;
fix 507 0 1 1 1 1 1;

#
# S1 Span Nodes
#
node 1000    0.000  316.250  199.500;
node 1001   43.200  316.250  199.500;
node 1002   86.400  316.250  199.500;
node 1003  129.600  316.250  199.500;
node 1004  172.800  316.250  199.500;
node 1005  216.000  316.250  199.500;
node 1006  259.200  316.250  199.500;
node 1007  302.400  316.250  199.500;
node 1008  345.600  316.250  199.500;
node 1009  388.800  316.250  199.500;
mass 1000    0.021122 0.0211220 0.0211220 0.0 0.0 0.0;
 set mass1000 0.0211220;
mass 1001    0.042244 0.0422440 0.0422440 0.0 0.0 0.0;
 set mass1001 0.0422440;
mass 1002    0.042244 0.0422440 0.0422440 0.0 0.0 0.0;
 set mass1002 0.0422440;
mass 1003    0.042244 0.0422440 0.0422440 0.0 0.0 0.0;
 set mass1003 0.0422440;
mass 1004    0.042244 0.0422440 0.0422440 0.0 0.0 0.0;
 set mass1004 0.0422440;
mass 1005    0.042244 0.0422440 0.0422440 0.0 0.0 0.0;
 set mass1005 0.0422440;
mass 1006    0.042244 0.0422440 0.0422440 0.0 0.0 0.0;
 set mass1006 0.0422440;
mass 1007    0.042244 0.0422440 0.0422440 0.0 0.0 0.0;
 set mass1007 0.0422440;
mass 1008    0.042244 0.0422440 0.0422440 0.0 0.0 0.0;
 set mass1008 0.0422440;
mass 1009    0.042244 0.0422440 0.0422440 0.0 0.0 0.0;
 set mass1009 0.0422440;

#
# S2 Span Nodes
#
node 2000  432.000  316.250  199.500;
node 2001  489.600  316.250  199.500;
node 2002  547.200  316.250  199.500;
node 2003  604.800  316.250  199.500;
node 2004  662.400  316.250  199.500;
node 2005  720.000  316.250  199.500;
node 2006  777.600  316.250  199.500;
node 2007  835.200  316.250  199.500;
node 2008  892.800  316.250  199.500;
node 2009  950.400  316.250  199.500;
mass 2000    0.049284 0.0492840 0.0492840 0.0 0.0 0.0;
 set mass2000 0.0492840;
mass 2001    0.056324 0.0563240 0.0563240 0.0 0.0 0.0;
 set mass2001 0.0563240;
mass 2002    0.056324 0.0563240 0.0563240 0.0 0.0 0.0;
 set mass2002 0.0563240;
mass 2003    0.056324 0.0563240 0.0563240 0.0 0.0 0.0;
 set mass2003 0.0563240;
mass 2004    0.056324 0.0563240 0.0563240 0.0 0.0 0.0;
 set mass2004 0.0563240;
mass 2005    0.056324 0.0563240 0.0563240 0.0 0.0 0.0;
 set mass2005 0.0563240;
mass 2006    0.056324 0.0563240 0.0563240 0.0 0.0 0.0;
 set mass2006 0.0563240;
mass 2007    0.056324 0.0563240 0.0563240 0.0 0.0 0.0;
 set mass2007 0.0563240;
```

```
mass 2008    0.056324 0.0563240 0.0563240 0.0 0.0 0.0;
 set mass2008 0.0563240;
mass 2009    0.056324 0.0563240 0.0563240 0.0 0.0 0.0;
 set mass2009 0.0563240;

#
# S3 Span Nodes
#
node 3000 1008.000  316.250  199.500;
node 3001 1051.200  316.250  199.500;
node 3002 1094.400  316.250  199.500;
node 3003 1137.600  316.250  199.500;
node 3004 1180.800  316.250  199.500;
node 3005 1224.000  316.250  199.500;
node 3006 1267.200  316.250  199.500;
node 3007 1310.400  316.250  199.500;
node 3008 1353.600  316.250  199.500;
node 3009 1396.800  316.250  199.500;
mass 3000    0.049284 0.0492840 0.0492840 0.0 0.0 0.0;
 set mass3000 0.0492840;
mass 3001    0.042244 0.0422440 0.0422440 0.0 0.0 0.0;
 set mass3001 0.0422440;
mass 3002    0.042244 0.0422440 0.0422440 0.0 0.0 0.0;
 set mass3002 0.0422440;
mass 3003    0.042244 0.0422440 0.0422440 0.0 0.0 0.0;
 set mass3003 0.0422440;
mass 3004    0.042244 0.0422440 0.0422440 0.0 0.0 0.0;
 set mass3004 0.0422440;
mass 3005    0.042244 0.0422440 0.0422440 0.0 0.0 0.0;
 set mass3005 0.0422440;
mass 3006    0.042244 0.0422440 0.0422440 0.0 0.0 0.0;
 set mass3006 0.0422440;
mass 3007    0.042244 0.0422440 0.0422440 0.0 0.0 0.0;
 set mass3007 0.0422440;
mass 3008    0.042244 0.0422440 0.0422440 0.0 0.0 0.0;
 set mass3008 0.0422440;
mass 3009    0.042244 0.0422440 0.0422440 0.0 0.0 0.0;
 set mass3009 0.0422440;

#
# Last S3 Span Node
#
node 4000 1440.000  316.250  199.500;
mass 4000    0.021122 0.0211220 0.0211220 0.0 0.0 0.0;
 set mass4000 0.0211220;

#
# Column-2A Nodes
#
node   20  432.000    0.000   63.500;
node   21  432.000  260.000   63.500;
```

```
mass   20   0.0162612 0.0162612 0.0162612 0.0 0.0 0.0;
 set mass20 0.0162612;
mass   21   0.0162612 0.0162612 0.0162612 0.0 0.0 0.0;
 set mass21 0.0162612;
fix 20 1 1 1 1 1 1;

#
# Column-2B Nodes
#
node   22  432.000    0.000  335.500;
node   23  432.000  260.000  335.500;
mass   22   0.0162612 0.0162612 0.0162612 0.0 0.0 0.0;
 set mass22 0.0162612;
mass   23   0.0162612 0.0162612 0.0162612 0.0 0.0 0.0;
 set mass23 0.0162612;
fix 22 1 1 1 1 1 1;

#
# Column-3A Nodes
#
node   30 1008.000    0.000   63.500;
node   31 1008.000  260.000   63.500;
mass   30   0.0162612 0.0162612 0.0162612 0.0 0.0 0.0;
 set mass30 0.0162612;
mass   31   0.0162612 0.0162612 0.0162612 0.0 0.0 0.0;
 set mass31 0.0162612;
fix 30 1 1 1 1 1 1;

#
# Column-3B Nodes
#
node   32 1008.000    0.000  335.500;
node   33 1008.000  260.000  335.500;
mass   32   0.0162612 0.0162612 0.0162612 0.0 0.0 0.0;
 set mass32 0.0162612;
mass   33   0.0162612 0.0162612 0.0162612 0.0 0.0 0.0;
 set mass33 0.0162612;
fix 32 1 1 1 1 1 1;

set long_abut_tag  1;
set trans_abut_tag 2;
set IDconcCore     3;
set IDconcCover    4;
set IDreinf        5;

# Longitudinal abutment material
uniaxialMaterial ElasticPPGap 1   76.360  -66.820 -0.75

# Transverse abutment material
uniaxialMaterial ElasticPPGap 2  381.800 -334.100 -0.50
```

```
#
# Cover Concrete
#
#  fc1U=-4.29 ksi
#  eps1U=-0.002023 in./in.
#  fc2U=0.0 ksi
#  eps2U=-0.005 in./in.
#  Ec=3733.391219789322 ksi
uniaxialMaterial Concrete01 4 -4.290 -0.002023 0.0 -0.005

#
# Core Concrete
#
#  fc1C=-4.464 ksi
#  eps1C=-0.002433 in./in.
#  eps2C=-0.010 in./in.
uniaxialMaterial Concrete04 3 -4.464 -0.002433 -0.01 3733.4 0.0 0.0 0.0

#
# Reinforcing Steel
#
#  Fy=40.0 ksi
#  Fu=40.0 ksi
#  Es=29000.0 ksi
#  ey=0.001379
#  eu=0.2 in./in.
uniaxialMaterial Hysteretic 5 20.0 0.0006897 40.0 0.0013793 40.0 0.20 -20.0 -0.0006897 -40.0 -
0.0013793 -40.0 -0.20 1.0 1.0 0.0 0.0 0.0

#
# Bents 2/3 Sections
#
#  H=60.5
#  B=16.0

#
#  Version A
#
section fiberSec 2300 {;

   # Define the core patch
   patch quadr 3 16 16 -28.115000000000002 5.865 -28.115000000000002 -5.865 25.615000000000002 -
5.865 25.615000000000002 5.865

   # Define the four cover patches
   patch quadr 4 1 4 -30.25 8.0 -28.115000000000002 5.865 25.615000000000002 5.865 30.25 8.0
   patch quadr 4 1 4 -28.115000000000002 -5.865 -30.25 -8.0 30.25 -8.0 25.615000000000002 -5.865
   patch quadr 4 4 1 -30.25 8.0 -30.25 -8.0 -28.115000000000002 -5.865 -28.115000000000002 5.865
   patch quadr 4 4 1 25.615000000000002 5.865 25.615000000000002 -5.865 30.25 -8.0 30.25 8.0
   #
   # Define reinfocement layers
   #
   # Top layer
   layer straight 5 3 1.27 25.615000000000002 5.865 25.615000000000002 -5.865;  # top layer reinforcement
   # Top middle layer
   layer straight 5 2 0.2 7.949999999999999 5.865 7.949999999999999 -5.865;  # top layer reinforcement
   # Bottom middle layer
   layer straight 5 2 0.2 -10.45 5.865 -10.45 -5.865;  # top layer reinforcement
   # Bottom layer
   layer straight 5 3 1.27 -28.115000000000002 5.865 -28.115000000000002 -5.865;  # bottom layer reinfocement
};  # end of fibersection definition
uniaxialMaterial Elastic 2310 1.0e+010
   section Aggregator 2320 2310 T -section 2300
   geomTransf Linear 2330 -1 0 0

#
#  Version B
#
section fiberSec 2340 {;

   # Define the core patch
   patch quadr 3 16 16 -27.9035 5.6535 -27.9035 -5.6535 25.615000000000002 -5.6535 25.615000000000002 5.6535

   # Define the four cover patches
   patch quadr 4 1 4 -30.25 8.0 -27.9035 5.6535 25.615000000000002 5.6535 30.25 8.0
   patch quadr 4 1 4 -27.9035 -5.6535 -30.25 -8.0 30.25 -8.0 25.615000000000002 -5.6535
   patch quadr 4 4 1 -30.25 8.0 -30.25 -8.0 -27.9035 -5.6535 -27.9035 5.6535
   patch quadr 4 4 1 25.615000000000002 5.6535 25.615000000000002 -5.6535 30.25 -8.0 30.25 8.0
   #
   # Define reinfocement layers
   #
   # Top layer
   layer straight 5 3 1.27 25.615000000000002 5.6535 25.615000000000002 -5.6535;  # top layer reinforcement
   # Top middle layer
   layer straight 5 2 0.2 7.949999999999999 5.6535 7.949999999999999 -5.6535;  # top layer reinforcement
   # Bottom middle layer
   layer straight 5 2 0.2 -10.45 5.6535 -10.45 -5.6535;  # top layer reinforcement
   # Bottom layer
   layer straight 5 3 2.25 -27.9035 5.6535 -27.9035 -5.6535;  # bottom layer reinfocement
};  # end of fibersection definition
uniaxialMaterial Elastic 2350 1.0e+010
section Aggregator 2360 2350 T -section 2340

#
# Columns 2/3 Sections
#
section fiberSec 2000 {;
```

```
    # Define the core patch
    patch quadr 3 16 16 -9.295 9.295 -9.295 -9.295 9.295 -9.295 9.295 9.295

    # Define the four cover patches
    patch quadr 4 1 4 -12.0 12.0 -9.295 9.295 9.295 9.295 12.0 12.0
    patch quadr 4 1 4 -9.295 -9.295 -12.0 -12.0 12.0 -12.0 9.295 -9.295
    patch quadr 4 4 1 -12.0 12.0 -12.0 -12.0 -9.295 -9.295 -9.295 9.295
    patch quadr 4 4 1 9.295 9.295 9.295 -9.295 12.0 -12.0 12.0 12.0

    # Define reinfocement layers
    # top layer reinforcement
    layer straight 5 2 1.56  9.295 9.295 9.295 -9.295;
    # bottom layer reinfocement
    layer straight 5 2 1.56 -9.295 9.295 -9.295 -9.295;
};  # end of fibersection definition
uniaxialMaterial Elastic 2001 1.0e+010
section Aggregator 2002 2001 T -section 2000

geomTransf Linear 2003 0 0 -1
geomTransf PDelta 2004 0 0 -1

#
# Span Elements
#
set Deck_Area 4436.25;
set Deck_E    3733.391;
set Deck_G    1500.0;
set Deck_J    61509000.0;
set Deck_Iy   63344000.0;
set Deck_Iz   427780.0;
geomTransf Linear 1000 0 1 0;
element elasticBeamColumn 1000 1000 1001 4436.3 3733.4 1500.0 61509000.0 63344000.0 427780.0
1000
element elasticBeamColumn 1001 1001 1002 4436.3 3733.4 1500.0 61509000.0 63344000.0 427780.0
1000
element elasticBeamColumn 1002 1002 1003 4436.3 3733.4 1500.0 61509000.0 63344000.0 427780.0
1000
element elasticBeamColumn 1003 1003 1004 4436.3 3733.4 1500.0 61509000.0 63344000.0 427780.0
1000
element elasticBeamColumn 1004 1004 1005 4436.3 3733.4 1500.0 61509000.0 63344000.0 427780.0
1000
element elasticBeamColumn 1005 1005 1006 4436.3 3733.4 1500.0 61509000.0 63344000.0 427780.0
1000
element elasticBeamColumn 1006 1006 1007 4436.3 3733.4 1500.0 61509000.0 63344000.0 427780.0
1000
element elasticBeamColumn 1007 1007 1008 4436.3 3733.4 1500.0 61509000.0 63344000.0 427780.0
1000
element elasticBeamColumn 1008 1008 1009 4436.3 3733.4 1500.0 61509000.0 63344000.0 427780.0
1000
```

```
element elasticBeamColumn 1009 1009 2000 4436.3 3733.4 1500.0 61509000.0 63344000.0 427780.0
1000
element elasticBeamColumn 2000 2000 2001 4436.3 3733.4 1500.0 61509000.0 63344000.0 427780.0
1000
element elasticBeamColumn 2001 2001 2002 4436.3 3733.4 1500.0 61509000.0 63344000.0 427780.0
1000
element elasticBeamColumn 2002 2002 2003 4436.3 3733.4 1500.0 61509000.0 63344000.0 427780.0
1000
element elasticBeamColumn 2003 2003 2004 4436.3 3733.4 1500.0 61509000.0 63344000.0 427780.0
1000
element elasticBeamColumn 2004 2004 2005 4436.3 3733.4 1500.0 61509000.0 63344000.0 427780.0
1000
element elasticBeamColumn 2005 2005 2006 4436.3 3733.4 1500.0 61509000.0 63344000.0 427780.0
1000
element elasticBeamColumn 2006 2006 2007 4436.3 3733.4 1500.0 61509000.0 63344000.0 427780.0
1000
element elasticBeamColumn 2007 2007 2008 4436.3 3733.4 1500.0 61509000.0 63344000.0 427780.0
1000
element elasticBeamColumn 2008 2008 2009 4436.3 3733.4 1500.0 61509000.0 63344000.0 427780.0
1000
element elasticBeamColumn 2009 2009 3000 4436.3 3733.4 1500.0 61509000.0 63344000.0 427780.0
1000
element elasticBeamColumn 3000 3000 3001 4436.3 3733.4 1500.0 61509000.0 63344000.0 427780.0
1000
element elasticBeamColumn 3001 3001 3002 4436.3 3733.4 1500.0 61509000.0 63344000.0 427780.0
1000
element elasticBeamColumn 3002 3002 3003 4436.3 3733.4 1500.0 61509000.0 63344000.0 427780.0
1000
element elasticBeamColumn 3003 3003 3004 4436.3 3733.4 1500.0 61509000.0 63344000.0 427780.0
1000
element elasticBeamColumn 3004 3004 3005 4436.3 3733.4 1500.0 61509000.0 63344000.0 427780.0
1000
element elasticBeamColumn 3005 3005 3006 4436.3 3733.4 1500.0 61509000.0 63344000.0 427780.0
1000
element elasticBeamColumn 3006 3006 3007 4436.3 3733.4 1500.0 61509000.0 63344000.0 427780.0
1000
element elasticBeamColumn 3007 3007 3008 4436.3 3733.4 1500.0 61509000.0 63344000.0 427780.0
1000
element elasticBeamColumn 3008 3008 3009 4436.3 3733.4 1500.0 61509000.0 63344000.0 427780.0
1000
element elasticBeamColumn 3009 3009 4000 4436.3 3733.4 1500.0 61509000.0 63344000.0 427780.0
1000

#
# Rigid Elements linking bents to spans
#
rigidLink beam 1000 102;
rigidLink beam 2000 203;
rigidLink beam 3000 303;
rigidLink beam 4000 402;
```

```
#
# Rigid Elements linking columns to bents
#
rigidLink beam 201 21;
rigidLink beam 205 23;
rigidLink beam 301 31;
rigidLink beam 305 33;

#
# Bent 1 Elements
#
element elasticBeamColumn 100 100 101 1e+008 1e+010 1e+010 1e+010 1e+010 1e+010 2330
element elasticBeamColumn 101 101 102 1e+008 1e+010 1e+010 1e+010 1e+010 1e+010 2330
element elasticBeamColumn 102 102 103 1e+008 1e+010 1e+010 1e+010 1e+010 1e+010 2330
element elasticBeamColumn 103 103 104 1e+008 1e+010 1e+010 1e+010 1e+010 1e+010 2330

#
# Abutment 1 ZeroLength Elements
#
element zeroLength 1 1 100 -mat 2 -dir 3
element zeroLength 2 2 100 -mat 1 -dir 1
element zeroLength 3 3 101 -mat 1 -dir 1
element zeroLength 4 4 102 -mat 1 -dir 1
element zeroLength 5 5 103 -mat 1 -dir 1
element zeroLength 6 6 104 -mat 1 -dir 1
element zeroLength 7 104 7 -mat 2 -dir 3

#
# Bent 2 Elements
#
element dispBeamColumn 200 200 201 5 2320 2330;
element dispBeamColumn 201 201 202 5 2360 2330;
element dispBeamColumn 202 202 203 5 2360 2330;
element dispBeamColumn 203 203 204 5 2360 2330;
element dispBeamColumn 204 204 205 5 2360 2330;
element dispBeamColumn 205 205 206 5 2320 2330;
element elasticBeamColumn 2020 201 202 1e-007 4e+003 1e-007 1e-007 6e+007 1e-007 2330
element elasticBeamColumn 2030 202 203 1e-007 4e+003 1e-007 1e-007 6e+007 1e-007 2330
element elasticBeamColumn 2040 203 204 1e-007 4e+003 1e-007 1e-007 6e+007 1e-007 2330
element elasticBeamColumn 2050 204 205 1e-007 4e+003 1e-007 1e-007 6e+007 1e-007 2330

#
# Bent 2 Column Elements
#
element beamWithHinges 20 20 21 2002 18.92 2002 18.92 3733.39 576.0 27648.0 27648.0 1500.0
55296.0 2004;
element beamWithHinges 22 22 23 2002 18.92 2002 18.92 3733.39 576.0 27648.0 27648.0 1500.0
55296.0 2004;

#
# Bent 3 Elements
```

```
#
element dispBeamColumn 300 300 301 5 2320 2330;
element dispBeamColumn 301 301 302 5 2360 2330;
element dispBeamColumn 302 302 303 5 2360 2330;
element dispBeamColumn 303 303 304 5 2360 2330;
element dispBeamColumn 304 304 305 5 2360 2330;
element dispBeamColumn 305 305 306 5 2320 2330;
element elasticBeamColumn 3020 301 302 1e-007 4e+003 1e-007 1e-007 6e+007 1e-007 2330
element elasticBeamColumn 3030 302 303 1e-007 4e+003 1e-007 1e-007 6e+007 1e-007 2330
element elasticBeamColumn 3040 303 304 1e-007 4e+003 1e-007 1e-007 6e+007 1e-007 2330
element elasticBeamColumn 3050 304 305 1e-007 4e+003 1e-007 1e-007 6e+007 1e-007 2330

#
# Bent 3 Column Elements
#
element beamWithHinges 30 30 31 2002 18.92 2002 18.92 3733.39 576.0 27648.0 27648.0 1500.0
55296.0 2004;
element beamWithHinges 32 32 33 2002 18.92 2002 18.92 3733.39 576.0 27648.0 27648.0 1500.0
55296.0 2004;

#
# Bent 4 Elements
#
element elasticBeamColumn 400 400 401 1e+008 1e+010 1e+010 1e+010 1e+010 1e+010 2330
element elasticBeamColumn 401 401 402 1e+008 1e+010 1e+010 1e+010 1e+010 1e+010 2330
element elasticBeamColumn 402 402 403 1e+008 1e+010 1e+010 1e+010 1e+010 1e+010 2330
element elasticBeamColumn 403 403 404 1e+008 1e+010 1e+010 1e+010 1e+010 1e+010 2330

#
# Abutment 4 ZeroLength Elements
#
element zeroLength 501 501 400 -mat 2 -dir 3;
element zeroLength 502 400 502 -mat 1 -dir 1;
element zeroLength 503 401 503 -mat 1 -dir 1;
element zeroLength 504 402 504 -mat 1 -dir 1;
element zeroLength 505 403 505 -mat 1 -dir 1;
element zeroLength 506 404 506 -mat 1 -dir 1;
element zeroLength 507 404 507 -mat 2 -dir 3;
```

10.2 OPENSEES SCRIPT FOR 3-SPAN GRAVITY LOADS

```
puts "gravity_loads_nom.tcl: Starting Gravity Load Analysis";

# 0 => no print output (default)
# 1 => print information on each step
# 2 => print information when convergence has been achieved
# 4 => print norm, dU and dR vectors
# 5 => at convergence failure, carry on, print error message, but do not stop analysis
set test_command_flag 1;

set mult -$g;
set S1_total_weight 0.0;
set S2_total_weight 0.0;
set S3_total_weight 0.0;
set S4_total_weight 0.0; # one last node over B4
set B1_total_weight 0.0;
set B2_total_weight 0.0;
set B3_total_weight 0.0;
set B4_total_weight 0.0;
set C2A_total_weight 0.0;
set C2B_total_weight 0.0;
set C3A_total_weight 0.0;
set C3B_total_weight 0.0;
set total 0.0;

pattern Plain 1 "Constant" {

   # Span 1
   for {set i 1000} {$i <= 1009} {incr i} {
      set var_name mass$i;
      set value [expr $$var_name];
      puts [format "node $i %.6f" $value];
      set gvalue [expr $mult*$value];
      load $i 0.0 $gvalue 0.0 0.0 0.0 0.0;
      set S1_total_weight [expr $S1_total_weight+$gvalue];
      set total [expr $total+$gvalue];
   }
   # Span 2
   puts "";
   for {set i 2000} {$i <= 2009} {incr i} {
      set var_name mass$i;
      set value [expr $$var_name];
      puts [format "node $i %.6f" $value];
      set gvalue [expr $mult*$value];
      load $i 0.0 $gvalue 0.0 0.0 0.0 0.0;
      set S2_total_weight [expr $S2_total_weight+$gvalue];
      set total [expr $total+$gvalue];
   }
```

```
# Span 3
puts "";
for {set i 3000} {$i <= 3009} {incr i} {
    set var_name mass$i;
    set value [expr $$var_name];
    puts [format "node $i %.6f" $value];
    set gvalue [expr $mult*$value];
    load $i 0.0 $gvalue 0.0 0.0 0.0 0.0;
    set S3_total_weight [expr $S3_total_weight+$gvalue];
    set total [expr $total+$gvalue];
}
# Last Span Node (4000)
puts "";
set var_name mass4000;
set value [expr $$var_name];
puts [format "node $i %.6f" $value];
set gvalue [expr $mult*$value];
load 4000 0.0 $gvalue 0.0 0.0 0.0 0.0;
set S4_total_weight [expr $S4_total_weight+$gvalue];
set total [expr $total+$gvalue];

# Bent 1
for {set i 100} {$i <= 104} {incr i} {
    set var_name mass$i;
    set value [expr $$var_name];
    set gvalue [expr $mult*$value];
    load $i 0.0 $gvalue 0.0 0.0 0.0 0.0;
    set B1_total_weight [expr $B1_total_weight+$gvalue];
    set total [expr $total+$gvalue];
}
# Bent 2
for {set i 200} {$i <= 206} {incr i} {
    set var_name mass$i;
    set value [expr $$var_name];
    set gvalue [expr $mult*$value];
    load $i 0.0 $gvalue 0.0 0.0 0.0 0.0;
    set B2_total_weight [expr $B2_total_weight+$gvalue];
    set total [expr $total+$gvalue];
}
# Bent 3
for {set i 300} {$i <= 306} {incr i} {
    set var_name mass$i;
    set value [expr $$var_name];
    set gvalue [expr $mult*$value];
    load $i 0.0 $gvalue 0.0 0.0 0.0 0.0;
    set B3_total_weight [expr $B3_total_weight+$gvalue];
    set total [expr $total+$gvalue];
}
# Bent 4
for {set i 400} {$i <= 404} {incr i} {
    set var_name mass$i;
```

```
        set value [expr $$var_name];
        set gvalue [expr $mult*$value];
        load $i 0.0 $gvalue 0.0 0.0 0.0 0.0;
        set B4_total_weight [expr $B4_total_weight+$gvalue];
        set total [expr $total+$gvalue];
    }

    # Column 2A
    set var_name mass21;
    set value [expr $$var_name];
    set gvalue [expr $mult*$value];
    load 21 0.0 $gvalue 0.0 0.0 0.0 0.0;
    set C2A_total_weight [expr $C2A_total_weight+$gvalue];
    set total [expr $total+$gvalue];

    # Column 2B
    set var_name mass23;
    set value [expr $$var_name];
    set gvalue [expr $mult*$value];
    load 23 0.0 $gvalue 0.0 0.0 0.0 0.0;
    set C2B_total_weight [expr $C2B_total_weight+$gvalue];
    set total [expr $total+$gvalue];

    # Column 3A
    set var_name mass31;
    set value [expr $$var_name];
    set gvalue [expr $mult*$value];
    load 31 0.0 $gvalue 0.0 0.0 0.0 0.0;
    set C3A_total_weight [expr $C3A_total_weight+$gvalue];
    set total [expr $total+$gvalue];

    # Column 3B
    set var_name mass33;
    set value [expr $$var_name];
    set gvalue [expr $mult*$value];
    load 33 0.0 $gvalue 0.0 0.0 0.0 0.0;
    set C3B_total_weight [expr $C3B_total_weight+$gvalue];
    set total [expr $total+$gvalue];
}



puts [format "Span 1 Weight: %.3f kips" $S1_total_weight];
puts [format "Span 2 Weight: %.3f kips" $S2_total_weight];
puts [format "Span 3 Weight: %.3f kips" $S3_total_weight];
puts [format "N4000  Weight: %.3f kips" $S4_total_weight];
puts [format "  Total Span Weights: %.3f kips"\
   [expr $S1_total_weight+$S2_total_weight+$S3_total_weight+$S4_total_weight]];
puts [format "Bent 1 Weight: %.3f kips" $B1_total_weight];
puts [format "Bent 2 Weight: %.3f kips" $B2_total_weight];
puts [format "Bent 3 Weight: %.3f kips" $B3_total_weight];
puts [format "Bent 4 Weight: %.3f kips" $B4_total_weight];
puts [format "  Total Bent Weights: %.3f kips"\
   [expr $B1_total_weight+$B2_total_weight+$B3_total_weight+$B4_total_weight]];
puts [format "Col 2A Weight: %.3f kips" $C2A_total_weight];
puts [format "Col 2B Weight: %.3f kips" $C2B_total_weight];
puts [format "Col 3A Weight: %.3f kips" $C3A_total_weight];
puts [format "Col 3B Weight: %.3f kips" $C3B_total_weight];
puts [format "  Total Column Weights: %.3f kips"\
   [expr $C2A_total_weight+$C2B_total_weight+$C3A_total_weight+$C3B_total_weight]];
puts [format "  Total Structure Weight: %.3f kips" $total];
puts [format "  Total Structure Mass  : %.6f kips-sec2/in." [expr $total/386.4]];
puts "";

# Gravity-analysis parameters -- load-controlled static analysis
set Tol 1.0e-8;                    # convergence tolerance for test
#set constraintsTypeGravity Plain;       # default;
set constraintsTypeGravity Transformation;       # default;
constraints $constraintsTypeGravity ;   # how it handles boundary conditions
numberer RCM;                         # renumber dof's to minimize band-width (optimization), if you want to
system BandGeneral;                   # how to store and solve the system of equations in the analysis (large
model: try UmfPack)
test EnergyIncr $Tol 30 $test_command_flag; # determine if convergence has been achieved at the end of
an iteration step
algorithm Newton;                     # use Newton's solution algorithm: updates tangent stiffness at every
iteration
set NstepGravity 10;                  # apply gravity in 10 steps
set DGravity [expr 1./$NstepGravity];   # first load increment;
integrator LoadControl $DGravity;       # determine the next time step for an analysis
analysis Static;                   # define type of analysis static or transient
set ok [analyze $NstepGravity];        # apply gravity

if {$ok != 0} {
   puts "PROBLEM: gravity_loads_nom.tcl";
} else {
   puts "DONE: gravity_loads_nom.tcl: ... Done Gravity Analysis";
}
```

10.3 OPENSEES SCRIPT FOR 3-SPAN EXTERNAL LOADS

```
source units.tcl;

# These strings are placeholders for the EQ files for the two horizontal
# directions 1 and 3 (file names with path, time between time steps (secs), and
# duration of records (secs)).
# Remember that the EQ filename use different units for delta_t and duration.
#
set _VAR_acc_filePath1 EQ1.acc;
set _VAR_acc_filePath2 EQ2.acc;
set _VAR_acc_delta_t 0.0;
set _VAR_acc_duration 0.0;

set _VAR_damping 1.0; # not varied yet by batch script

# Set by the batch script so that debug mode is always turned off when doing EQ runs.
set _VAR_use_debug_mode $true;

set use_EQ_dir_1 $true;
set use_EQ_dir_3 $true;

puts "external_loads_nom.tcl: Starting External Load Analysis (EQ/Pushover/Cyclic)";

# 0 => no print output (default)
# 1 => print information on each step
# 2 => print information when convergence has been achieved
# 4 => print norm, dU and dR vectors
# 5 => at convergence failure, carry on, print error message, but do not stop analysis
set test_command_flag 1;

# Pick ONE of the following to be true; the others should be false.
set do_EQ $true;
set do_pushover $false;
set do_cyclic $false;

#####################################################################################

if {$do_EQ} {
   puts "doing EQ load type"

   set units_conver 2.54; # acc files are in cm/sec2

   # DYNAMIC ground-motion analysis -------------
   if {$use_EQ_dir_1} {
      set accelSeries1 "Series -dt $_VAR_acc_delta_t -filePath \"$_VAR_acc_filePath1\"\
            -factor [expr $_VAR_external_loads * $_VAR_g_factor / $units_conver]";
      puts "\naccelSeries1: $accelSeries1\n";
      pattern UniformExcitation 2 1 -accel $accelSeries1;
```

```
}

if {$use_EQ_dir_3} {
   set accelSeries2 "Series -dt $_VAR_acc_delta_t -filePath \"$_VAR_acc_filePath2\"\
         -factor [expr $_VAR_external_loads * $_VAR_g_factor / $units_conver]";
   puts "\naccelSeries2: $accelSeries2\n";
   pattern UniformExcitation 3 3 -accel $accelSeries2;
}

set eigen_value [eigen 1];
set damping_value [expr 0.05*$_VAR_damping];
rayleigh 0. 0. 0. [expr 2*$damping_value/pow($eigen_value,0.5)];

if {[regexp 2in50 $_VAR_acc_filePath1]} {
   set DtAnalysis $Dt_short;
   puts "Using Dt_short ($Dt_short) for DtAnalysis value";
} elseif {[regexp 10in50 $_VAR_acc_filePath1]} {
   set DtAnalysis $Dt_long;
   puts "Using Dt_long ($Dt_long) for DtAnalysis value";
} else {
   puts "A record other than 2in50 or 10in50 is being used ... exiting";
   exit;
}

#set DtAnalysis 0.0015;

set Nsteps [expr int($_VAR_acc_duration/$DtAnalysis)];
set TolDynamic 1.e-8;           # Convergence Test: tolerance

wipeAnalysis;
#constraints Plain;
constraints Transformation;
numberer Plain;
system BandGeneral;
test NormDispIncr $TolDynamic 10 $test_command_flag;
algorithm Newton;
integrator Newmark 0.5 0.25;
analysis Transient;
set ok [analyze $Nsteps $DtAnalysis]; # returns ok=0 if analysis was successful

set testTypeDynamic EnergyIncr;  # Convergence-test type
set maxNumIterDynamic 10;        # maximum number of iterations
set algorithmTypeDynamic ModifiedNewton;

if {$ok != 0} {; # analysis was not successful.
   # ---------------------------------------------------------------------------
   # change some analysis parameters to achieve convergence
   # performance is slower inside this loop
   #    Time-controlled analysis
   set ok 0;
   set controlTime [getTime];
```

```
while {$controlTime < $_VAR_acc_duration && $ok == 0} {
  set controlTime [getTime]
  set ok [analyze 1 $DtAnalysis]
  if {$ok != 0} {
    puts "Trying Newton with Initial Tangent .."
    test NormDispIncr $TolDynamic 10 $test_command_flag;
    algorithm Newton -initial
    set ok [analyze 1 $DtAnalysis]
    test $testTypeDynamic $TolDynamic $maxNumIterDynamic $test_command_flag;
    algorithm $algorithmTypeDynamic
  }
  if {$ok != 0} {
    puts "Trying Broyden .."
    algorithm Broyden 8
    set ok [analyze 1 $DtAnalysis]
    algorithm $algorithmTypeDynamic
  }
  if {$ok != 0} {
    puts "Trying NewtonWithLineSearch .."
    algorithm NewtonLineSearch .8
    set ok [analyze 1 $DtAnalysis]
    algorithm $algorithmTypeDynamic
  }
  if {$ok != 0} {
    puts "Trying reducing the time step by 2: dt=[expr $DtAnalysis/2]"
    set ok [analyze 1 [expr $DtAnalysis/2]]
  }
  if {$ok != 0} {
    puts "Trying reducing the time step by 10: dt=[expr $DtAnalysis/10]"
    set ok [analyze 1 [expr $DtAnalysis/10]]
  }
  if {$ok != 0} {
    puts "Trying reducing the time step by 100: dt=[expr $DtAnalysis/100]"
    set ok [analyze 1 [expr $DtAnalysis/100]]
  }
  # Try the previous methods with the smaller timestep
  set Dt_new [expr $DtAnalysis/100];
  if {$ok != 0} {
    puts "Trying Newton with Initial Tangent .."
    test NormDispIncr $TolDynamic 10 $test_command_flag;
    algorithm Newton -initial
    set ok [analyze 1 $Dt_new]
    test $testTypeDynamic $TolDynamic $maxNumIterDynamic $test_command_flag;
    algorithm $algorithmTypeDynamic
  }
  if {$ok != 0} {
    puts "Trying Broyden .."
    algorithm Broyden 8
    set ok [analyze 1 $Dt_new]
    algorithm $algorithmTypeDynamic
  }
```

```
         if {$ok != 0} {
            puts "Trying NewtonWithLineSearch .."
            algorithm NewtonLineSearch .8
            set ok [analyze 1 $Dt_new]
            algorithm $algorithmTypeDynamic
         }
         if {$ok != 0} {
            puts "EQ:: PROBLEM: [getTime]";
         }
      }
   };   # end if ok !0

   if {$ok == 0} {
      puts "EQ:: Ground Motion DONE. End Time: [getTime]"
   }

} elseif {$do_pushover} {

   set IDctrlNode 325;
   set IDctrlDOF 3;

   pattern Plain 100 Linear {
      load 325 0.0 0.0 [expr 0.05*100.0] 0.0 0.0 0.0;
   }

   set Dmax [expr 0.000015*266.0];
   set Dmax [expr 0.02*266.0];
   puts "Dmax=$Dmax";

   set Dincr [expr 0.000005*266.0];

set Nsteps [expr int($Dmax/$Dincr)];                 # number of pushover analysis steps

set ok [analyze $Nsteps];          # this will return zero if no convergence problems were encountered
# ----------------------------------------------if convergence failure-------------------------
variable testTypeStatic EnergyIncr ;        # Convergence-test type
#variable TolStatic 1.e-8;
variable TolStatic 1.e-6;
#variable maxNumIterStatic 6;
variable maxNumIterStatic 20;
variable algorithmTypeStatic Newton;

if {$ok != 0} {
   # if analysis fails, we try some other stuff, performance is slower inside this loop
   set Dstep 0.0;
   set ok 0
   while {$Dstep <= 1.0 && $ok == 0} {
      set controlDisp [nodeDisp $IDctrlNode $IDctrlDOF ]
      set Dstep [expr $controlDisp/$Dmax]
      set ok [analyze 1];  # this will return zero if no convergence problems were encountered
         if {$ok != 0} {;                              # reduce step size if still fails to converge
         set Nk 4;          # reduce step size
         set DincrReduced [expr $Dincr/$Nk];
         integrator DisplacementControl  $IDctrlNode $IDctrlDOF $DincrReduced
         for {set ik 1} {$ik <=$Nk} {incr ik 1} {
            set ok [analyze 1]; # this will return zero if no convergence problems were encountered
            if {$ok != 0} {
               # if analysis fails, we try some other stuff
               # performance is slower inside this loop    global maxNumIterStatic;
               # max no. of iterations performed before "failure to converge" is ret'd
               puts "Trying Newton with Initial Tangent .."
               #test NormDispIncr   $Tol 2000 $test_command_flag
               #test NormDispIncr   $Tol 100 $test_command_flag
               test NormDispIncr   $TolStatic 100 $test_command_flag
               algorithm Newton -initial
               set ok [analyze 1]
               test $testTypeStatic $TolStatic      $maxNumIterStatic   $test_command_flag
               algorithm $algorithmTypeStatic
            }
            if {$ok != 0} {
               puts "Trying Broyden .."
               algorithm Broyden 8
               set ok [analyze 1 ]
               algorithm $algorithmTypeStatic
            }
            if {$ok != 0} {
               puts "Trying NewtonWithLineSearch .."
               algorithm NewtonLineSearch 0.8
               set ok [analyze 1]
               algorithm $algorithmTypeStatic
            }
            if {$ok != 0} {;   # stop if still fails to converge
               set fmt1 "%s Pushover analysis: CtrlNode %.3i, dof %.1i, Disp=%.4f %s";

               puts [format $fmt1 "PROBLEM" $IDctrlNode $IDctrlDOF [nodeDisp $IDctrlNode
$IDctrlDOF] $LunitTXT]
               return -1
            }; # end if
         }; # end for
         integrator DisplacementControl  $IDctrlNode $IDctrlDOF $Dincr;    # bring back to original
increment
      }; # end if
   };   # end while loop
};     # end if ok !0
# ---------------


} elseif {$do_cyclic} {

   #puts "external_loads_nom.tcl: ... Done Cyclic Analysis";

} else {
   puts "\nexternal_loads_nom.tcl: ERROR: invalid load type"
   exit;
}
```

OTREC
OREGON TRANSPORTATION RESEARCH AND EDUCATION CONSORTIUM

P.O. Box 751
Portland, OR 97207

OTREC is dedicated to stimulating and conducting collaborative multi-disciplinary research on multi-modal surface transportation issues, educating a diverse array of current practitioners and future leaders in the transportation field, and encouraging implementation of relevant research results.